# ABSTRACT

Title of Dissertation: THE GATING MECHANISM OF THE LARGE MECHANOSENSITIVE CHANNEL IN *Escherichia coli* AND EFFECTS OF GAIN-OF-FUNCTION MUTAIONS

Chien-Sung Chiang, Doctor of Philosophy, 2005

Dissertation directed by: Dr. Sergei Sukharev, Associate Professor
Department of Biology

The mechanosensitive channel of large conductance (MscL) in *Escherichia coli* is perhaps the best-characterized mechanosensitive protein. The structure of the *Mycobacterium tuberculosis* ortholog has been solved recently by X-ray crystallography, but the structural rearrangements associated with gating remain obscure. Based on the crystal structure, a homology model of *E. coli* MscL had been built and the gating process was proposed (Sukharev et al., 2001). I experimentally verified these working models. The result demonstrates that the iris-like expansion of M1 helixes does occur during the gating transition. In addition to the hydrophobic M1 gate, the S1 segments unresolved in the original crystal structure were easily cross-linked with pairs of cysteines and prevented opening, consistent with the proposed function of a second gate.

Although the early models predicted a wide-open conformation with cytoplasmic S3 domains separated, the current data strongly suggest that S3 domains are in fact stably associated in both closed and open conformations.

The open-state model predicts an in-plane expansion of the channel protein of about 23 $nm^2$. The analysis of multiple MscL dose-response curves, accounting for non-homogeneity of channels in a population, (i.e. variable energy or area changes for individual channels), estimated the total channel expansion ~20 $nm^2$ and the transition energy ~52 kT, consistent with molecular models of the open state. Gain-of-function (GOF) mutants with hydrophilic or charged substitutions in the main hydrophobic gate stably occupy low-conducting substates. The character of perturbations introduced in the main gate by GOF substitutions strongly supports the two-gate mechanism in which the first sub-transition (C→S) can be viewed as the opening of the M1 gate formed by the first transmembrane domains, resulting in an expanded leaky conformation (S). The second sub-transition (S→O) can be attributed to the separation of the N-terminal (S1) gate resulting in the fully conductive channel

# THE GATING MECHANISM OF THE LARGE MECHANOSENSITIVE CHANNEL IN *Escherichia coli* AND EFFECTS OF GAIN-OF-FUNCTION MUTATIONS

By

Chien-Sung Chiang

Dissertation submitted to the Faculty of the Graduate school of the
University of Maryland at College Park in partial fulfillment
of the requirements for the degree of
Doctor of Philosophy
2005

Advisory Committee:

Associate Professor Sergei Sukharev, Chair/Advisor
Professor Dorothy Beckett, Dean's Representive
Professor Marco Colombini
Assistant Professor Roger W. Davenport
Professor Richard Payne

©Copyright by
Chien-Sung Chiang
2005

# DEDICATION

It is my great pleasure to dedicate this dissertation to my loving father, stepmother, farther-in-law, and mother-in-law and in memory of my mother, a woman of great intellect, who was an inspiration to everyone around her.

# ACKNOWLEGEMENTS

I deeply thank my advisor, Dr. Sergei Sukharev, for leading me to the world of microbial ion channels, and for his great patience, insightful research guidance and financial support during past six years. I am indebted to members of my dissertation committee, Drs. Dorothy Beckett, Marco Colombini, Roger W. Davenport and Richard Payne for their review and valuable critique to my proposal and dissertation. I am very grateful to previous laboratory members, Monica Betanzos, Paul Gray and Slava Gendel, and current members Dr. Andriy Anishkin, Lena Shirinian, Bradley Akitake, Dr. Kishore Kamaraju, Dr. Grzegorz Jezierski, and visiting scholar Dr. Yuri Ermakov, and Lois Reid at the Biology Department for their help and encouragement that made my stay pleasant in College Park. I especially appreciate Dr. Anishkin, Monica, Slava and Lena who contributed their work to my dissertation.

I also want to show my love and respect for brothers and sisters in my church cell group who give me their prayers, affection and care in their special ways. To my beloved, supporter, listener, and discerning wife, Yin-Ying, I could not finish this study without your understanding.

I thank God the most. I thank you for your salvation and giving me grace in this journey.

# TABLE OF CONTENTS

# LIST OF TABLES

# LIST OF FIGURES

# LIST OF ABBREVIATION

| | |
|---|---|
| DTT | dithiothreitol |
| EDTA | ethylene diamine tetraacetic acid |
| GOF | gain-of-function |
| HEPES | N-[2-hydroxyethyl] piperazine-N'-[2-ethanesulfonic acid] |
| IPTG | isopropyl-β-D-thiogalactopyranoside |
| LB | Luria-Bertani medium |
| ME | β-mercaptoethanol |
| MLB | modified Luria-Bertani medium |
| NEM | N-ethylmaleimide |
| PAGE | polyacrylamide gel electrophoresis |
| PCR | polymerase chain reaction |
| SDS | sodium dodecyl sulfate |

# GENERAL INTRODUCTION

Mechanosensation involves a wide range of physiological processes critical for survival of many organisms. We can sense a light touch or pinch applied to the skin, and feel the size and the shape of an object as well as the texture of its surface. We discriminate subtle differences in sounds, as evident from our ability to understand speech, or enjoy music. Somatosensory fibers in tissues, specialized mechanosensory endings underneath the skin and delicate arrays of hair cells in the cochlea are the receptor cells that implement mechanotransduction (Smith, 2000). Non-sensory somatic cells are capable of responding to mechanical challenges as well. Blood flowing through an artery, air passing through the airways, body fluid filtered through the kidney, and movement of a meal through the intestine, all exert pressure and shear force on the lining of tubular structures formed by non-sensory somatic cells. Moreover, the tension or relaxation of the body's musculature as well as joint positions, though controlled unconsciously, is permanently monitored to control the static orientation and movements of our body, the function collectively named proprioception (Smith, 2000). Humans are capable of perceiving an extremely wide range of the mechanical stimuli. It is peculiar that the sensitivity of hair cells is at the level of thermal energy, and due to the special signal integration scheme we can discern sounds even through the 'roar' of Brownian motion (Hudspeth, 1997). Despite of the decades of intensive research on various mechanosensory systems and large amount of data, the actual molecules responsible for mechanosensation and the way they convert force into biological responses remains largely unknown. While 'slow' responses to force such as tissue remodeling are ascribed to signaling through integrin cell adhesion complexes (Ingber, 2003), it is commonly

accepted that ion channels directly activated by mechanical tension mediate 'fast' mechanosensation in most instances (Hamill and Martinac, 2001).

The patch-clamp recording technique (Hamill et al., 1981) made it possible to resolve ion conduction events at a single-molecule level in membranes of practically any cell. This led to the discovery of the first mechanosensitive (MS) ion channels in the skeletal muscle of chick embryo (Guharay and Sachs, 1984), and latter MS channels had been documented in more than 30 types of cells (Sackin 1995), including yeast (Gustin et al., 1988) and bacteria (Martinac et al., 1987; Zoratti and Petronilli, 1988; Sukharev et al., 1993). Most of these channels, however, have proved difficult to purify because channels are not expressed at high levels within individual cells and agonists/and antagonists that specifically bind with high affinity to mechanically gated channels were unavailable. Nonetheless, *Escherichia coli* MS channels are preciously exceptional. They can be extracted from the bacterial membranes by solubilization in a detergent, and functionally reconstituted in liposomes amenable to patch-clamp recording (Sukharev et al., 1993). Using patch clamping of reconstituted fractions as an assay for the presence of mechanosensitive channels, the large conductance (MscL) channel protein of *E. coli* was enriched and gel-purified. The partial sequence of the protein soon led to the cloning of the *mscL* gene (Sukharev et al., 1994).

The use of the forward genetics proved to be a powerful means in identifying molecular players involved in mechanosensation. Progress has been accelerated through the use of genetic screens in the nematode *Caenorhabditis elegans*, *Drosophila* fruit flies, and zebrafish *Danio rerio* (Ernstrom and Chalfie, 2002). Several eukaryotic candidate MS ion channels were identified by this approach. In addition, analysis of inherited

deafness or other diseases in humans also promises to lead to identify molecules which mediate mechanosensation in vertebrates (Ernstrom and Chalfie, 2002).

**Multiplicity of MS channels**

MS ion channels are structurally diverse. They have been discovered in all three fundamental branches of the phylogenic tree, Bacteria, Archaea and Eukarya. MS channels found in distant groups of eukaryotic organisms include the DEG/ENaC family, TRP family, and mammalian two-pore $K^+$ channels. The DEG/ENaC family is named after the first two sub-families identified: degenerins, the *C. elegans* genes that in their mutant form cause cell swelling and degeneration (Driscoll and Chalfie, 1991) and ENaCs, subunits of vertebrate epithelial amiloride-sensitive $Na^+$ channel (Canessa et al, 1993, 1994). The TRP family is named for the first member identified: a *Drosophila* protein needed for sustained photoreceptor response, encoded by the *trp* (*transient receptor potential*) locus (Cosens & Manning, 1969; Minke et al., 1975). In prokaryotes, MS channels were first documented in bacteria (Martinac et al., 1987; Zoratti and Petronilli, 1990; Sukharev et al., 1993), followed by their discovery in Archaea (Le Dain et al., 1998). Members of main eukaryotic channel families required for sensation of mechanical stimuli are briefly introduced below.

***DEG/ENaC family*** Genetic analysis of *C. elegans* has identified approximately 18 mutated *mec* genes (mechanosensory abnormal), which specifically disrupt gentle lateral and posterior body touch sensation and, therefore, encode candidate mediators of touch sensitivity. Two degenerin-like genes, *mec*-4 and *mec*-10, were postulated as candidates for MS channel (Driscoll and Chalfie, 1991; Huang and Chalfie, 1994). MEC-4 and

MEC-10 proteins with two putative transmembrane domains are likely to work as parts of intricate protein machines, anchored on both sides of the membrane to structural elements of the cytoskeleton and extracellular matrix (Ernstrom and Chalfie, 2002). Co-expression in *Xenopus* oocytes demonstrated that mutated MEC-4 and MEC-10 subunits with other associated MEC proteins form the $Na^+$-specific ion channel (Goodman et al., 2002; Chelur et al., 2002).

ENaCs and ASICs (for acid-sensitive ion channels) are the subfamilies found exclusively in vertebrates (Kellenberger and Schild, 2002). While the epithelial αβγ ENaC is expressed in the kidney, the channels containing β and γ subunits of ENaC, but not α, were detected in mechanosensory neurons of the dorsal root ganglia (DRG) and several sites of mechanosensation: rat paw (Drummond et al., 2000), trigeminal sensory neurons (Fricke et al., 2000), and arterial baroreceptor nerve endings (Drummond et al., 1998). ASIC2a and ASIC3 are co-expressed in DRG and cutaneous mechanoreceptors as well (Alvarez de la Rosa et al., 2002; Price et al., 2000; Garcia-Anoveros et al., 2001). They form heteromultimeric channels (Alvarez de la Rosa et al., 2002), and the knockouts display compromised skin mechanosensation (Price et al., 2000; 2001). *Drosophila* genome also encodes 24 DEG/ENaC proteins (Goodman and Schwarz, 2003). Only 2 of them have been characterized so far. One of them is called Pickpocket (PPK or dmdNaC1) (Adams et al., 1998; Darboux et al., 1998). PPK displays limited expression in multiple dendritic sensory neurons titling the body wall of late-stage embryos and early larvae, which was thought to play a role in touch sensation (Adams et al., 1998). Further knockout studies suggest an essential role of PPK in mechanosensory

signal transduction of proprioceptive sensory information from individual larval segments (Ainsley et al., 2003).

***Trp* family** In *C. elegans*, none of the genes required for lateral body touch cell function (eg. MEC-4 and MEC-10) have been implicated in nose touch sensitivity. The osm-9 gene responsible for nose touch sensation was then found through positional cloning (Colbert et al., 1997). It encodes a protein with six putative transmembrane domains and, phylogenetically, falls in the TRPV (V for vanilloid) branches of the TRP superfamily. Subsequently, four additional OSM-9 family members were identified and named OSM-9/capsaicin receptor-related proteins (OCR-1 to OCR-4) (Tobin et al., 2002). The combined expression of OSM-9 with OCR-2 in defined neurons of *C. elegans* is necessary for numerous sensory functions, including mechanosensation (nose touch), olfaction, and osmosensation (avoidance of high osmolarity) (Tobin et al., 2002). The vertebrate homolog of OSM-9, TRPV4, that senses osmolarity or other mechanical stimuli has been cloned recently (Strotmann et al., 2000; Liedtke et al., 2000; Wissenbach et al., 2000; Delany et al, 2001). It is expressed at high levels in the kidney, liver and heart (Strotmann et al., 2000), and also found in inner-ear cells, Merkel cell and neurons of the circumventricular organs in the brain that sense systemic osmotic pressure (Liedtke et al., 2000). The mice lacking TRPV4 gene showed a markedly reduced sensitivity of the tail (Suzuki et al., 2003) and compromised ability to regulate blood osmolarity (Liedtke et al., 2003), which are compatible with a role of TRPV4 in mechanosensation and osmoregulation. TRPV4 is also activated by various physical and chemical stimuli, such as heat (~above $35^{o}$ C), phorbols and endogenous ligands, which are able to induce $Ca^{2+}$ entry (Nilius et al., 2003). Understanding the function of TRPV4 has become more

complicated due to its multimodal behavior and the uncertainty as to what is the primary stimulus for gating.

Homology searches with *Drosophila* genome identified two additional genes that fall within the TRPV channel family: CG4536 and CG5842 (Tobin et al., 2002; Littletom and Ganetzky, 2000). CG4536 is most closely related to the nematode OSM-9 and CG5842 is an ortholog of nematode OCR. The CG5842 channel-named Nanchung or Nan is osmosensitive (Kim et al., 2003). An antibody to Nan labeled the ciliated endings of chordotonal neurons in Johnston's organ, the ear of the fly. In behavioral tests, Nan mutants completely lacked antennal sound-evoked potentials, demonstrating that Nan is an essential element for the auditory mechanotransduction in *Drosophila* (Kim et al., 2003).

A classical mutant screen in *Drosophila* produced another TRP channel needed for mechanosensation. The *Drosophila* nompC (for no mechanoreceptor potential) encodes an unusual TRP channel with 29 ankyrin repeats preceding the transmembrane domains (Walker et al., 2000). NOMPC is sufficiently different; thus, it defines a new branch of the TRP superfamily: the TRPNs. The nompC gene is expressed specifically in mechanosensory neurons underneath the bristles and chordotonal organs in fly. The nompC mutants show loss of almost all transduction current (~90%) examined from individual bristles, suggesting that NOMPC likely serves as a mechanosensory transduction channel in tactile bristal response of *Drosophila*. However, nompC mutants show only partially compromised fly hearing (Walker et al., 2000), suggesting the products play a modulatory role in fly hearing. Using the fly nompC sequence to search the zebrafish genome, Sidi et al. (2003) isolated a cDNA that encodes a vertebrate

NOMPC. In situ hybridization showed nompC in the hair cells of the larval zebrafish inner ear. Fish larvae were deaf and exhibited circular swimming behavior consistent with a vestibular defect, when the zebrafish embryos were injected with antisense oligonucleotides (Sidi et al., 2003). The evidence indicates that NOMPC is necessary for hair cell transduction in zebrafish. However, there is as yet no trace of an ortholog of either NOMPC or Nanchung in human beings. What might be the transduction channel in human hair cells is still a mystery.

***Mammalian two-pore $K^+$ channels*** The two-pore types mammalian $K^+$ channels with four transmembrane domains include TREK (TWIK-1 related $K^+$ channel, TWIK-1 for tandem of P domains in a weak inward rectifying $K^{\pm}$ channel) and TRAAK (TWIK-1 related arachidonic acid-stimulated $K^{\pm}$ channel). Human TREK-1, TREK-2 and TRAAK are consistently found in the brain and believed to be part of the leakage channel pool responsible for maintaining the resting potential in neurons (Patel and Honore, 2001). They appear to sense membrane tension directly and function as mechano-gated channels when transiently expressed in COS cells (green monkey kidney cell line) and *Xenopus* oocytes. However, the cytoskeleton could act as a repressor of channel activity and allow a dynamic tuning of the stretch sensitivity of the channels as examined in the case of TRAAK (Maingret et al., 1999). Similar to TRPV4, two-pore $K^+$ channels show a multimodal behavior, when channel activity can be elicited not only by mechanical stimuli, including osmotic stress and membrane stretch, but also by decreased intracellular pH, temperature, or cAMP-dependent phosphorylation (Patel et al., 2001).

A summary of cloned channels involved in mechano- and osmosensation that belong to several unrelated families with different membrane topology is presented in

Table I-1. It is intriguing that MS channels from unrelated families can be employed in different parts of the same organism. Even a simple prokaryote *E. coli* is equipped with at least three types of MS channels: the mechanosensitive channels of mini conductance (MscM), small conductance (MscS) and large conductance (MscL). Two known MS proteins in bacteria, MscS and MscL, belong to two distinct families with no homology or structural similarity (Pivetti et al., 2003). In the nematode *C. elegans*, members of DEG/ENaC and Trp protein family are involved in mechanosensory perception in two separate anatomical zones, in the lateral-posterior area and in the nose. In *Drosophila*, Trp-type channels, NOMPC and Nanchung, are found in external sensory organs, whereas internal multidendritic sensory neurons employ the DEG/ENaC channel PPK. A more complicated picture unfolds in mammals. TRPV4 is implicated in the osmosensory function in most cells, whereas polycystins (PKD1 and PKD2), representing a subfamily within the TRP family, are required for the fluid flow-induced mechanotransduction by the primary cilia in the kidney epithelium (Nauli et al., 2003). ENaC subunits are located in baroreceptor nerve endings and can be involved in detecting vessel stretch, while its relatives, ASICs, are believed to play a critical role in cutaneous sensation. Additionally, mammalian TREK channels are proposed to carry out osmoprotective function in nerve systems (Patel and Honore, 2001), whereas a splice-variant of calcium-dependent big conductance $K^+$ channel ($K^+_{Ca}$, maxiK, BK) can be responsible for MS channel activities in the heart (Tang et al., 2003).

**Table I-1.** Families of channels and their mechanosensitive representatives (excerpt from Sukharev and Anishkin, 2004, with modification)

| Family | MS channel species | Organism/location |
|---|---|---|
| **DEG/ENaC** (2 TM) | Mec-4, Mec-10 | *C. elegans,* lateral and posterior touch neurons [Driscoll and Chalfie, 1991; Huang and Chalfie, 1994] |
| | ASIC(1-4) | Multiple isoforms in the mammalian NS. Best characterized in sensory neurons and endings [Krishtal, 2003] |
| | ENaC | Vertebrate transporting epithelia. β and γ subunits are found in DRG neurons, aortic baroreceptors and cutaneous sensory organs [Welsh et al., 2002] |
| | PPK | Multiple dendritic neurons of Drosophila. Implicated in proprioception [Adams et al., 1998]. |
| **TRP** (usually 6TM) | Osm-9, Ocr-2 | Ciliated endings of anterior polymodal sensory neurons of *C. elegans* [Colbert et al.,1997; Tobin et al., 2002] |
| | TRPV4 | Mammalian osmosensitive channel, widely expressed, especially in epithelial tissues [Liedke et al., 2000] |
| | nanchung | *Drosophila* ortholog of Ocr channels, expressed in chondrotonal auditory organs [Kim et al., 2003]. |
| | NompC | *Drosophila* bristle mechanoreceptors [Walker et al., 2000], zebrafish otic hair cells [Sidi et al., 2003] |
| | polycystins 1 and 2 | PKD1 and 2 are coexpressed in the primary cilium of the mammalian kidney epithelium [Nauli et al., 2003], sensory neurons in male copulatory organs of *C. elegans* [Barr and Sternberg, 1999] |
| | Yvc1p | Stretch-activated channel from yeast vacuole [Zhou et al., 2003] |
| **$K^+_{Ca}$** channel (7TM) | $SAC_{Ca}$ | K+-specific MS current in the heart [Tang et al, 2003] |
| **Kir**-inward rectifiers (2TM) | $K_{ATP}$<br>$K_{ACH}$ | Mechanically-modulated $K^+$-currents in the heart [measured from native tissues, Van Wagoner, 1993; Pleumsamran and Kim, 1995] |
| **Two-pore $K^+$** channels (4TM) | TREK (1,2), TRAAK | Polymodal $K^+$ channels in mammalian CNS activated by stretch, unsaturated fatty acids and low pH [Patel and Honore, 2002] |
| **MscS** (yggB) (3TM) | MscS,<br>MscK | Stretch-activated efflux channels in the inner membrane of *E. coli* [Levina et al., 1999] Homologs found in most bacteria, archaea, fission yeast *Schizosaccharomyces pombe* and plant *Arabidopsis. thaliana* [Pivetti et al., 2003]. |
| **MscL** (2TM) | MscL | Stretch-activated osmotic release valve in the inner membrane of *E. coli* [Sukharev et al. 1994]. Orthologs in most free-living bacteria. One distant homolog found in the fungus *Neurospora crassa* [Pivetti et al., 2003] |
| **Archaeal MSCs** (various) | MscTA<br>MscMJ | channels from *Thermoplasma acidophilium* and *Methanococcus jannashii* with a loose homology to MscL [Kloda and Martinac, 2001] |

**Models of MS channel gating**

There are two main hypotheses about how an external force may activate mechanosensitive ion channels (Hamill and Martinac, 2001). In the first type, two-dimensional tension within the lipid bilayer could directly activate the channel. Reconstitution of purified bacterial channel proteins in liposomes yields functional MS channels. This has been demonstrated with *E. coli* stretch-activated channels such as MscS (Sukharev, 2002), MscL (Hase et al., 1995; Blount et al., 1996), and the archaeal MS channels (Kloda and Martinac, 2001). In the second (tethered) model, the channel is attached to the cytoskeleton and/or the extracellular matrix. Through movements or distortions of such scaffolds the stress is transmitted and focused at the channel gate. Although the biochemical identification of the different elements of this system has proven difficult, genetic data in *C. elegans,* although indirect, strongly favors this model. In addition, a potential mechanism by which a channel indirectly responds to mechanical stimuli may exist. For instance, opening of MscS in a spheroplast by osmotic swelling was shown to be almost instantaneous (Cui and Adler, 1996). However, an attempt to activate TRPV4 expressed in human embryonic kidney cells by osmotic swelling showed a delayed activation of the current (tens of seconds), leaving some doubt of whether TRPV4 is directly activated by mechanical stimuli (Strotmann et al., 2000). Latest experiments done by Vriens et al., (2003) suggest that mechanosensation could involve a release of TRPV4-activating messenger, 5', 6'-epoxyeicosatrienoic acid (5', 6'-EET), that may in turn open TRPV4. Thus, in response to mechanical stimuli, activators might be released from a mechanosensitive cell itself or an associated cell, triggering a paracrine reaction leading to channel activation.

**Why bacterial MS channels are good model systems?**

Research in the past years has produced many new candidates for eukaryotic mechano-gated ion channels as described above. However most eukaryotic mechanosensory systems are complex and the function of mechanically-gated channels is usually inferred from genetic data, cellular/tissue localization of proteins, and functional manifestations in the mutant or knockout animals. In general, the evidence for the mechano-activated channel function remains mostly circumstantial and a heterologous expression combined with electrophysiological examination does not always give a definitive answer about the character of channel gating, or in some instances is simply impossible. Mechanosensory cells are not always easily accessible with a glass electrode (such as the touch neurons under the cuticle of *C. elegans*). Moreover, many eukaryotic candidate mechanosensors are presumed to form multi-component protein complexes. Elaborate protein-protein interactions are not easy to reconstitute in a heterologous system and obtain functional expression. So far, the gating mechanisms of putative eukaryotic mechanosensitive ion channels remain largely unknown.

Bacterial MS channels became good models for mechanistic biophysical studies as they provide a 'simpler' alternative to complex vertebrate systems. They have several advantages. First, the genes for the two main types of MS channels in *E. coli* have been cloned and their products re-expressed (Sukharev et al., 1994; Levina et al., 1999). The bacterial MS proteins survive purification from detergent extracts and reconstitution into liposomes (Sukharev et al., 1993), permitting *in vitro* studies. Second, they were shown to gate just by tension in the lipid bilayer with no requirement of any additional elements (Blount et al., 1996a; Sukharev et al., 2002), making them 'simple' molecular models for

studies of primary events in mechanosensory transduction. Third, the small gene size of MscL (0.4 kb) and MscS (0.8 kb) allows exhaustive *in vitro* mutagenesis to study the structure -function relationships. Fourth, it permits random mutagenesis (as was done for *mscL* and *mscS*), expression of mutagenized libraries in knock-out strains followed by functional screens for loss- or gain-of-function phenotypes (Ou et al., 1998). Fifth, the channel can be studied directly with the patch-clamp technique since the technology of patch-clamping bacteria has been developed (Martinac et al., 1987) and multiple mutants as well as complete *mscL and mscS* knock-out strains (Blount et al, 1996a; Levina et al.,1999) are now available. Preparation of giant spheroplasts with over-expressed mutated bacterial MS proteins is now relatively simple and permits straightforward functional examination of mutant channels. Sixth, the conductance of the channels is exceptionally large, of 1nS for MscS and 3.2 nS for MscL (when measured in the standard recording solution: 200mM KCl, 90 $MgCl_2$, 10 $CaCl_2$, pH 6), thus permitting high signal-to-noise ratio and good time resolution. The discrete subconductance states are distinguishable in both MscL and MscS at a fast recording, allowing an easy access to their occupancies and further extraction for physical parameters for transitions between different states. Seventh, recent advances in structural biology have provided crystallographic snapshots of MscL from *Mycobacterium tuberculosis* (Chang et al., 1998) and MscS from *E. coli* (Bass et al., 2002). Molecular dynamics (MD) simulations can be performed based on the known MS tertiary structures providing insight to the conformational dynamics of the MS channels when they are simulated in a lipid membrane. Finally, more than 35 MscL and 40 MscS homologs (Maurer & Dougherty, 2001; Pivetti et al., 2003) from different types of bacteria have been cloned and

sequenced to date, permitting identification of conserved regions and homology modeling. The proposed homology models could be examined by designed experiments or simulated by molecular dynamics. Thus, bacterial MS channels represent excellent model systems for understanding how a mechanosensitive ion channel may work.

**MscL as 'simple' model**

The large conductance mechanosensitive channel MscL, first identified in *E. coli* (Sukharev et al., 1994), appears to be a ubiquitous component of cell envelopes of essentially all free-living bacteria. Together with MscS, it acts as an osmolyte "safety release" system activated under hypoosmotic shock (Blount et al., 1997, Levina et.al., 1999). The 136 amino acid EcoMscL protein has two identifiable transmembrane (TM) domains (M1 and M2). This was confirmed by biochemical studies of the MscL membrane topology (Blount et al., 1996a), which also showed that the loop connecting the two TM domains is in the periplasm, whereas both $NH_2$ and COOH termini are cytoplasmic (Fig. I-1). The EcoMscL complex has been proposed to function as a homopentamer (Sukharev et al., 1999a).

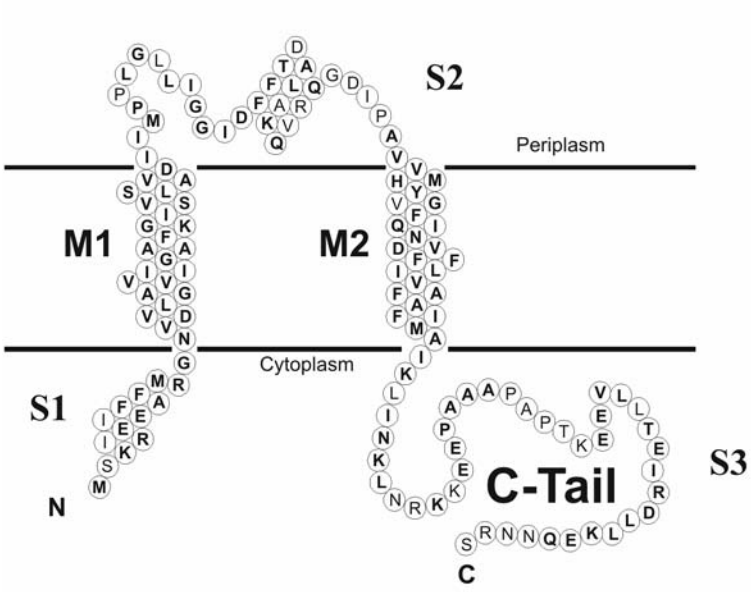


**Figure I-1.** Amino acid sequence and membrane topology of the EcoMscL subunit peptide (Blount et al., 1996b).

***Thermodynamics and kinetics of Eco*MscL** Based on the unitary conductance and assumed pore length, the open pore diameter for EcoMscL has been estimated as ~30 Å (Cruickshank et al. 1997; Sukharev et al., 1999b). Attempts of sieving measurements on MscL using larger organic molecules suggested the pore diameter of about 40 Å (Cruickshank et al. 1997). This implies a very large-scale conformational transition from the closed to the open state. MscL also requires extremely high tension for activation with the midpoint $T_{1/2}$ at 11.8 dynes/cm when reconstituted in liposomes (Sukharev et al., 1999b). The initial measurements of the slope of the dose-response curves (open probability versus tension) of EcoMscL reconstituted in azolectin liposomes estimated the entire protein expansion as 6.5 $nm^2$ (Sukharev et al. 1999b), which was somewhat small taking into account that the cross-sectional area of the conducting pore should be as large as 10 $nm^2$. A two-state kinetic analysis of traces obtained in liposome-reconstituted patches demonstrates that the rate constant for the forward transition (close-to-open, $K_{on}$) has 2.5 times steeper tension dependence than the rate constant for the backward transition (open-to-close, $K_{off}$). This means that the energy barrier is positioned closer to the open state on the reaction coordinate $\Delta A$, and thus the channel must be pre-expanded to a large extent in the transition state before reaching the open state. Time-resolved recordings have shown that EcoMscL is not a binary channel, but has at least four open conducting states and a closed state. It has been shown that the rate constants for the upper subconducting states are essentially tension-independent, indicating that a substantial conductance increase (S1-O) (80%) occurs with a relatively small (30% of total) change in the cross-sectional area of the protein (Fig. I-2A) (Sukharev et al., 1999b). A cartoon shown in Fig. I-2B illustrates the relative change of channel

dimensions during the gating. The proposed two-gate mechanism will be discussed below.

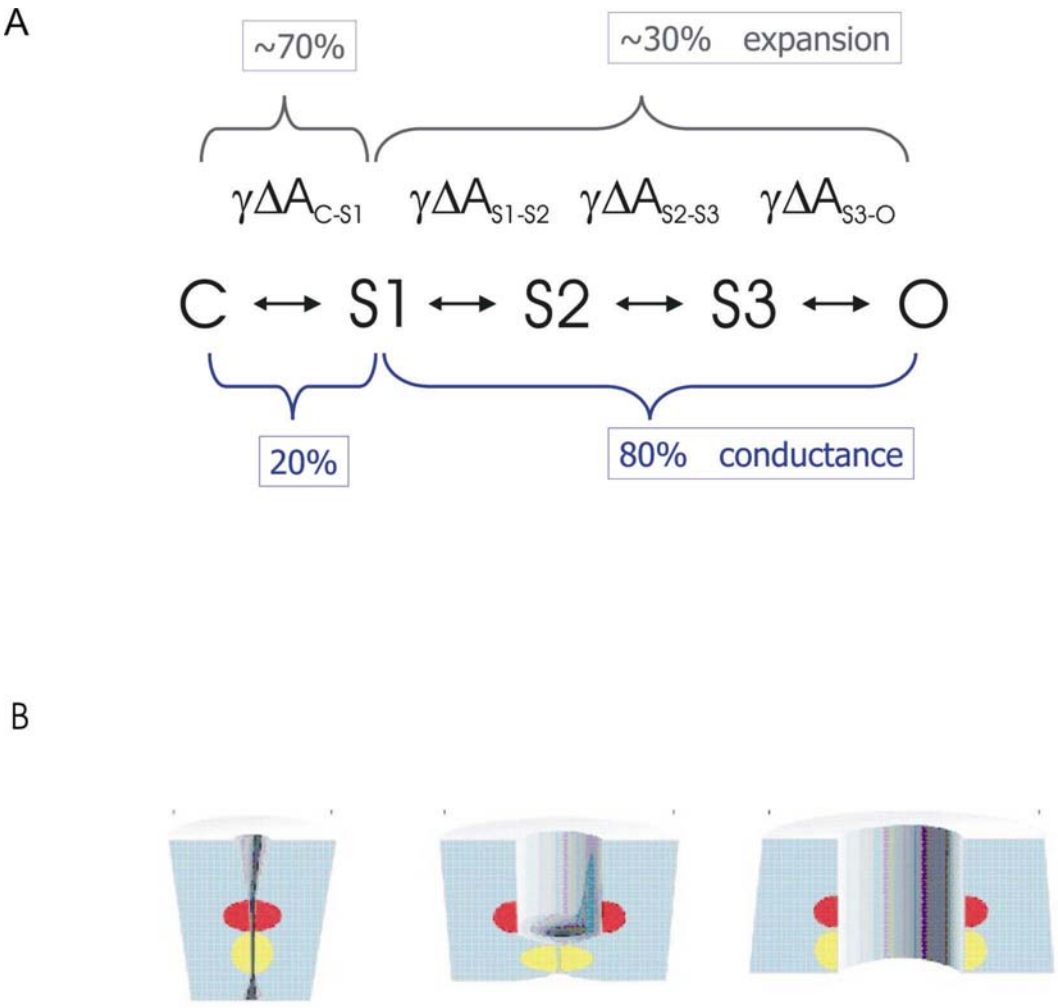


**Figure I-2** (A) Comparison of conductances and in-plane area changes between the closed state, low subconducting state S1 and the open state. (B) Cartoon models depict relative changes of channel dimensions in closed, low-conductance expanded and open states. The two gates proposed in the model are highlighted: the hydrophobic central gate (red) and the cytoplasmic gate (yellow).

***Gain-of-function mutations*** Much information from the molecular dissection of *E. coli* MscL channels by in-vitro mutagenesis (reverse genetics) has been carried out following the discovery of MscL gene. Many papers describe the effects of deletion and substitution mutations (see review by Sukharev et al., 1997, Oakley et al., 1999) and proteolysis (Ajouz et al., 2000) on gating pressure and kinetics. To determine functionally important residues in the most unbiased way, Ou et al. (1998) performed forward genetics. The approach included saturating random mutagenesis followed by screens for mutations that inhibit the growth of host bacteria. The presumption was that mutations in the gate region can make the channel leaky or opened at a significantly lower tension threshold, thus making the mutant channel toxic for the host cell. This allowed isolation of numerous gain-of-function mutants (GOF). Expression of such mutant channels caused leakage of cytoplasmic solutes, especially $K^+$, even when subjected to a slight hypo-osmotic shock. In excised patches, the mutant channels gated at membrane tensions that were less than that required for gating of the wild-type MscL. Surprisingly, most of the identified GOF mutations were clustered in the cytoplasmic half of the M1 domain. The most severe mutations are substitutions of small or hydrophobic amino acids with hydrophilic and especially charged ones (G22N, G22D, V23D, G26S, and G30R). Systematic changes of G22 to every other amino acid showed that the threshold for MscL activation is proportional to the hydrophobicity of the substitute (Yoshimura et al. 1999). Systematically placing charges in at position 22 (G22S) by using methanethiosulfonate reagents (Yoshimura et al. 2001) indeed cause the channel to open at low stretch force. These experiments gave the first idea where the channel gate might be. MscL opening entails breaking the hydrophobic interactions at this region and water is probably

excluded from the hydrophobic constriction of the closed MscL, but increased hydration of this region due to hydrophilic substitutions strongly destabilizes the closed state. One of GOF mutants, G22N, fluctuated mainly between the closed and the substate without full opening in the absence of suction. The occupancy of the low substate attained saturation at relatively low pressures, whereas the further transition to the fully open state required much higher pressure (Yoshimura et al., 1999). This separation of the first and second transitions attracted my attention and the detailed analysis of this type of gating in G22N and other GOF mutants presented below became one of the most clear illustrations of the sequential action of two gates in MscL.

***Structure of TbMscL.*** The crystal structure of the MscL homologue from *M. tuberculosis* (TbMscL) has been determined to a 3.5Å resolution in what is proposed to be the closed conformation (Chang et al., 1998). The TbMscL structure is a pentamer with the loop between the transmembrane domains of each subunit (TM1 and TM2), extending out of the membrane into the periplasm. The TM1 helix crosses the membrane with its N-terminus on the cytoplasmic side and creates the bulk of the pore. The loop connecting TM1 and TM2, without a distinctive secondary structure, creates a flap on the extracellular surface and dips into the pore region. Connected to the pore loop, the TM2 helix crosses the membrane and projects into the cytoplasm along the outside of the channel. All transmembrane helices of each subunit are tilted with the five TM1 helices coming together at their cytoplasmic ends. Thus, the closed channel looks like a funnel, extending outward above the membrane on the periplasmic side and narrowing at the cytoplasmic end. A number of polar residues lining the TM1s, including four threonines, lysine and aspartate, forms the ion-conduction pathway of the funnel. Two hydrophobic

residues, isoleucine 14 and valine 21 of each TM1 create the tight constriction of the channel at the cytoplasmic end, approximately 2 Å in diameter. This narrowest part of the channel has been proposed to function as the gate since the side-chain rings of these two hydrophobic residues protrude into the pore likely providing a hydrophobic barrier to ion permeation.

***Gating models.*** Based on the TbMscL crystal structure and studies of GOF mutants, early models postulated that tension first breaks the hydrophobic gate and straightens all TM helices up into a barrel-stave structure such that all 10 helices line the pore throughout the transmembrane region (Spencer et al., 1999, Batiza et al., 1999). The model of the closed conformation of EcoMscL is presented in Fig. 1.3 (center) with the barrel-stave model of the open state on the left. The detailed analysis of this model has shown that the hydrophobic cytoplasmic part of M2 helix can hardly be exposed to water, making the barrel-stave (10-helix) arrangement of the pore highly unlikely (Sukharev et al., 2001). A more plausible scenario suggests that pore opening takes place through an iris-like movement of M1 helices sliding one along another, leading to their separation at the constriction site (Fig. 1.3, right). This type of helical movement involves much larger expansion accompanied with a substantial flattening of the entire channel complex. In the fully open and intermediate expanded states the pore is lined mostly by the tilted M1 helices bearing a polar face, whereas M2 helices remain on the periphery facing the lipid.

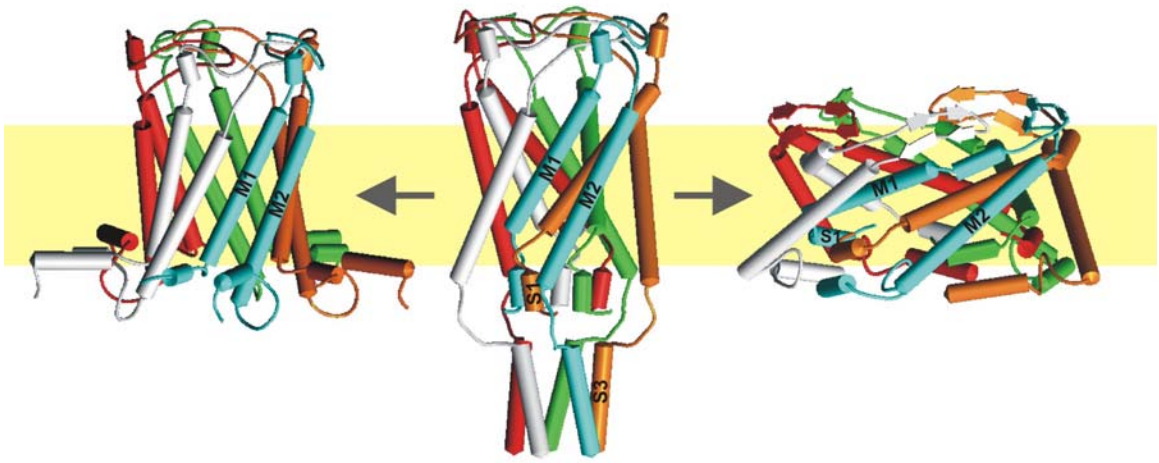


**Figure I-3.** Cartoon representations of the closed structure (middle) of *E. Coli* MscL that undergoes two possible gating pathways as viewed from the side in the plane of the membrane (yellow area). Each subunit shows different colors for clarity. Two possible open conformations are shown: a barrel-stave structure in which 10 membrane-spanning helixes form the conductive pore (left) and the tilted structure in which only 5 TM1 helices line the pore (right). These early models propose separation of cytoplasmic S3 domains, however, as will be described in Chapter 1, these domains more likely remain stably associated in all conformations.

The existence of a low conductive or silent pre-expanded state implies that the channel has an internal gate, which occludes the conductive pathway in the intermediate state. The conserved N-termini domain, which was unsolved in TbMscL, was hypothesized to be the second, cytoplasmic gate (Fig. I-2 B). The collaborative work of Dr. Sukharev and Dr. Guy resulted in a homology model of EcoMscL built after the crystal structure of TbMscL. It was also possible to model the gating transitions for each of these channels by introducing small translational and angular displacements to the helices that allowed to arrive from the fully closed to fully open conformation (Sukharev et al., 2001). It should be noted that EcoMscL turned out to be a much better object for experimental examination. The observed high activation threshold of TbMscL, especially when the channel is expressed in *E. coli* (Moe et al., 2000), makes it very difficult to work with.

This "tilting" mechanism of MscL gating transition appears to be more realistic and its general predictions can be summarized as follows: (1) the entire channel complex undergoes a large iris-like expansion, transforming from a tall and narrow to a short and wide conformation and essentially only M1 (not M2) is forming the pore lining in the open conformation; (2) M1 and M2 helices are likely to undergo a concerted tilting motion without changing their relative positions substantially; (3) the transition from the fully closed to the pre-expanded low-conducting state is likely to be accompanied by a full hydration of the pore; (4) the transition from the low-conducting pre-expanded state to the fully open state occurs after the separation of the hypothetical S1 bundle under tension transmitted via the S1-M1 linkers from the channel barrel. Validation of these modeling predictions comprises the specific aims of my thesis.

**Specific aims and the organization of the Thesis**

**(1) To test the stereochemical aspect of the gating mechanism of EcoMscL.** The above 'tilting' models of the EcoMscL gating transition represent a working hypothesis that was generated using subjective computational methods of molecular modeling. Whether or not the proposed mechanism is correct, this has to be tested in experiments. The model predicts the proximities between specific residues in either the closed or open conformations thus making the system amenable to the disulfide trapping approach. The predictions specify relative positions of transmembrane helices in the closed and open conformations as well as positions of N- and C-terminal exramembranous domains. The **first chapter** describes the experiments performed using the disulfide cross-linking technique in combination with patch-clamping. The results generally support the tilting model.

**(2) To assess the spatial scale of the gating transition of EcoMscL *in situ.*** To satisfy the ~3 nm open pore diameter, a large conformation change should take place during the gating transition. The model predicts that M1 helix of one subunit remains in a close apposition to the M2 helix of the adjacent subunit throughout the gating process, and both helices tilt together by about $40^{o}$ and move outward by at least 1.2 nm. The average increase in cross-sectional area of the protein complex can be estimated as 23 $nm^2$. However, in the initial characterization of EcoMscL reconstituted in azolectin liposomes (Sukharev et al. 1999b), the slope of the open state occupancy with tension estimated the protein expansion as only 6.5 $nm^2$, which is quite different from the model prediction. In an effort to reconcile this discrepancy, in the **second chapter** I describe the assessment of the spatial scale and gross energetics of EcoMscL conformational transition *in situ,* which

was performed by examining single-channel currents and dose-response curves recorded from channel populations in giant spheroplasts.

**(3) Examination of the energetic and spatial parameters of GOF mutations.** GOF channels, which carry hydrophilic or charged substitutions in the hydrophobic pore constriction (cytoplasmic half of M1 helix), are gated at membrane tension that are less than that required for the gating of the wild-type MscL and *E. coli* harboring GOF mutations show growth impairment (Ou et al., 1998). Many of GOF mutants, V23D, G22N, display two-step opening, first between the closed state and the substate, and then at higher tensions, between the substate and fully open state. Analysis of easily openable "gain-of-function" mutants with pronounced subconducting states may provide invaluable information about the sequence of events along the transition pathway. In **chapter three**, I systematically examine the energy requirement, the in-plane area changes and the positions of activation barriers for mild (V23T) and severe (G22N and V23D) GOF mutants of MscL. The observed parameters are consistent with the hypothesis that the primary (M1) gate opens first. This step is associated with a large pore expansion and corresponds to the moments of full hydration of the pore interior favored by hydrophilic substitutions. This first step is followed by the separation of cytoplasmic S1 gate associated with a smaller barrel expansion. In our gating model, the flexible linkers ($^{13}R^{14}G^{15}N$) connecting S1 to M1 helices are the main force-transmitting elements between the barrel and the secondary (S1) gate. To verify the role of S1-M1 linkers, linker extension mutants, GG14 and GAG14, were generated and their gating patterns were recorded. The results uphold their tension-transmitting role during the gating transition.

# MATERIALS AND METHODS

## Mutagenesis

Cysteine substitutions were introduced by the 'megaprimer' mutagenesis technique involving two rounds of PCR, as described in Yoshimura et al. (1999). Wild type *mscL* cloned into the pB10b vector as a BglII-XhoI fragment was used as a primary template. Mutations were verified by automated sequencing. The same pB10b vector containing $P_{UVlac}$ promoter was used to express all mutants in either PB104 *mscL*$^-$ cells (Blount et al, 1996a) for patch-clamp analysis, or in MJF455 *mscL*-, *mscS*$^-$ cells (Levina et al., 1999) for biochemical cross-linking experiments. Severe gain-of-function mutants V23D and G22N (Ou et al., 1998) were gifts from Dr. Ching Kung (University of Wisconsin-Madison).

## Disulfide cross-linking experiments

Iodine ($I_2$) was used as an oxidant in all cysteine cross-linking experiments as described by Pakula and Simon (1992). Depending on the setting, the concentration of Iodine was varied between 0.025 and 0.5 mM. To trap the protein in the putative closed conformation, the expressed cells grown in regular Luria-Bertani (LB) medium were induced with Isopropyl-B-D-thiogalactopyranoside (IPTG) (Research products International, Mt. Propsect, IL), harvested and French-pressed. Membranes were collected and subjected to 0.2 mM $I_2$ for 5 min. The reactions were terminated by washing $I_2$ out with 5-min incubation with 5 mM N-ethylmaleimide (NEM) to block free cysteines. The non-reducing SDS sample buffer contained 0.2 M iodoacetate. The cross-linking products were separated in a non-reducing SDS-PAGE and visualized on western

blots with antibodies against the C-terminal domain of MscL (Blount et al., 1996a). The expanded/open conformations were trapped by shocking cells osmotically in the presence of the oxidant. MJF455 expressed cells were pre-grown in LB supplemented with 0.25 M NaCl (850 mOsm). Cells were washed with isoosmotic buffer (adjusted with sorbitol) and subjected to different shocks in the presence of 1 mM EDTA and 0.5 mM iodine added a few seconds prior to reaction. The cells were French-pressed; the membranes were pelleted by a 35 min centrifugation at 16,000 rpm, and the patterns of MscL cross-linking were visualized with western blots as above.

**Spheroplast preparation**

Giant spheroplasts were prepared essentially as described previously (Martinac et al., 1987). *E. coli* pB104 *mscL*-, *recA*- cells harboring the pB10b vector with MscL gene under the control of a lac-inducible promoter were grown in this study. A culture was shaken overnight in LB medium containing 100 uM ampicillin at 37$^{o}$ C, 255 rpm, then diluted 1:100 in the same medium and incubated for 3 h to an $OD_{600}$ of 0.4-0.8. This culture was then diluted 1:10 into modified Luria-Bertani (MLB) medium containing 100 uM ampicillin and additional 60 ug/ml cephalexin (Sigma Chemical Co, St. Louis, MO) to block cell septation. The culture was shaken for 1.5 h at 37$^{o}$ C, until single-cell filaments reached 50-150 um in length. In most cases, wild-type and mutant MscL was induced by adding final 1 mM IPTG in the MLB culture for an extra 30 min. The filaments were then harvested and giant spheroplasts were formed by hydrolyzing the peptidoglycan layer with lysozyme (0.2 mg/ ml) at room temperature (22-24$^{o}$ C). In order to obtain a low number of channels per patch for wild type and V23T, no IPTG was

added during the culture. To avoid death in cultures of severe GOF mutants (V23D, G22N, GG14-V23D and GAG-V23D), 1 mM IPTG was added for only 5 min, prior to the reaction.

**Electrical recording**

The standard patch-clamp technique (Hamill et al., 1981) was used to record MscL single-channel current in excised inside-out patches of giant spheroplasts as originally described by Martinac et al. (1987). Patch electrodes were pulled from capillaries (100 uL disposable microliter pipets; Fisherbrand, Fisher Scientific, Pittsburg, PA) by a Flaming/Brown micropipette puller (P-97, Sutter Insuments, Novato, CA) and were not fire-polished before use. All pipettes had bubble numbers in 100% ethanol of 4-5 corresponding to a resistance ~5 M Ω filled with the solution containing (in mM): 200 KCl, 90 $MgCl_2$, 10 $CaCl_2$ and 5 HEPES, pH 6 titrated with 10M KOH. The bath solution contained the same ingredients plus 0.3M sucrose to osmotically stabilize the spheroplasts. To achieve reducing conditions in some experiments, recordings were made in the same buffer containing an additional 200 mM β-mercaptoethanol or 10 mM dithiothreitol (DTT). In some cases (F7C, F10C), the pipette solution also contained 200 mM β-mercaptoethanol to ensure the completion of the reaction. In cysteine cross-linking experiments (I32C/N81C, A20C/L36C), 0.08mM iodine ($I_2$) used as an oxidant was filled in the pipette. All channel currents were recorded using an Axopatch 200B amplifier (Axon Insuments, Forster city, CA). The holding potential was +20 mV in the pipette and all activation currents along pressure gradients were done at room temperature. The current, filtered at 8 kHz by the build-in low pass Bessel filter of the amplifier and an

external 8-pole Bessel filter (Model 3381 filter, Krohn-Hite Corporation, Avon, MA), was digitized at 25 kHz with DigData 1322A data acquisition board and analyzed using the pCLAMP6 software (Axon Insuments, Forster city, CA). To reduce the noise and better resolve short subconducting states, in some experiments patch electrodes were coated with dental wax (Kerr Corporation, Romulus, MI). Currents in such instances were filtered at 30 kHz and sampled at a 100 kHz. Suction applied by a screw-driven syringe to the patch-clamp pipette was measured with a pressure gauge (PM015D, World Precision Insuments, Sarasota, FL). After the seal establishment and patch excision, negative pressure was ramped up at a rate of about 60 mm Hg per second until endogenous MscS channels were fully activated, then the pressure was increased more slowly until initial MscL activation was achieved. In order to record dose-response curves, following the activation of the first MscL, the pressure was increased in smaller increments of about 10 mm Hg and kept constant for approximately 5~10 s between the steps.

To assess the 'stiffness' of MscL channels, the threshold of wild-type or mutant MscL gating was compared to that of MscS usually present in the same patch. The 'threshold' was expressed as the ratio of the pressure required to evoke first opening of MscL (or a mutant MscL) relative to the pressure at which half of MscS channel open. For GOF MscLs showing a stable low substate, the pressure sufficient to enter the substate was taken as the threshold. For a more precise quantification, the pressure at which half of MscS channels were activated ($p_{½}^{MscS}$) could be used as a tension calibration point, as reported previously. According to previous measurements in spheroplasts (Cui and Adler, 1996) and liposomes (Sukharev, 2002), the tension mid-

point for MscS activation ($\gamma_{½}^{MscS}$) is close to 5.5 dyne/cm. Pressures were converted to tensions using the formula: $\gamma = (p / p_{½}^{MscS})$ x 5.5 dyne/cm, which can be deduced from the law of Laplace for a spherical surface.

**Dose-response curves measured with mean current**

The open probability ($P_o$) could be calculated for each pressure step as the mean integral current divided by the maximum current which was attained at saturating pressures ($P_o = I/ I_{max}$). For any given pressure step, the mean integral current is the sum of currents passing through all conductive states.

The dose-response curves for MscL were fitted with the two-state Boltzmann-type model:

$$P_o/P_c = \exp [-(\Delta E - \gamma \Delta A)/kT] \qquad (1)$$

where $P_o$ and $P_c$ are the open and closed state probabilities, $\Delta E$ is the energy difference between the states in an unstressed membrane, $\Delta A$ is the in-plane protein area change upon the gating transition, $\gamma$ is membrane tension, and $kT$ has conventional meaning (Howard and Hudspeth, 1988; Sachs, 1992; Sukharev et al., 1999). Technically, plots of $P_o/P_c$ versus tension were fitted with the exponential equation $P_o/P_c = b \exp^{a\gamma}$, where coefficients $a = \Delta A/kT$ and $b = \exp(-\Delta E/kT)$, respectively. Then the gating parameters, $\Delta E$ and $\Delta A$, can be extracted.

**Amplitude histograms**

To identify the substates, continuous traces were recorded at constant pipette pressures. Only single-channel fragments were taken into consideration. Following baseline

correction that removed drift and some obvious MscS fluctuations, all-points histograms of single-channel trace and normalized probability density histograms were constructed using HISTAN, a software written in Matlab by Dr. Andriy Anishkin. The amplitudes of ionic current through the channel were normalized to the amplitude of the fully open state. To include the baseline noise and fluctuations around the fully open state into the histogram, the range of conductances taken for analysis was set between -0.1 and 1.1. Probability density histograms were fitted by a sum of Gaussian functions, representing the occupancies of the closed and open states and a variety of subconductance levels. Although the positions, occupancies and widths of Gaussian peaks were independent adjustable parameters, it was possible to obtain reasonably accurate fits for wild-type and GOF MscL (discussed in the chapter 2 and 3) with essentially the same set of positions for peaks, which reflect common amplitudes of subconducting states. To present the average probabilities of various conducting states as a function of tension, two-dimensional (2-D) histograms (probability over the conductance-pressure plane) were generated by pulling together probability density histograms of each tension from three to seven activation curves. The gaps between fixed tension values was then filled using an interpolation procedure that creates a smooth surface of log probability.

**Thermodynamic and kinetic analyses of substates**

The ability of a channel to undergo expansion in the plane of the membrane is the specific property that makes it responsive to external tension applied to the lipid bilayer. In the linear approximation, at equilibrium, the ratio of probabilities of any two states can be related by the Boltzmann equation:

$$P_J/P_i = \exp\,[-(\Delta E_{ji} - \gamma \Delta A_{ji})/kT]$$

where $P_i$ and $P_j$ are the state occupancies obtained from the single channel probability density histograms, $\Delta E_{ji}$ is the energy difference between the states in an unstressed membrane, $\Delta A_{ji}$ is the in-plane protein area change upon the transition, $\gamma$ is membrane tension, and $kT$ is thermal energy (Howard et al., 1988; Sachs, 1992; Sukharev et al., 1999b).

In Chapter 3, the rate constants for selected transitions in wild-type and V23D MscL were determined using the QuB package (Qin et al., 2000). The baseline-corrected single-channel fragments of traces were idealized in a two-state approximation using SKM, and then the major rate constants were fitted using MIL. For wild-type MscL, which is characterized with a single rate-limiting step (Sukharev et al., 1999b), the entire closed-to-open interval was counted as a single transition. At low and intermediate tensions, V23D mutant dwells predominantly in the low substate $S_{0.13}$, from which it visits upper substates and the fully open state, and returns back to the low substate. It clearly shows two separate sub-transitions: C→ $S_{0.13}$ and $S_{0.13}$ → O. The rate constants were determined as functions of tension for the second sub-transition (Chapter 3).

The kinetics of transitions provides information about the position of the rate-limiting barrier. For the closed and open states separated by a single barrier, the two rate constants can be written in the Eyring's form:

$k = \frac{k_B T}{h} \exp(-\Delta E^* / kT)$, where $k$ is an experimental rate constant either on rate or off rate, $k_B$ is the Boltzmann constant, $h$ is Plank's constant, and $\Delta E^*$ is the free energy of activation from a measured rate constant. For a mechanosensitive channel, the open

probability of the channel is biased by the external work, $\gamma\Delta A$. As seen in Fig. I-4, $\Delta E^*$ for on rate can be calculated by $\Delta h_b - \gamma\Delta A_{cb}$ and $\Delta E^*$ for the off rate can be calculated by $\Delta h_b - \Delta E + \gamma\Delta A_{ob}$.

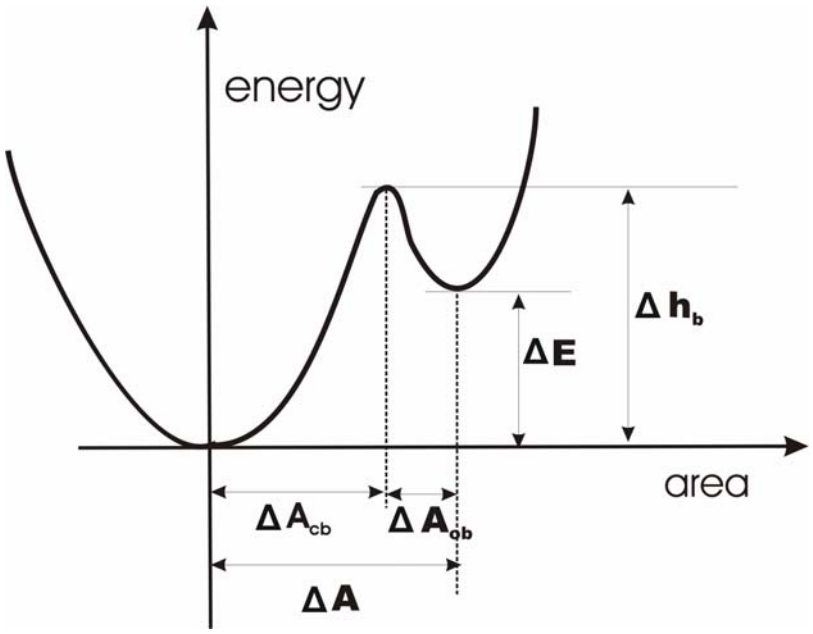


**Figure I-4.** Process of a reaction according to the Eyring rate theory. The energy and space parameters for closed and open wells are denoted.

Therefore, $k_{on} = k_0 \exp[-(\Delta h_b - \gamma \Delta A_{cb})/kT]$ and $k_{off} = k_0 \exp[-(\Delta h_b - \Delta E + \gamma \Delta A_{ob})/kT]$ where pre-exponential coefficient, $k_0 = \frac{k_B T}{h}$ , $\Delta E$ is the energy difference between closed and open wells, $\Delta h_b$ is the height of the barrier looking from the closed well, $\Delta h_b$-$\Delta E$ is the height of the barrier as seen from the open well, and $\Delta A_{cb}$ and $\Delta A_{ob}$ are the area differences between the bottoms of closed or open well to the tip of the barrier. By taking logarithms and then derivatives on γ, the logarithmic slopes of the rate constants give area differences between the equilibrium positions of the states and that of the rate-limiting barrier, i.e. $\frac{d \ln k_{on}}{d\gamma} = \Delta A_{cb}/kT$ and $\frac{d \ln k_{off}}{d\gamma} = -\Delta A_{ob}/kT$.

**Protein area calculations**

As discussed in the chapter 2, the molecular models of the closed (conformation 2) and the open state that satisfies the 3.1 nS unitary conductance (conformation 11) were taken from model (Sukharev et al., 2001). Smooth outer-boundary accessible surfaces were created by 5 Å rolling spherical probe using the PDBAN program written by Dr. A. Anishkin. The solvent-accessible surface was sliced into 1 Å-thick sections with planes perpendicular to the pore axis and the cross-sectional areas of individual slices was calculated. The areas of two protein slices located at the positions ±12 Å from to the mid-plane of the membrane, i.e. near the hydrophobic core boundaries, were averaged, and the numbers taken as in-plane cross-sectional areas for a particular conformation.

**Statistical modeling of the population response to varied parameters**

The amount of channel expansion $\Delta A_o = 23.3$ nm$^2$ was estimated from molecular models (see chapter 2), and the corresponding energy of the transition, $\Delta E_o = 58.9\ kT$ was calculated using eqn 1 and the condition of $\gamma_{½} = 10.4$ dyne/cm determined in experiments (see Results of the chapter 2). These values were taken as the initial 'single-channel' parameters for simulations. Sets of normally distributed random numbers $\Delta E_i$ and $\Delta A_i$ with different standard deviations were generated using the "randn" function of Matlab. The standard deviations were varied, between 1 to 20 $kT$ for $\Delta E$ (around the mean of 58.9 $kT$), and between 0.5 and 3.5 nm$^2$ for $\Delta A$ (around the mean of 23.3 nm$^2$). Pairs with fixed $\Delta E$ and random $\Delta A$, random $\Delta E$ and fixed $\Delta A$, or both random parameters modeled individual channels in a population. $P_o/P_c\,(\gamma)$ curves for each channel were generated using eqn.1 and then superimposed to simulate the dose-response curves of the entire population containing 50 or 100 channels. The slope of the simulated curve was then determined using the Boltzmann fitting procedure as for experimental curves and the apparent parameters $\Delta E_{app}$ and $\Delta A_{app}$ were extracted.

# Chapter 1

# Gating mechanism of MscL channel: experimental validation of the stereochemistry of the opening transition


## Abstract

The crystal structure of MscL from *Mycobacterium tuberculosis* and homology models of *E. coli* MscL developed recently provide a framework for analyzing molecular gating mechanisms. The purpose of disulfide cross-linking experiments described below is to test the stereochemical aspect of the models. The results confirm the helical positions in the modeled closed state of *E. coli* MscL and demonstrate that the iris-like expansion of M1 helixes does occur during the gating transition, upholding the proposed helix-tilt model. Throughout the gating process, the M1 helix of one subunit and M2 helix of the adjacent subunit do not change their relative positions substantially and must tilt together. In addition to the hydrophobic M1 gate, the S1 segments unresolved in the original crystal structure were easily cross-linked with pairs of cysteines, which support their close proximity and possibly bundle-like arrangement. Cross-links between S1 domains also prevented opening, consistent with the proposed function of a second gate. Although the early models predicted a wide-open conformation with cytoplasmic S3 domains separated, the current data strongly suggest that S3 domains are in fact stably associated in both closed and open conformations.

**Analysis of Models**

In the crystal structure of TbMscL and in the homology model of EcoMscL, the closed conformation is characterized by tight packing of M1 helices forming the pore constriction. The constriction was identified as the primary gate region in the original crystal structure (Chang et al., 1998) and, independently, the residues lining the constriction were implicated in the gating process by mutagenesis studies (Ou et al., 1998). In the constriction region of EcoMscL, the pore is lined and practically occluded by hydrophobic side chains of residues L19 and V23 ($Ile^{14}$ and $Val^{21}$ in TbMscL) located near the $NH_2$-terminal end of the transmembrane helix M1. The pore in that region is narrow (~3-4 Å in diameter) and, due to its hydrophobicity, most likely is completely dehydrated. How big should the conformational transition that would allow for a conductance of 3 nS be? The conductance of the EcoMscL pore is a linear (non-saturable) function of specific buffer conductivity (at least up to 2 M KCl), indicating a large aqueous pore where the ions behave the same way as in the bulk solution. Macroscopic estimates suggest that the pore should be about 3 nm in diameter (Cruickshank et al. 1997, Sukharev et al., 1999b). To achieve this, a large-scale change of protein conformation would be necessary. In the iris-like model of pore opening discussed above, M1 helices slide one along another, leading to a wide separation of the constriction region with M1 helices lining most of the pore. This type of movement also involves flattening of the entire channel protein.

The proposed models of EcoMscL gating specify helical positions and most probable conformations of side chains in the closed, fully open and several intermediate

states. These atomic-scale models make several concrete predictions concerning the proximities of specific pairs of residues:

1. *Relative positions of M1 helices.* M1 helices are in the most upright position in the closed state, forming the narrowest constriction. The beta carbon of A20 is separated from the alpha carbon of G22 of the neighbor by 4Å in the closed state (conformation 2, see Sukharev et al, 2001). Similarly, I24 and G26 residues are only 4.5 Å apart.

As the barrel expands toward the fully open state, A20 comes close to L36 (4.8 Å in conformation 9) and after arrival to the most expanded conformation 11, it remains near L36 (4.4 Å), but also becomes proximal to V37 and I40 (~5 Å). I24 in the expanded conformation becomes proximal to V37, I40 and I41. When changed to cysteines, these residues may form disulfide bridges potentially stabilizing the open state.

2. *Relative positions of M1 and M2.* In the TbMscL crystal structure and EcoMscL homology model, M1 and M2 helices of neighboring subunits form extensive areas of buried contact and their interaction in EcoMscL is additionally stabilized by the K31-D84 partially buried salt bridge. The strong interactions between M1 and M2 appear to be the major factor that secures the entire MscL complex together and implies that the two helices should tilt together as a unit during the gating transition. Several pairs of residues are predicted to be in the contact zone with the closest distances between A28 and F85 or V88 and between I32 and N81 (4-6 Å). If the helixes do not change their relative positions substantially and tilt together, the channel should be able to open with or without a disulfide bridge between cysteines in the corresponding positions.

3. *Positions of putative S1 domains.* N-terminal domains were heavily modified for the purpose of TbMscL isolation and were unresolved in the crystal structure. In the

homology model of EcoMscL, these domains were proposed to form the cytoplasmic gate. Kinetic studies suggest an expanded but low-conducting intermediate state of the channel (Sukharev et al., 1999b). In this conformation apolar contacts formed by M1s are supposed to be completely broken, the pore is predicted to be fully hydrated and the fact that the conductance is low (15-20% of fully open current) implies that the pore remains occluded by another gate. The conserved and clearly amphipathic S1 helices, which were predicted to form a short bundle, are the best candidates for the role of the second gate. The most conserved hydrophobic residues F7 and F10 should pack inside the bundle and their interactions as well as possible salt bridges on the periphery may stabilize the short bundle. When changed to cysteines, F7C's or F10C's on adjacent subunits may cross-bridge and lock the channel in its partially or completely closed conformation. In the fully open conformation S1 may pack along the M2 helix of another subunit (not adjacent, but one over) and form apolar contact partially stabilized by interactions between I3 (S1) and I96 (M2).

4. *Cytoplasmic S3 helices.* Sequence analysis shows a highly conserved stretch between positions 119 and 130 in EcoMscL predicted to be an amphipathic helix. In the crystal structure of TbMscL, C-terminal helices are indeed associated in a pentameric bundle, but the orientation of helices seems to be distorted as negatively charged residues are buried inside the bundles whereas apolar residues occur on the periphery. In the initial models, the C-terminal S3 domains were re-packed such that all conserved aliphatic side chains (L121, L122, I125, L128, and L129) would pack inside the petameric bundle, burying the large hydrophobic surface. Because expansion of the transmembrane barrel is associated with substantial flattening of the transmembrane segments, the initial model

proposed that S3 helices may compensate for the flattening by interacting with lipids at the cytoplasmic surface of the membrane and form part of the pore entrance. The conformation of S3 helices, however, required experimental validation. The strategy described below includes introduction of either stabilizing modifications, such as L121C/ L122C or L128C/ L129C substitutions allowing for disulfide formation, or bundle-destabilizing mutations such as L121T/L122T/L128T/L129T. Functional analysis of such mutants and comparison with WT MscL must give the answer to the question of whether the S3-bundle separates during the functional cycle. If indeed the bundle separates, the S3-S3 cross-links should prevent channel opening or severely restrain it. Conversely, destabilizing mutations should make the channel 'softer'. The absence of significant effects on gating would suggest that the bundle remains intact in all conformations.

In the sections below, I examine the stereochemical aspect of atomic models, the way they predict the fully open and fully closed channel conformations. I chose the disulfide cross-linking approach, which is irreversible under strongly oxidizing conditions, and it 'traps' all Cys-Cys encounters, even very rare. For the first time I have been able to conduct disulfide trapping experiments during patch-clamp recording and directly observe effects of disulfide bonds formation on the channel behavior. I acknowledge a substantial contribution from Mrs. Monica Betanzos (laboratory technician) who generated most of the cysteine mutants and performed biochemical cross-linking experiments verifying the probabilities of cross-links. Additional mutants in the C-terminal domain were generated by Vyacheslav Gendel (undergraduate student) and Lena Shirinian (technician).

## Results and Discussion

### The closed-state arrangement of M1 helices

Fig. 1-1 shows the inner part of the EcoMscL barrel (S1 and M1 helices) in a putative closed conformation. In the contacts between adjacent M1 helices, Ala 20 faces Gly 22 and Ile 24 faces Gly 26 (the distances between β-carbons of Ala 20 or Ile 24 and α-carbons of corresponding glycines are about 5Å). Under ambient conditions (room $T^o$, atmospheric oxygen), the subunits of the A20C/G22C or I24C/G26C double mutants produce mostly monomers and dimers, as seen on western blots following the separation in non-reducing SDS-PAGE (panel B). This indicates a moderate degree of cross-linking. Upon oxidation with iodine, the I24C/G26C mutant cross-links immediately into pentamers, which migrate in gels slightly faster than the 5x band of the previous mutant. These particular pentamers may have a more compact conformation in SDS gels due to the complete cross-linking into closed-loop structures. Cross-linking of the A20C/G22C mutant is less complete, it shows preferential tetrameric products with no monomers, but visible amounts of dimers, trimers, and pentamers. Single-channel traces recorded from giant spheroplasts expressing each of the double mutants were either silent in the entire range of pipette pressures up to the patch breakdown at 250-350 mm Hg (activation pressure ratio, ~1.8-2.3, relative to MscS; MscL usually opens at ~1.5), or revealed mostly incomplete openings (8 patches out of 20 for I24C/G26C, Fig. 1-1C), illustrating the partially cross-linked state of the channel under ambient oxygen. Exposure to reducing reagent, 200 mM mercaptoethanol (ME), increased the activity of I24C/G26C MscL (3 out of 4 patches, Fig. 1-1C). The complete interlinking of the channel complex

via cysteine pairs at positions 24 and 26 constrains the closed-state EcoMscL structure to the conformation similar to the crystal structure of TbMscL.

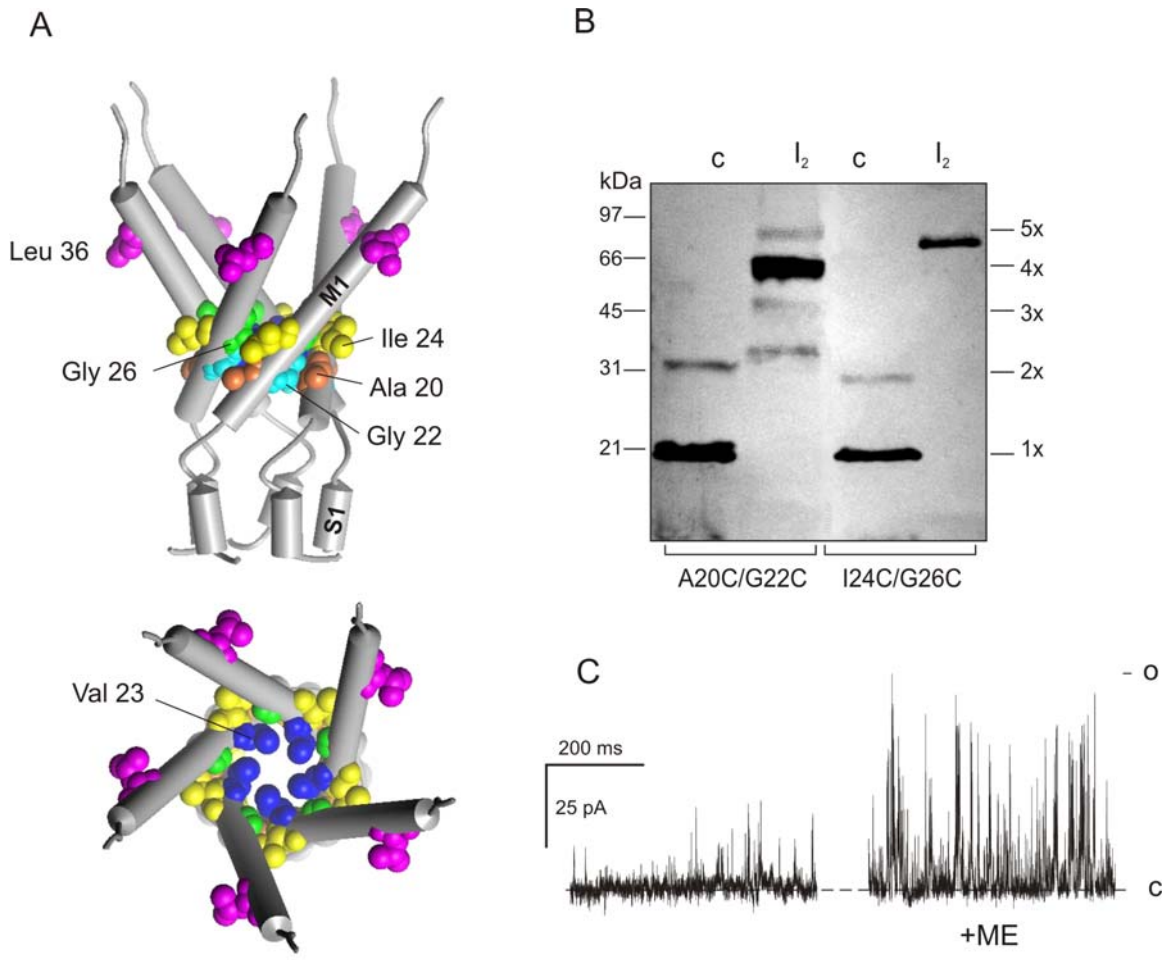


**Figure 1-1.** The closed conformation of MscL inner helices. (A) A fragment of the EcoMscL model showing M1 and S1 helices from the side (top panel) and the view from the periplasm into the pore (bottom). (B) Western blot representing cross-linking patterns of A20C/G22C and I24C/G26C under ambient oxygen (control) and in the presence of 0.2 mM $I_2$. (C) Traces of I24C/G26C channels recorded under ambient oxidizing conditions and in the presence of 200 mM of mercaptoethanol (ME) in bath and pipette (at pressures of - 230 and -200 mm Hg, respectively).

**The expanded state of the barrel**

The two open pore models of Fig. I -3 (see Introduction) make very different predictions about the interactions of the M1 helices. In the '5- helix pore' model (Fig. I-3, *righ*), residues near the beginning of one M1 helix interact with residues near the end of the adjacent helix; whereas, in the '10-helix barrel-stave' model (Fig. I-3, *left*) no M1 residues interact with M1 residues of an adjacent subunit and the N- and C-termini of adjacent M1 helices remain far apart. Since the precise conformation of the open channel is difficult to predict, we considered a range of open '5-helix pore' models, in which the tilts of M1 varied from $60^o$ for the least expanded to $74^o$ for most expanded. The distance between residues Ala 20 and Leu 36 of adjacent M1's remain within the reach of a disulfide bond (<6 Å) in all of these conformations (Fig. 1-2A ), but is shortest in conformations characterized by 630 to 670$Å^2$ pore lumen cross-section and 70 to $73^o$ tilts of M1.

The experimental conditions for disulfide cross-linking in intact cells under hypotonic shock were developed and performed for the *E. coli* MJF 455 *mscL*$^-$*/mscS*$^-$ cells. In brief, cells expressing each of the mutants were pre-grown in a high-osmotic medium and then subjected to osmotic shocks of various magnitudes by mixing into a diluted medium containing iodine as an oxidant. 1 mM of EDTA was added to the shock medium to destabilize the outer membrane and provide rapid access of $I_2$ to the inner membrane. Without osmotic challenge, the double A20C/L36C mutant forms multiple cross-linking products under these conditions, ranging from dimers to tetramers (Fig. 1-2 B, *left-most lane*). Osmotic shock in the presence of the oxidant results in the appearance of a prominent fifth band in a manner dependent on the strength of the shock (Fig. 1-2B).

This sharp band migrates slightly faster than the expected pentamer band, which suggests that complete cross-linking into compact circular products is likely to occur.

In order to see the effect of the Cys 20 to Cys 36 disulfide bond formation on single-channel currents, I expressed the single A20C and L36C mutants and the double mutant in PB104 cells, generated giant spheroplasts and subjected them to patch-clamping. In the control experiments without the oxidant, application of pressure gradients to the patch evoked nearly normal MscL currents with single A20C, or L36C mutants. The A20C/L36C double mutant was similar but was activated at slightly higher pressures and had a shorter mean open time than WT MscL. Application of iodine to the pipette had no effect on L36C (5 out of 5 patches), but often inactivated the A20C mutant (4 out of 5 patches). Although β-carbons of Ala 20 on adjacent subunits are separated by about 10Å in the static (symmetrical) model, the dynamics of M1 helices may permit coupling of cysteines at these positions. When patches with the A20C/L36C double mutant were exposed to 0.08 mM iodine in the pipette, irreversible inactivation occurred in 18 out of 24 patches (Fig. 1-2 C, *upper trace*), consistent with high probability of Cys 20-Cys 20 cross-links. Indeed, cross-linking of adjacent M1 helices prevents opening. In six other patches, three channels exhibited a locking of the channel in a subconducting state (Fig. 1-2C, *middle trac*e) and three others were locked in the fully open state (Fig. 1-2C, *bottom trace*). The traces show that while the activating pressure in the pipette is kept constant, the channel suddenly enters a regime in which it never visits the completely closed state until the rupture of the patches (from 10 seconds to 4 minutes), indicative of stabilization of the expanded conformation. In a model built after the crystal structure, A20 and L36 are ~20 Å away from each other. Cross-linking evidence in

osmotically shocked cells and single channel recordings strongly support the helix-tilt model of EcoMscL gating. Recently a study of the structural rearrangements associated with EcoMscL gating was carried out, using site-directed cysteine screening and electron paramaganetic resonance (EPR) measurement (Perozo et al., 2002), which independently confirmed that M1 helices are highly tilted and primarily line the pore.

**Figure 1-2.** Interhelical contacts between adjacent M1 helices in the closed conformation and functional verification of '5-helix-tilt' model. (A) Molecular models of the EcoMscL in the closed and open conformations. Notice upon opening A20 from one subunit contacts L36 of another subunit. (B) In the presence of iodine (0.1 mM), A20C/L36C under isosmotic condition displays four bands, whereas under hypoosmotic downshock the pentamer forms as observed by the appearance of the fifth band on the gel. The numbers in the bottom of the gel show the strength of the hypo-osmotic shock by shifting bacterial culture from hyperosmolarity to dilute medium (C) In the presence of iodine in the pipette (0.08 mM), patch-clamping of A20C/L36C reveals that the channel is locked in either the closed state (upper trace, 75% of patches, 18 of 24) or open state (middle and lower traces, 25% of patches, 6 out of 24).

A

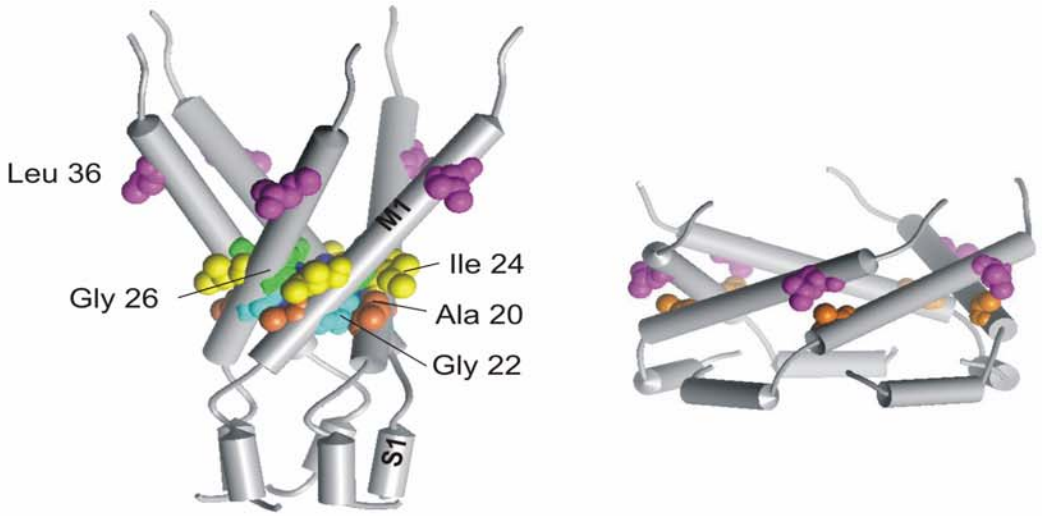
Leu 36
Gly 26
M1
Ile 24
Ala 20
Gly 22
S1

B

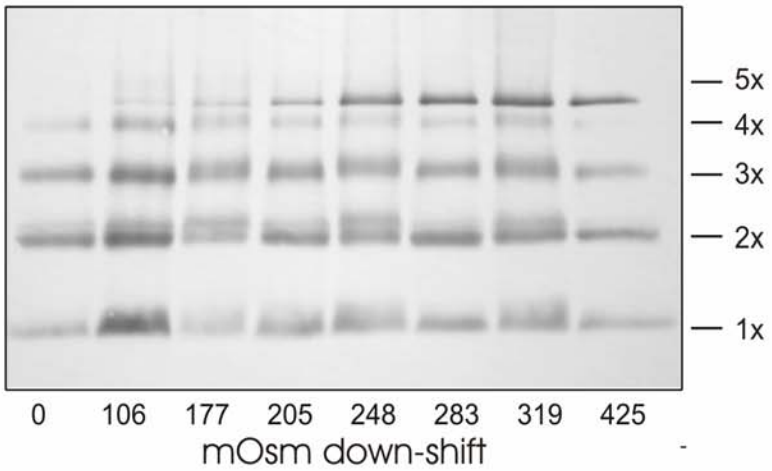
5x
4x
3x
2x
1x
0
106
177
205
248
283
319
425
mOsm down-shift

C

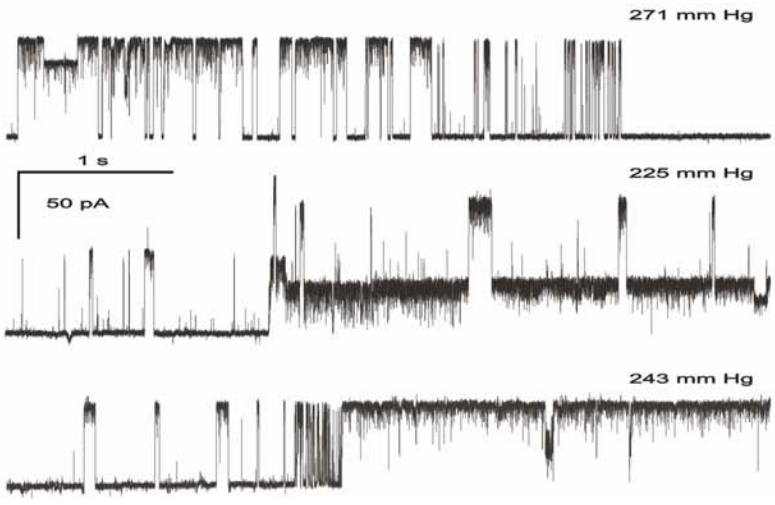
271 mm Hg
1 s
50 pA
225 mm Hg
243 mm Hg

**M1 and M2 transmembrane helices tilt together**

In the proposed gating models, extensive contacts between M1 and M2 helices of neighboring subunits remain relatively unaltered throughout the opening process (Sukharev et al., 2001). To verify this structural detail, the I32C/N81C mutant that covalently bridges M1 and M2 of adjacent subunits was engineered. In the models, the presence of the disulfide bridge occurs in the closed, intermediate and open conformations, and therefore is not expected to prevent the channel opening. The proximity of I32 and N81 is shown in Fig. 1-3A. In the presence of 0.025-0.05 mM of $I_2$ in the medium, the subunits of the I32C/N81C double mutant link readily into closed pentamers as shown by the western blot (Fig.1- 3B*, middle lane*). Pentamers form with equally high probability after treatment with iodine followed by osmotic downshock (Fig.1- 3B*, right lane*), suggesting M1 and M2 would form cysteine-bridge upon iodine treatment and then likely tilt together in response to the osmotic downshock throughout the gating process and osmotic shock does not perturb the cross-linking. In the patch-clamp experiments without an oxidant, the double mutant was activated at an activation threshold of ~1.4 relative to MscS, slightly smaller than that in the wild type (~1.5), and exhibited a 'spiky' phenotype characterized by very short mean open time. Nonetheless, the mutation did not affect the open channel conductance response to applied pressure in a patch, suggesting that basic open-shut conformational change is preserved. In the excised inside-out patches, application of iodine through the pipette to the outer surface of the membrane, which mimics the cross-linking conditions in whole cells, affected neither WT nor the I32C/N81C mutant. The trace in Fig. 1-3C recorded after 60 minutes of exposure to 0.08 mM iodine reveals no difference in the unitary channel conductance

or kinetic pattern compared with the initial non-oxidized channel. Note that the I32C/N81C pair is near the extracellular surface and must be accessible to lipid-soluble iodine, which was present in the pipette in a concentration that caused 100% cross-linking in whole-cell experiments and in isolated membranes (Fig. 1-3B). The Cys 32-Cys 81 disulfide bridges, which must form in the patch under such conditions, do not impede channel gating, indicating that M1 and M2 helices do not change their relative position substantially during the gating transition, and therefore they must tilt as a unit.

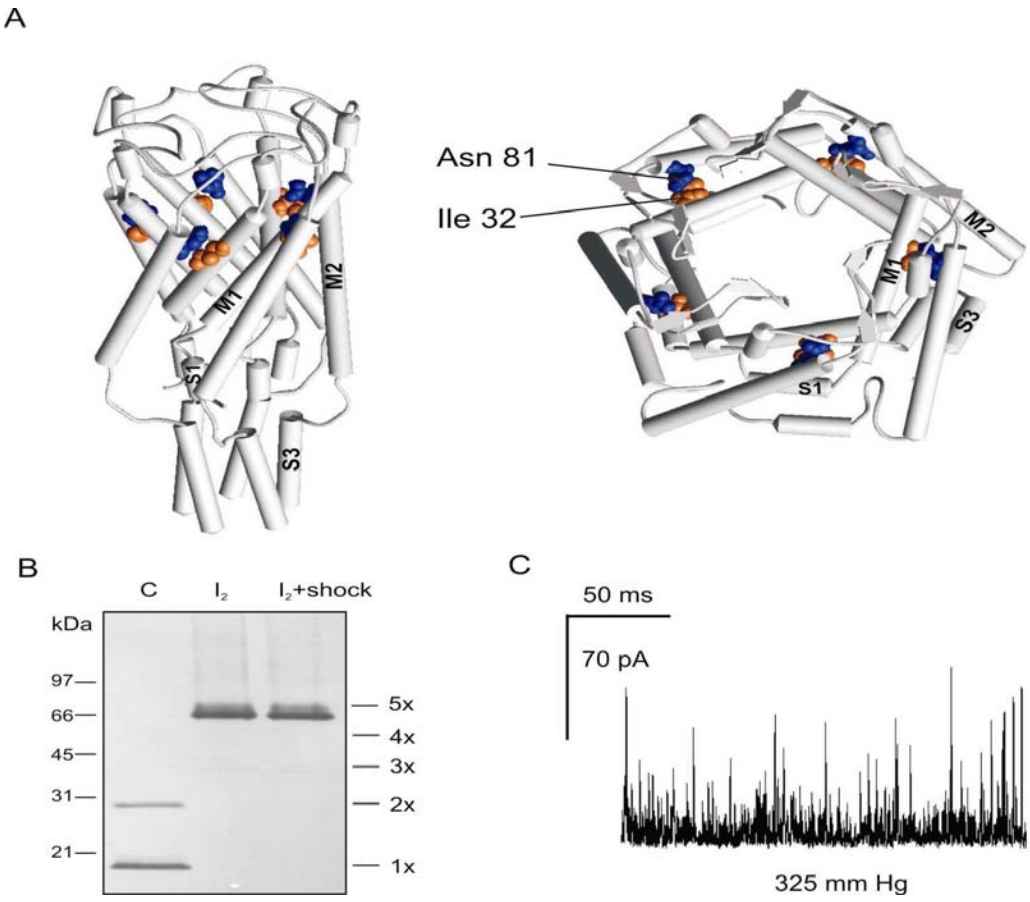


**Figure 1-3.** The I32C/N81C disulfide bridges cross-link the entire complex, but do not prevent the channel from opening. The relative positions of the residues Ile 32 (blue) and Asn 81 (orange) do not change in the course of the transition, such that the disulfide bridge satisfies both the closed and open conformations (A). The western blot (B) shows that I32C/N81C subunits form dimers under ambient oxygen and cross-link into complete pentamers in the presence of 0.05 mM $I_2$ equally well without or with a 425 mOsm osmotic shock (indicated as $I_2$ and $I_2$+shock, respectively). (C) A typical single-channel trace recorded from I32C/N81C MscL after 60 min exposure to 0.08 mM iodine in the pipette, which is identical to those recorded in control patches without oxidant (not shown).

**N-terminal domains (S1) function as a cytoplasmic gate**

The MscL gating model based on the analysis of single-channel currents involves two gates, the M1 hydrophobic gate, which opens first, and the S1 cytoplasmic gate opening second (Fig. 1-4A). The hypothesis that the S1 bundle occludes the pore was tested by substituting cysteines for specific S1 residues and determining whether these residues are proximal in adjacent subunits in closed state of channel, and if so, whether cross-linking of S1 segments prevents channel opening. Individual residues in the core of the bundle with β carbons < 7 Å apart should cross-link subunits when replaced with cysteine. This was supported by the western blot after protein separation by non-reducing electrophoresis gel. Both F7C and F10C mutants formed disulfide bridges spontaneously in the presence of ambient air oxygen (Fig. 1-4B, *left*). In the inside-out patch, no or very few incomplete short-lived MscL currents (2 out of 17 patches) were observed in F10C spheroplasts as the suctions were close to the lytic pressure (about > 2.3 times the MscS threshold) of the patch membrane. F7C occasionally displayed short-lived current at the pressure ratio up to 2 (5 out of 15 patches). When the patch was incubated with a reducing agent, 200 mM ß-mercaptoethanol (ME), in both the pipette and bath solution, F10C disulfide bridges are reduced slowly (Fig. 1-4, *right*). Partial openings appear gradually, presumably due to the reduction of one of two possible disulfide bridges (12 out 17 patches, 30 min incubation). These are followed in about an hour by complete ~3 nS openings (2 patches). The F7C mutant was fully activated within 30 min with 200 mM ß-mercaptoethanol applied in the pipette and bath solution, and the reaction went faster when a moderate suction of about 50 mm Hg was applied to the pipette (5 out of 8

patches). This suggests that the F7C structure has more conformational freedom than F10C, being easily expanded and more accessible to ß-mercaptoethanol.

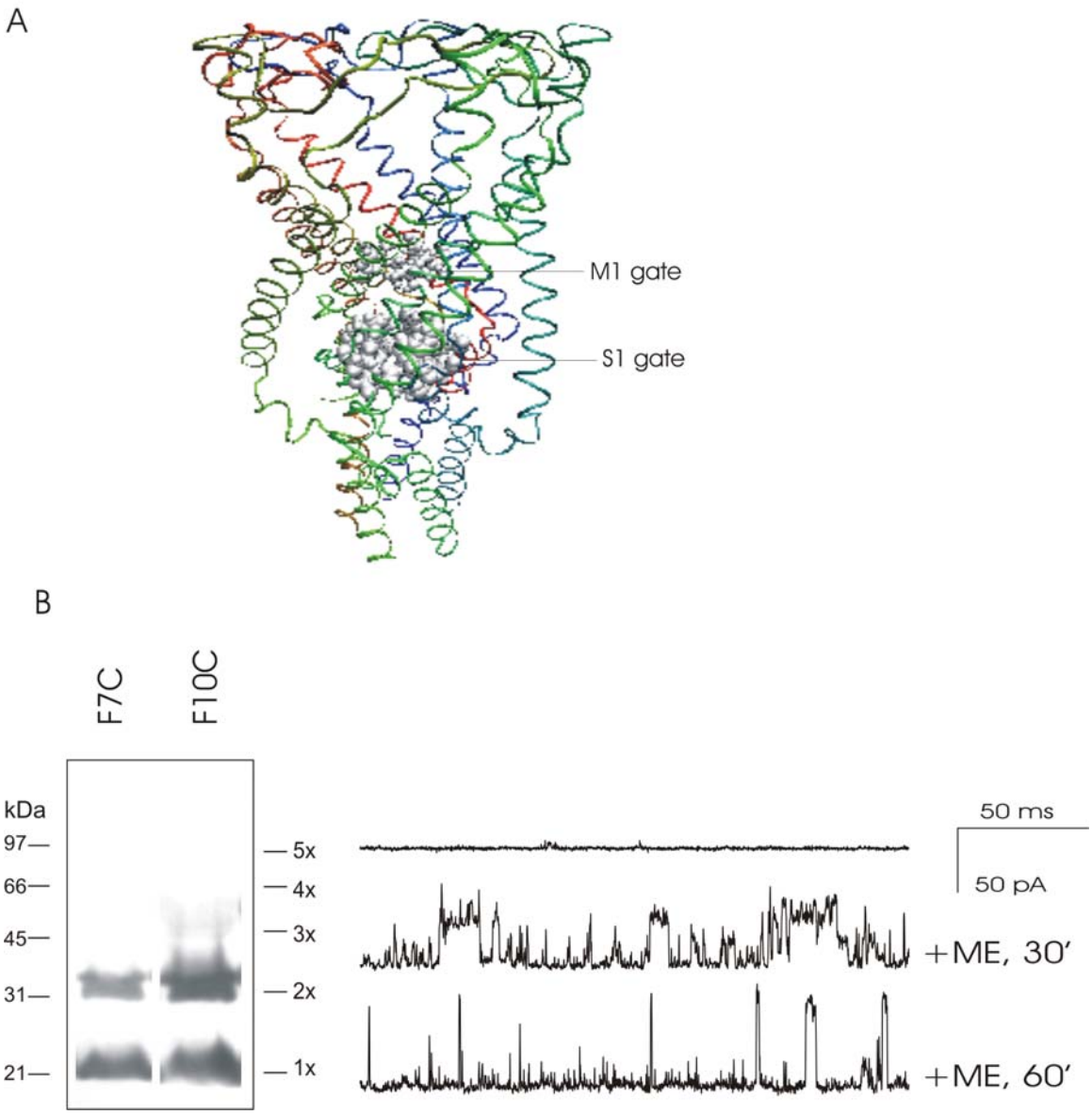


**Figure 1-4.** Functional verification of S1 gate (A) The polypeptide backbone of EcoMscL closed model, showing the hydrophobic gate made by valine 23 rings (M1 gate) and cytoplasmic gate formed by phenylalanine 7 and phenylalanine10 side chain rings (S1 gate) (B) Disulfide bridges of F7C and F10C under the ambient oxygenation revealed on the western blot (left). Single-channel traces obtained with F10C mutant after incubation for 0 min (top), 30 min (middle) and 60 min (bottom) with 200 mM ß-mercaptoethanol (ME) in the pipette and bath solution.

**The C-terminal domains (S3) stably associate throughout the gating process**

The 3D crystal structure of TbMscL revealed a pentameric channel (Chang et al., 1998). The sequence of the COOH terminus of MscL homologs is similar to that of the oligomerization domain of the cartilage protein COMP (Fig.1-5A), which has five-fold coiled-coil structure stabilized by apolar interaction inside the bundle and by salt bridges on the periphery (Malashkevich et al., 1996). Although the C-terminal cytoplasmic helices in the TbMscL crystal structure appear to be in close contact, detailed examination of the COOH-terminal bundles in the crystal structure, when crystallized in the very low pH (3.6-3.8), reveals that many hydrophobic side chains are exposed to the outside, whereas hydrophilic and some charged side chains are packed inside the bundle (Chang et al., 1998). A homology model of EcoMscL that better satisfies hydrophobicity criteria was proposed (Fig. 1-5B, *bottom illustration*). The alignment of S3 domains for twenty MscL homologs uncovers the consensus motif, `LLxEIRDLLK`, which has a pattern of a strongly amphipathic helix. To examine whether S3 domains form a bundle-like structure at rest, and whether the bundle remains stable or separates upon the channel opening, the highly conserved leucines in S3 were replaced by cysteines. Double cysteine mutants L121C/L122C and L128C/L129C of EcoMscL were first generated. The cross-linking patterns for double mutants L121C/L122C-6His and L128C/L129C-6His under ambient oxygen or oxidized conditions by iodine or $H_2O_2$ showed the same multimerization patterns, whereas reduction with DTT resulted in a monomeric form (Fig. 1-6). If the S3 domains change their conformation substantially during the gating process, then their immobilization via covalent cross-linking should affect the dose-response curves and single-channel currents. Based on the cross-linking pattern on the

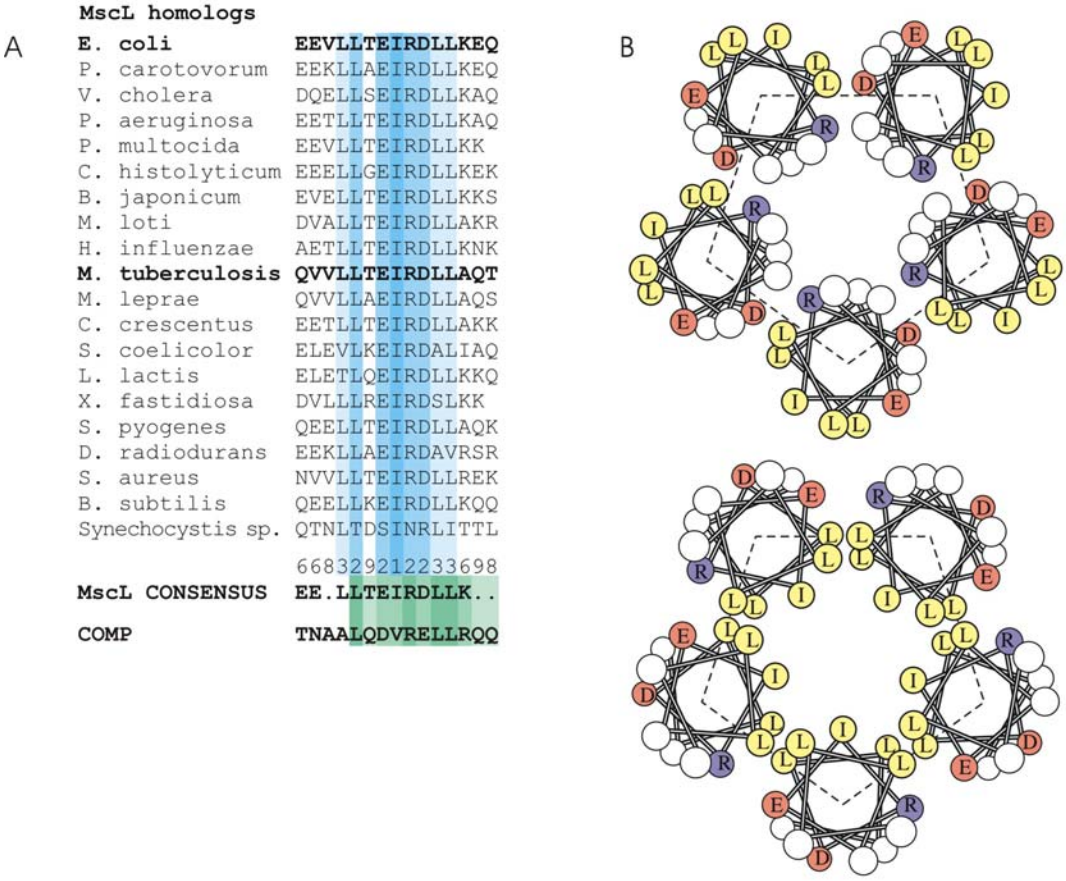


**Figure 1-5.** (A) Sequence analysis of conserved C-terminal regions of MscL and comparison with the cartilage protein COMP (cartilage oligomeric matrix protein). Alignment of S3 domains (residues 118-132 for EcoMscL) for nineteen representative MscL homologs from different bacterial species, the consensus and the sequence of the third heptad of the oligomerization domain of COMP. (B) Helical wheel representations of the packing of helices in the crystal structure of TbMscL (upper) and in EcoMscL modeled after COMP (below).

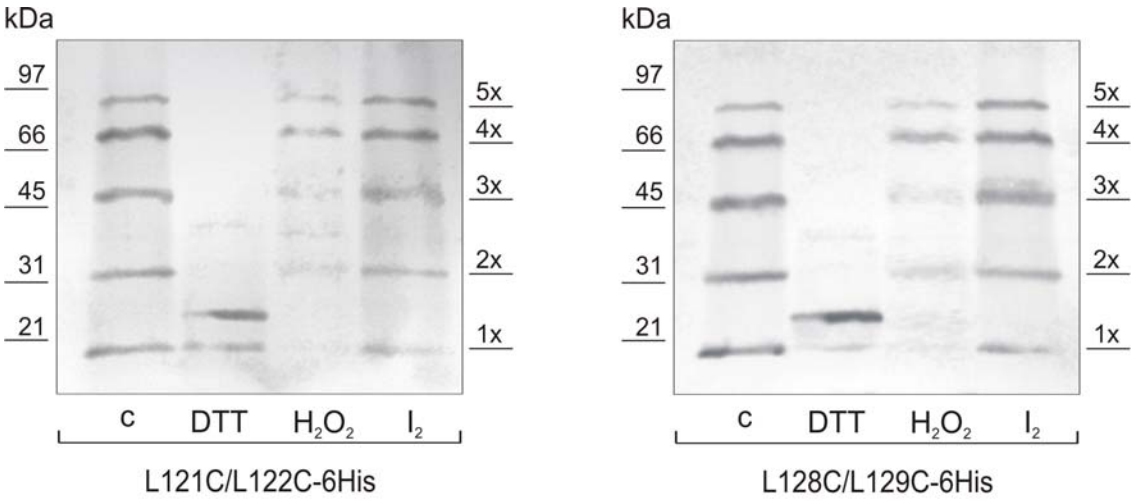


**Figure 1-6.** Disulfide crosslinking in C-terminal double cysteine MscL mutants. The patterns were visualized with the Western blot technique. Crosslinking conditions are denoted as c (control) - ambient oxygen, DTT (10 mM), $H_2O_2$ (0.3%), $I_2$ (0.1 mM), duration of all treatments was 15 min.

western blot, we considered that ambient oxygen is as effective in bridging cysteine pairs L121C/L122C and 128C/L129C mutants as a strongly oxidizing medium. Surprisingly, the L121C/L122C and L128C/L129C mutants, though, with S3 domains inter-linked by disulfide bonds, exhibited a similar degree of activation as WT MscL when examined by patch clamping (Fig. 1-7 A, B). The half tension point, $\gamma_{0.5}$ (dyne/ cm), where the channel open probability is 0.5, is 10.5 $\pm$ 0.6 (n = 10) for wild type, 10.5 $\pm$ 0.5 (n = 5) for L121C/L122C, and 10.6 $\pm$ 0.2 (n = 8) for 128C/L129C. The mutated channels gate normally with S3 domains inter-linked by disulfide bonds, suggesting that S3 domains of native MscL likely keep their association via several rings of hydrophobic residues throughout the gating process. When patches were subjected to reducing conditions by bathing in 25 mM DDT for 60 min, the channels open early in response to a similar increase of pipette pressure but the maximal current and the total number of active channels did not increase (Fig. 1-7 B). A shift of activation curves observed in the double cysteine mutants upon transferring to the reducing medium was similar to one recorded for cystein-less WT MscL in the presence of DTT (for both WT and cysteine mutants, $\gamma_{0.5}$ shifts from ~10.5 dyne/cm to ~8.9 dyne/cm). An apparently non-specific effect of reduction, also reported for cysteine-less MscS (Koprowski and Kubalski, 1999), is most likely due to the reduction of disulfide bonds in the surrounding proteins, which may change the mechanical properties of the membrane as a whole. Fig. 1-8 presents fragments of single-channel traces of L121C/L122C and L128C/L129C and their all-points histograms in a normal buffer and in buffer containing 25 mM DTT. It can be seen that under ambient oxygen double cysteine mutants gated similarly to WT, but changed

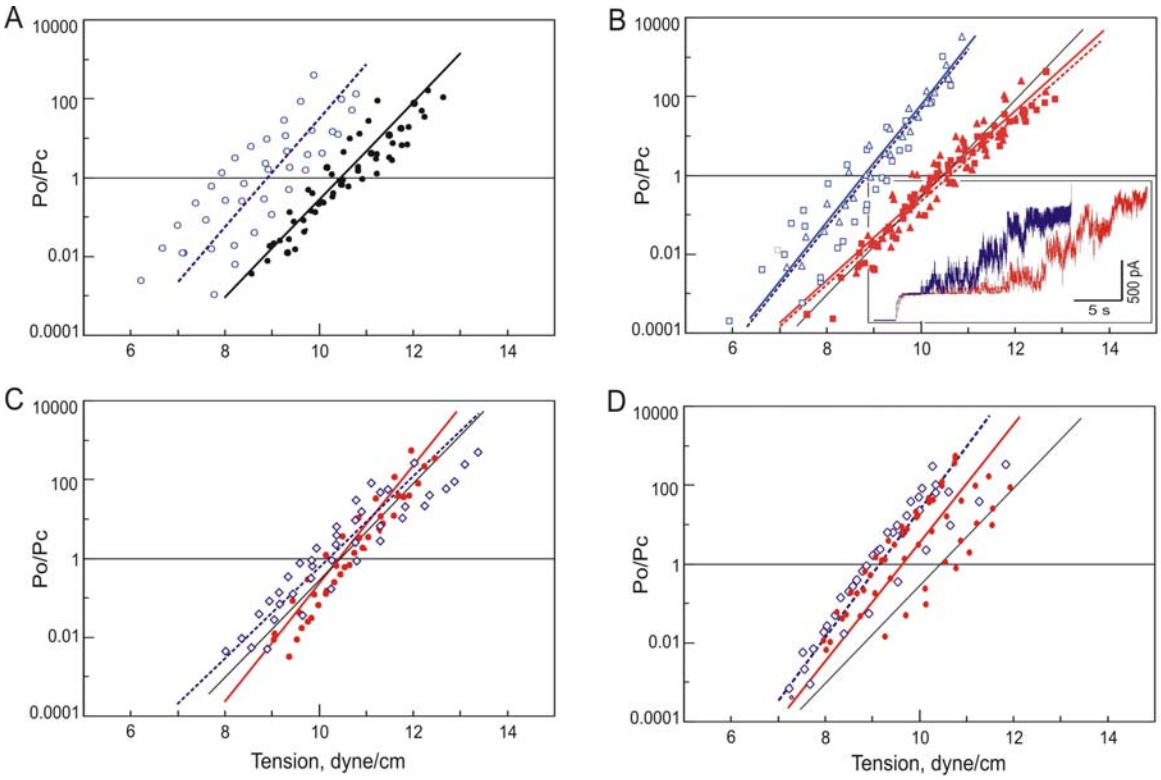


**Figure 1-7.** Dose-response curves for WT MscL and S3 domain mutants. Four to seven curves measured on independent patches were plotted and fitted according to the two-state model (see Methods). (A) WT MscL measured under ambient conditions (filled circles, black solid line) or in the presence of 25 mM DTT (blue open circles, dotted line). (B) L121C/L122C (squares, solid line) and L128C/L129C (triangles, dotted line) measured under ambient (red) or reducing (blue) conditions. Inset: a typical activation trace of L128C/L129C MscL measured under ambient conditions (red) or in the presence of 25 mM DTT (blue) in the same patch, in response to a similar sequence of pressure steps. (C) L121A/L122A (red) and L121T/L122T (blue) measured under ambient conditions. (D) The data for the quadruple L121A/L122A/L128A/L129A (red circles and solid line) and L121T/L122T/L128T/L129T (blue diamonds and dotted line). The black solid line representing WT MscL is given as reference in each panel.

the pattern upon reduction, occupying more short-lived low-conductance substates. We suspected this atypical behavior might result from loosening the S3 association. To verify this notion further we introduced small side chain substitutions for the highly conserved leucines in S3, which was expected to weaken the interactions between S3 domains. The L121A/L122A, L128A/L129A and L121T/L122T double mutants as well as the quadruple L121A/L122A/L128A/L129A and L121T/L122T/L128T/L129T mutants were produced. The dose-response curves for the double alanine and threonine mutants were similar to the curve for WT control (Fig. 1-7 C, D), with a similar $\gamma_{0.5}$ (L121A/L122A, 10.4 $\pm$ 0.5 (n = 6); 128A/L129A, 10.1 $\pm$ 1.3(n = 4), L121T/L122T, 10.2 $\pm$ 0.7 (n = 7); wild type, 10.5 $\pm$ 0.6 (n = 10)). The alanine or threonine quadruple substitutions further weaken the interactions between S3 bundles and produce slightly 'softer' phenotypes. $\gamma_{0.5}$ of L121A/L122A/L128A/L129A and L121T/L122T/L128T/L129T, is 9.7 $\pm$ 0.7 (n = 7) and 9.2 $\pm$ 0.5 (n = 4) respectively, smaller than that of wild type ($P < 0.05$). Single channel recordings show that L121A/L122A and L128A/L129A mutant significantly increased the occupancy of short-lived low-conductance substates, similar to the gating pattern of L121C/L122C mutant upon disulfide reduction (Fig. 1-8). Reduced cysteines are smaller and more polar than leucines and the gating pattern of cysteine mutants upon disulfide reduction is expected to be comparable to the effect of alanine substitution at the same positions. Our results indicate that replacing leucines with smaller alanines or reducing double cysteine mutants with DTT is likely to cause partial S3 bundle dissociation and increase dynamics of S3 domains or M2-S3 linkers. They may interact with the conducting pathway of the pore and lead to multiple short-lived substates.

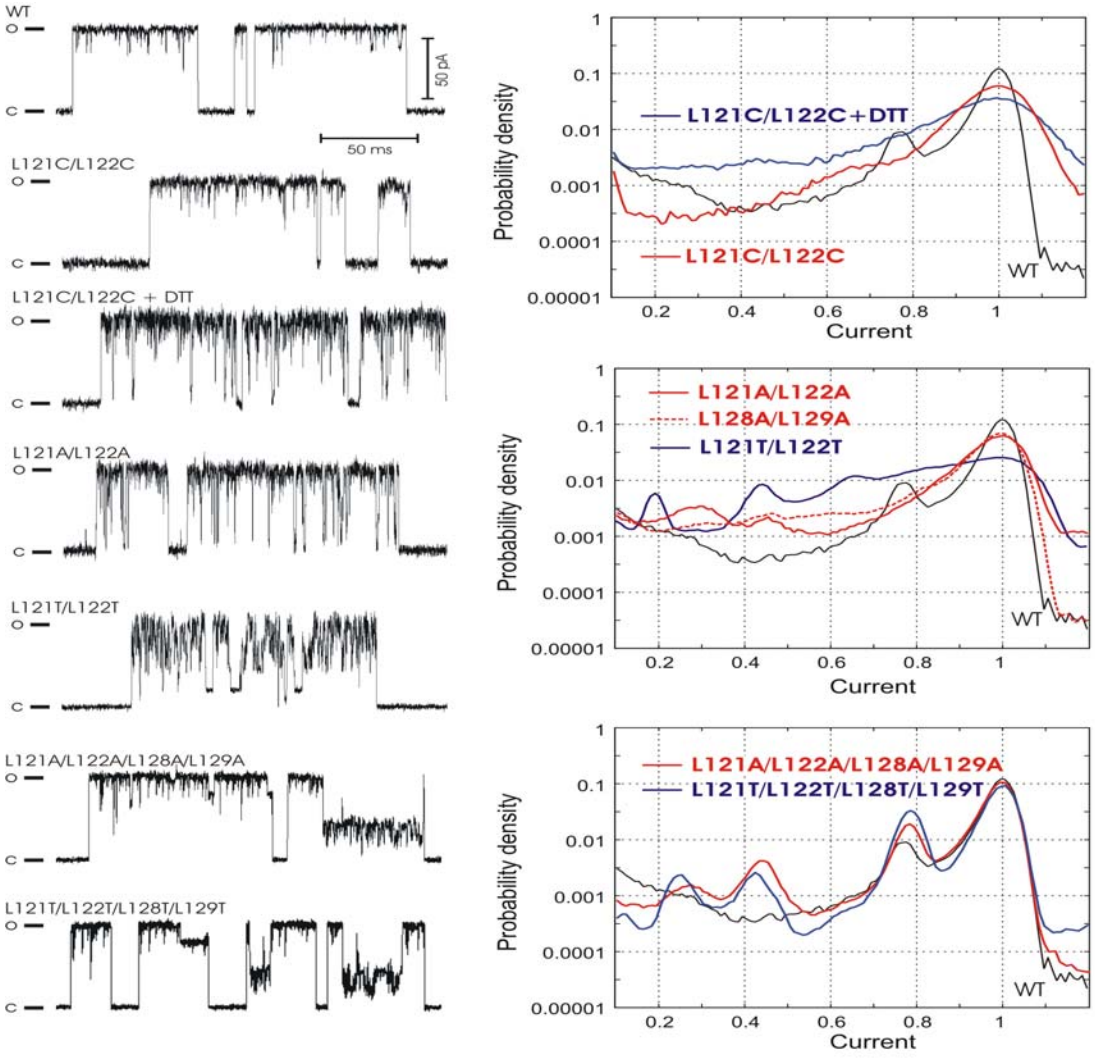


**Figure 1-8.** Representative single-channel traces (left) and probability density amplitude histograms (right) for WT MscL and mutants with alanines, threonines or cysteines substituting for conserved leucines in S3. Cysteine mutants were characterized under ambient or reducing conditions. The histograms for WT are shown in all panels as reference (black solid line). Histogram Analysis was done for typically 5-min recording (n= 3) at constant pipette pressures in the range of open probabilities ($P_o$) between 0.01 and 0.08.

More polar threonines at positions 121 and 122 caused further reduction of the occupancy of the fully open state, favoring multiple short-lived substates, also long-lived states of about 0.65, 0.45 and 0.2 of full conductance (Fig.1-8). Peculiarly, the quadruple mutants with all four leucines substituted exhibit less pronounced short substates than the double mutants, but considerably more pronounced long-lived substates with amplitudes of 0.45 and 0.25 relative to the fully open state (Fig.1-8). The short-lived substates are less prominent in quadruple mutants probably because their bundles are completely disrupted and there is no interaction that would hold disordered C-termini near the pore entrance. The frequent long-lived substates could be because channels are prevented from closing completely by the 'foot-in-the-door' action of loose S3 domains or linkers.

In conclusion, the experiments presented here support the closed-state arrangement of transmembrane helices (cross-link between cysteines 24 and 26) and a uniquely large iris-like conformational rearrangement of the MscL protein during the gating transition (open-state stabilizing cross-link between cysteines at positions 20 and 36). M1 and M2 should tilt together as a unit as suggested by the cross-link between cysteines 32 and 81. The data also suggest S1's interact with each other in the closed conformation (cross-links between cysteines in equivalent positions 7 or 10), forming a cytoplasmic gate. In contrast to what was proposed in the early model, S3 domains are stably associated in both closed and open conformations (multiple cross-links in the C-terminal domain).

# Chapter 2

# Analysis of open probability, dose-response curves and the molecular scale of MscL protein expansion


## Abstract

Despite increasing evidence for the open-state conformation of MscL, the energetic description of its complex gating remains incomplete. The previously estimated in-plane expansion of MscL (Sukharev et al., 1999b) is considerably smaller than predicted by molecular models. To resolve this discrepancy, I conducted a systematic study of currents and dose-response curves for WT MscL in *E. coli* giant spheroplasts. Using the all-point histogram method and calibrating tension against the threshold for the small mechanosensitive channel (MscS) in each patch, I found that the distribution of channels among the subconducting states is significantly less dependent on tension than the distribution between the closed and conducting states. The analysis suggests that the rate-limiting barrier and the major channel expansion occur between the closed state and a low-conducting substate, which is consistent with the previously-proposed gating scheme (Sukharev et al., 1999b). At –20 mV, all substates together occupy approximately 26% of the open time in the entire range of tensions examined. When compared to the ideal two-state channel which switches between the fully closed and fully open states, these substates reduce the mean integral current by about 6%, essentially independent of tension. This allows us to present $P_o$ as the ratio of the mean integral current at a given tension step to the mean current at saturating tensions. Dose-response ($P_o$-tension) curves determined with the alternative threshold method are indistinguishable from the curves

determined using integral current. The apparent energy and area differences between the fully closed and fully open states, ΔE and ΔA, extracted from 29 independent dose-response curves varied in a linearly correlated manner while the midpoint tension stayed around 10.4 dyne/cm. Statistical modeling suggests slight variability of gating parameters among channels in each patch, causing a strong reduction and correlated spread of apparent ΔE and ΔA. The slope of initial parts of activation curves, with a few channels being active, gave estimates of ΔE=51±13 $kT$ and ΔA=20.4±4.8 $nm^2$, the latter being consistent with structural models of MscL which predict ΔA =23 $nm^2$.

## Introduction

An atomic-scale homology model of closed *E. coli* MscL (EcoMscL) has been built based on the solved TbMscL crystal structure (Chang et al., 1998). Several hypothetical open conformations were proposed (Sukharev et al., 2001). As was described in Chapter 1, the models of the EcoMscL in the closed and open (expanded) states with tilted helices were supported by cysteine cross-linking experiments *in situ*, as well as with patch-clamp experiments on cysteine mutants. While the stereochemical aspect of MscL opening is becoming better understood, the thermodynamic description remains not only incomplete, but also inconsistent with the atomic model predictions. A previous thermodynamic treatment of multi-channel recordings made in liposomes in the framework of the two-state model (Sukharev et al., 1999b) estimated the intrinsic energy of MscL transition as 19 $kT$ and the in-plane expansion as 6.5 $nm^2$, the latter being too small to accommodate the highly conductive pore. The dose-response curves recorded *in situ* from giant spheroplasts in preliminary trials have estimated $\Delta A$ as 10-15 $nm^2$, which is larger than in liposomes, but still half of what the structural models predict. It seemed important to find what caused this apparent systematic discrepancy and to estimate the true values for $\Delta A$ and $\Delta E$.

In this chapter, I conduct a systematic study of single-channel traces and dose-response curves for EcoMscL in patches excised from giant spheroplasts. I utilize the activation pressure of MscS as a reference point to assess the tension acting on MscL. By analyzing occupancies of major subconducting states as a function of tension, I validate the use of the integral current recorded from multi-channel patches as a measure of $P_o$ and the two-state model for gross thermodynamic description of MscL gating. The results

allow us modify an extended kinetic scheme of MscL in accordance with the dependencies of subconducting states on tension. Although a large variance of apparent $\Delta E$ and $\Delta A$ was observed from 29 independent dose-response curves, intriguingly the midpoint tension remained around 10.4 dyne/cm. To solve this puzzle, Dr. Andriy Anishkin came up with a hypothesis of possible channel variability in each patch. We then performed statistical modeling to test this idea. Simulated results show that when the channel population in the patch is non-uniform, the observed gating parameters ($\Delta E$ and $\Delta A$) may be substantially lower than the intrinsic ('true') parameters characterizing individual channels. By measuring the 'limiting slope' of the left-most regions of does-response curves, I found a more realistic value for $\Delta A$ that better corresponds to the model predictions.

## Results

### Pressure-current responses of spheroplast patches and the tension scale

Current traces from two representative patches with 52 and 5 MscL channels are shown in Fig. 2-1 A and B, respectively. Both recordings were made in spheroplasts in inside-out configuration at -20 mV (pipette positive). The average number of channels per patch was 50±5 (n = 11) in induced cells and 5±2 (n = 20) in non-induced spheroplasts. The later number of channels per patch illustrates the 'leakage' of the vector promoter. This minimal level of expression combined with possible clustering of channels, did not permit reproducible recordings from true single-channel patches.

Prior to MscL activation, the small mechanosensitive channel (MscS), (Martinac et al., 1987; Sukharev et al., 1993) endogenous to the host strain, always activated at a

lower suction (arrow), exhibiting the unitary current of ~25 pA, under given ionic conditions (see Methods). MscL exhibits first openings (~75 pA, asterisk) at suction 1.5~1.6 times higher than what is required to open MscS, consistent with previous observations (Blount et al., 1996b). MscL activities increase with pressure and in both instances reach saturation. At a pressure application rate of 50-60 mm Hg/s, as shown in the trace, MscS channels activate in an almost threshold-like manner and the steep onset marks the mid-point of its activation by pressure ($p_{½}^{MscS}$), which corresponds to the tension of $\gamma_{½}^{MscS}$ = 5.5 dyne/cm, as reported previously (Cui and Adler, 1996; Sukharev, 2002). Assuming that the patch is a hemispherical cup and its radius of curvature (r) does not change in this range of pressures, the relation $\gamma/\gamma_{½}^{MscS} = p/p_{½}^{MscS}$ can be derived from the law of Laplace: $\gamma = pr/2$. Thus, determination of $p_{½}^{MscS}$ allows us to calibrate tension in each patch, and presents activation curves measured in different pressure ranges in a unified tension scale and treat the curves statistically.

Having $p_{½}^{MscS}$ one can also estimate the effective patch radius $r$ for a given size of pipettes, which provides information about patch geometry. In twenty-one independent trials, $p_{½}^{MscS}$ was determined as 148±29 mm Hg. Based on this data, the law of Laplace produces $r$ = 0.58±0.12 μm, with the actual distribution illustrated in Fig. 2-1A (inset). Assuming that patches are hemispherical caps delineated by about 60° angle relative to the axis of the pipette (Sukharev et al., 1999b), their areas can be calculated as

$$\text{Area} = 2\pi(1-\cos(\alpha))\times r^2 ,$$

where r is the radius of the patch, α is the angle relative to the axis of the pipette. This gives an estimation of Area = 1.1±0.5 $\mu m^2$ (n = 21).

**Figure 2-1.** Activation of MscL by transbilayer pressure gradients. (A) Patch-clamp recordings of channels at - 20 mV (pipette positive) from spheroplasts expressing the wild-type MscL after induction with IPTG (1 mM, 30 min). A total of 52 channels were observed at the pressure close to saturating. (B) MscL activities recorded without IPTG induction. Five channels are observed in this particular experiment. The pressure traces measured in mm Hg are shown below each current trace. The points of half-maximal activation of MscS and first openings of MscL are indicated by arrows and asterisks, respectively. Using pressure that elicits half-maximal activation of MscS, $p_{½}^{MscS}$ (which corresponds to tension of 5.5 dyne/cm) the pressure scale was converted into the scale of tensions. Inset represents the distribution of radii of curvature (r) calculated from the Law of Laplace in twenty-one patches sampled with standard 5 MOhm pipettes.

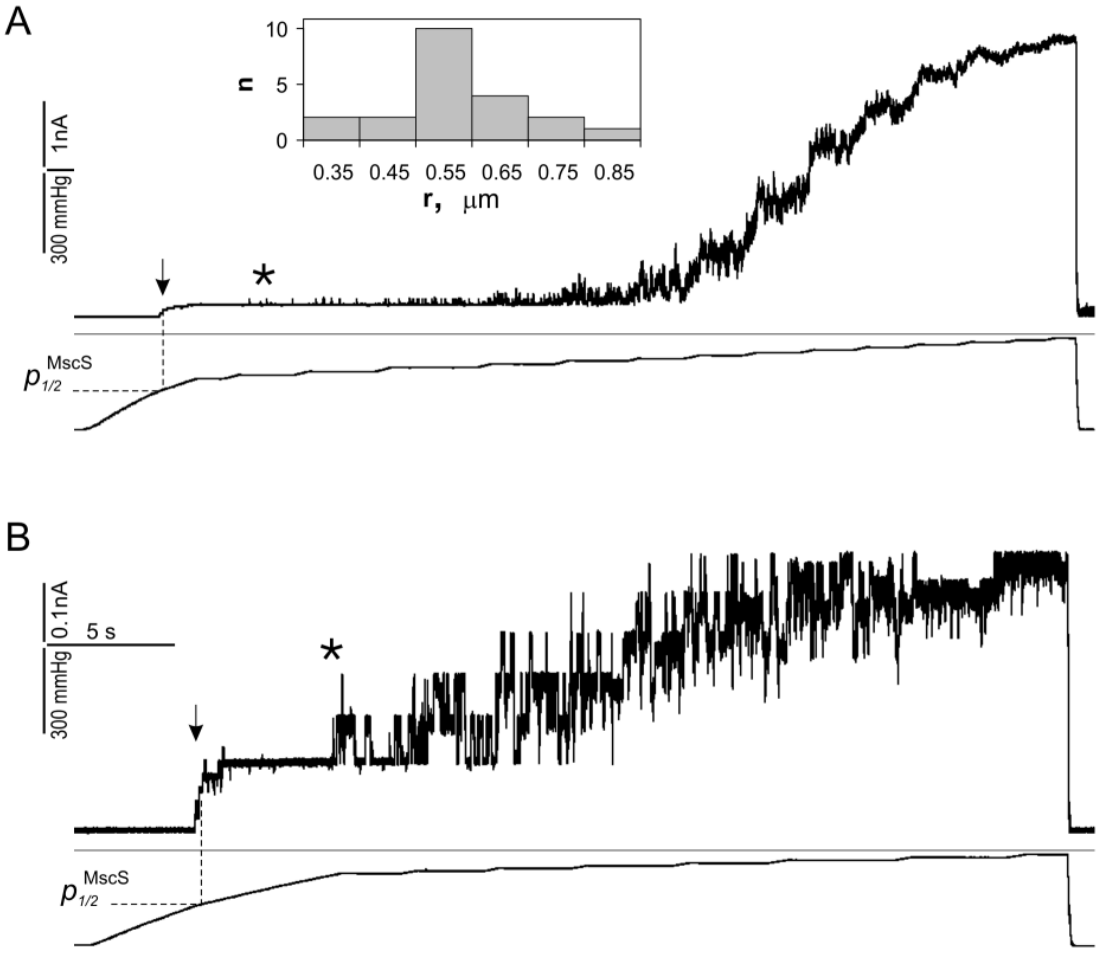
A
10
5
0
n
0.35 0.45 0.55 0.65 0.75 0.85
r, μm
1nA
300 mmHg
*
p 1/2 MscS
B
0.1nA
5 s
300 mmHg
*
p 1/2 MscS

**The structure of subconducting states**

Fig. 2-2A shows the fragment of a typical MscL trace recorded at -20 mV. The openings activated by moderate suction display short-lived substates seen as downward flickers from the fully open state (< 0.5 ms long) and distinct long-lived subconductance levels (> 2 ms). The short-lived substates are visited predominantly from the fully open state. Transitions to similar short substates are also observed from the long-lived substates. A typical all-point amplitude histogram constructed from a 5-min long continuous recording is presented on the panel B. A reasonably good fit of the experimental histogram by a sum of nine Gaussian curves indicates several discernable peaks with amplitudes of 0.22, 0.54, and 0.78 relative to the amplitude of the fully open state. The fit also suggests the presence of less prominent and more scattered intermediate levels centered near 0.7 and 0.93. The accuracy of fitting also required two low-populated peaks positioned near 0.33 and 0.45, and two more peaks with amplitudes of 0.07 and 0.13; however, the closeness of 0.07 to the highly populated closed state reduces the confidence of its exact position and occupancy. The prominent peak at 0.78 represents the long-lived subconducting state ($L_{0.78}$) visited predominantly from the fully open state. $L_{0.78}$ is kinetically different from short-lived substates $S_{0.22}$, $S_{0.45}$, $S_{0.70}$ and $S_{0.93}$. The occupancies of the closed and conductive states varied in different trials, while positions of the peaks were reproducible with the accuracy of 2 %. The short substates $S_{0.22}$, $S_{0.45}$, $S_{0.70}$ and $S_{0.93}$ are visited not only from the fully open state, but also show up as brief (10-40 μs) intermediate stair-like levels observed during opening or closing transitions (not shown). These levels correspond to the amplitudes of short substates (0.28, 0.71, and 0.90) previously reported in liposome-reconstituted patches (Sukharev et al., 1999b). Because the fragments of

liposome recordings were much shorter than those used in the present work, the substate with the relative amplitude near 0.45 and long-lived substate 0.78 were unaccounted in the previous analysis.

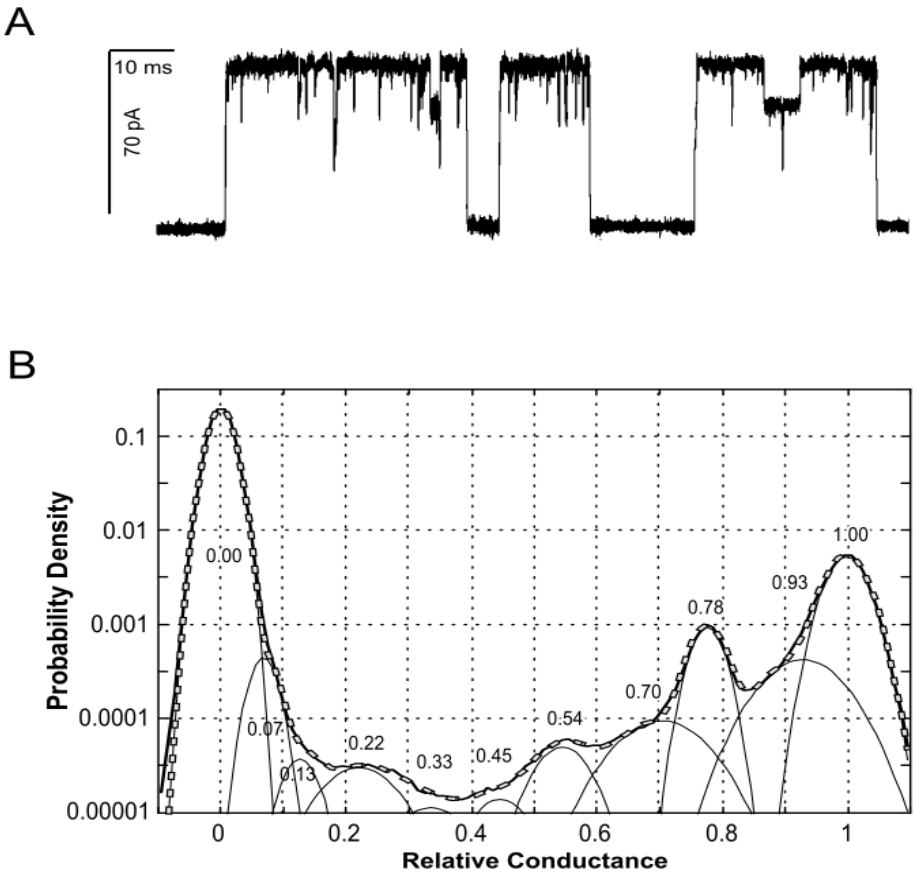


**Figure 2-2.** Representative single channel currents of MscL recorded in a 30 kHz bandwidth from an inside-out patch at -20 mV (A). A 0.15-second fragment of a 5-min trace is shown with openings as upward deflections. The all-point amplitude histogram (B) compiled of 120 bins (solid envelope curve) includes the entire 5-min dataset. It was fitted by a sum of eleven Gaussian distributions (dashed line). The peak positions shown by numbers represent amplitudes of subconducting states relative to the amplitude of the fully open state.

**Effect of tension on subconducting states**

To address the question of whether the mean integral current would be an adequate measure of open probability of MscL at each pressure step, I analyzed the relative occupancies of conducting states with tension (see below). The relative occupancy (or probability density) discussed in Fig. 2-3 is defined as the ratio the substate (or fully open state) occupancy to the total occupancy of all conducting states (substate plus fully open state), thus representing the proportion of time a state is occupied when the channel conducts at a given tension. A number of traces containing 3-5 channels were recorded in the range of open probabilities between 0.02 and 0.85. Amplitude histograms for one-channel fragments recorded at constant tensions were generated and compiled as a smooth 2-D diagram using the HISTAN software written by Dr. Andriy Anishkin (Fig. 2-3A). The surface represents the probability density for conducting states with amplitudes between 0.1 and 1.1, as a function of tension. The total probability of conducting states at each tension was normalized to be unity. The ridge on the far right edge represents the fully open state, whereas the lower ridge next to it corresponds to the prominent $L_{0.78}$. The elevated point in the corner closest to the viewer indicates the presence of low-conducting substates, which gradually disappear as tension increases. The inset above shows the actual open probability (calculated from the mean integral current of the entire channel population) plotted against tension in the same scale. It is evident from the diagram that while $P_o$ changes by more than two orders of magnitude in the given range of tensions, the shape of the landscape remains essentially the same and the relative occupancies of major subconducting states do not change substantially. Fig. 2-3B represents the numerical data obtained from Gaussian fits of ten averaged amplitude

histograms (cross-sections of the above surface at different tensions). The relative occupancy of short subconducting states $S_{0.22}$ (diamonds, ♦) and $S_{0.93}$, (solid triangles, ▲) slowly decrease, whereas the relative occupancy of the long-lived $L_{0.78}$ (filled circles, ●) increases. The slopes of the tension dependencies indicate relatively small, but measurable differences in in-plane areas occupied by the substates. By computing the relative occupancy ratio of any sub-conductive state to the open state along the tension gradient, we were able to compare the free energy change and apparent protein expansion between the two states. The areas of $S_{022}$ and $S_{0.93}$ are estimated to be smaller than that of the fully open state by 3.4 and 1.9 $nm^2$, respectively. The increase of $L_{078}$ occupancy with tension suggests that this conformation of the channel is wider by about 1.8 $nm^2$ than the open state. Correspondingly, the effective area changes for $C \rightarrow S_{022}$ , $C \rightarrow S_{0.93}$ and $C \rightarrow L_{078}$ transitions would represent 74%, 85% and 114% of the apparent area change for the entire closed to open ($C \rightarrow O$) transition (12.8 $nm^2$, in its uncorrected form as deduced from multi-channel dose-response curves, see below). This is consistent with the model which includes one dominant tension-dependent transition ($C \rightarrow S_{022}$ ) and with previous observations (Sukharev et al., 1999b) that once MscL makes a transition from the closed state to the low conducting substate, it quickly becomes distributed between the fully open state and a group of upper substates with shallow dependencies on tension.

**Figure 2-3.** Relative occupancies of the MscL conductive substates as a function of applied tension. (A) The 2-D amplitude histogram representing the relative probability of a single MscL channel to be in a particular conductive state at different tensions is compiled from 10 independent traces. The x-axis indicates the magnitude of applied tension, $\gamma$, relative to the mid-point tension for MscL activation, $\gamma_{½}$ ; the y-axis shows the relative conductance of ion channel normalized to the conductance of the fully open state. The z-axis displays the probability density in logarithmic scale. The inset above is the plot of open probability ($P_o$) versus $\gamma/\gamma_{½}$, which represents a simultaneous fit of ten dose-response curves with eqn. $P_o = 1 / [\ 1 + \exp(\ \Delta E - \gamma\ \Delta A)/\ k_B T\ ]$. (B) Occupancies of conductive states derived from amplitude histograms, as the one in Fig. 2-2, recorded at different tensions. Only the relative occupancies of $S_{0.22}$ (solid diamond), $L_{0.78}$ (solid circles) and $S_{0.93}$ (solid triangles) versus tension are presented. The combined relative occupancy of all 9 substates together (open triangles) as well as occupancies of the fully open state (solid squares) remained practically constant over the range of tensions relative to the total occupancy of all conducting states taken as unity. Open squares represent the effective amplitude of the integral current, which is the sum of all substate occupancies multiplied by the corresponding amplitudes.

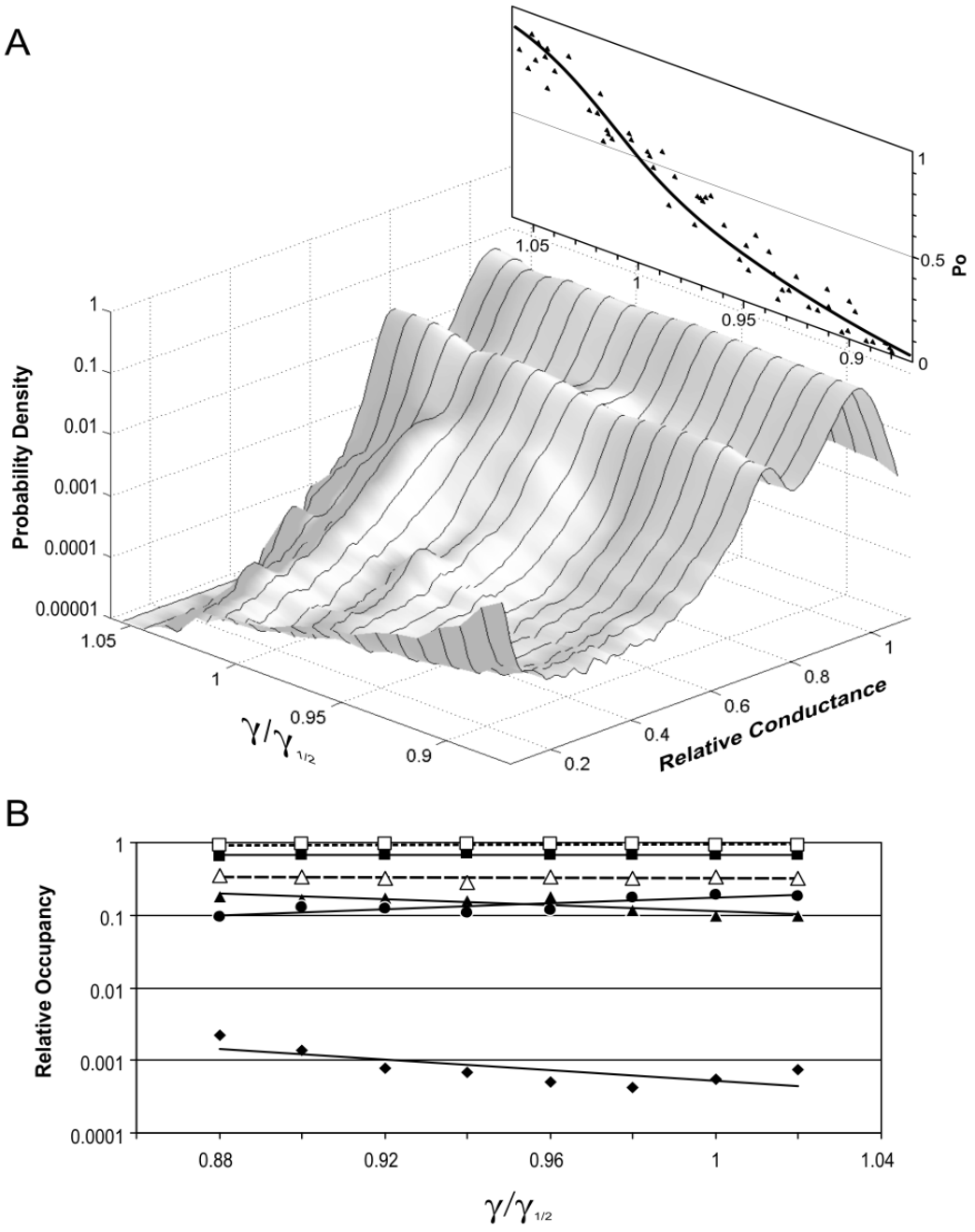
A
Probability Density
1
0.1
0.01
0.001
0.0001
0.00001
1.05
1
0.95
0.9
γ/γ1/2
0.2
0.4
0.6
0.8
1
Relative Conductance
Po
1
0.5
0
B
Relative Occupancy
1
0.1
0.01
0.001
0.0001
0.88
0.92
0.96
1
1.04
γ/γ1/2

**Determination of open probability ($P_o$)**

*Threshold method*

For a channel with multiple conducting states, such as MscL, the definition of open probability is not unequivocal. At its simplest, $P_o$ can be defined as the fraction of time the channel conducts above a certain threshold, residing in any of non-closed states or 1-$P_c$, (Fig 2-4A). Because MscL has a number of short-lived substates, some of which are low-conducting, the threshold can be set at the level of 0.1 of the fully open conductance to capture most of them. The threshold method easily applies to single-channel traces, but also works reasonably well for patches with a small number of channels ($n \leq 5$). The application of this approach is illustrated below.

If a patch contains not one, but N channels, then N regularly placed thresholds should be used to separate and count the number of channels that are open at each moment (see Fig 2-4 B, an example for 3-channel patch). An all-point histogram separated with the threshold levels to (N+1) parts will give the probabilities to see 0, 1, 2, …, N channels open at a given tension ($P\binom{N}{0}, P\binom{N}{1}, P\binom{N}{2}, \ldots, P\binom{N}{N}$ correspondingly). Since the channel gating (closure or opening) is characterized by binary variables, the binomial probability distribution can be used to describe the outcomes of an event. The total probability of seeing a certain number of channels (k) being open can be calculated through the probability of one independent channel to be in open state ($P_o$) in the patch:

$$P\binom{N}{k} = \frac{N!}{k!\cdot(N-k)!} \cdot (P_o)^K \cdot (1-P_o)^{N-k},$$

the factorial coefficient represents number of possible outcomes.

From the total probabilities of seeing all channels being closed or 1, 2 … k channels being opened at the same time, it permits us to estimate the open probability of an individual channel ($P_o$) in the patch. Any of the following formulas or the combined average value can be used for estimations of $P_o$:

$$P_o = 1 - P\binom{N}{0}^{1/N}$$

$$P_o = P\binom{N}{N}^{1/N}$$

also $P_o$ estimated by solving polynomial equations

Below is an example of a typical amplitude histogram from a recording of three MscL channels in a patch (Fig. 2-4B). The thresholds are positioned at 0.1, 1.1, and 2.1 in x-axis relative to the fully open conductance. The leftmost peak at the position 0 in x-axis corresponds to the closed state. For the case of three channels in the patch, the above-mentioned formulas can be written as:

$$P\binom{3}{0} = (1 - P_o)^3$$

$$P\binom{3}{1} = 3 \cdot (1 - P_o)^2 \cdot P_o$$

$$P\binom{3}{2} = 3 \cdot (1 - P_o) \cdot P_o^2$$

$$P\binom{3}{3} = P_o^3$$

Individual channel $P_o$ is calculated as follows:

$$P_o = 1 - P\binom{3}{0}^{1/3}$$

$$P_o = P\binom{3}{3}^{1/3}$$

or obtained $P_o$ from solving any individual polynomial, $P\binom{3}{1} = 3 \cdot (1 - P_o)^2 \cdot P_o$ or $P\binom{3}{2} = 3 \cdot (1 - P_o) \cdot P_o^2$; a combined average $P_o$ would give a fair estimation.

Note that the amplitude threshold technique can be easily applied when the number of MscL channels in the patch is less than 6; in recordings containing more channels, however, smearing of levels makes the threshold assignment difficult. In this case, an integral current method can be used to estimate probability of an individual channel to be in open state.

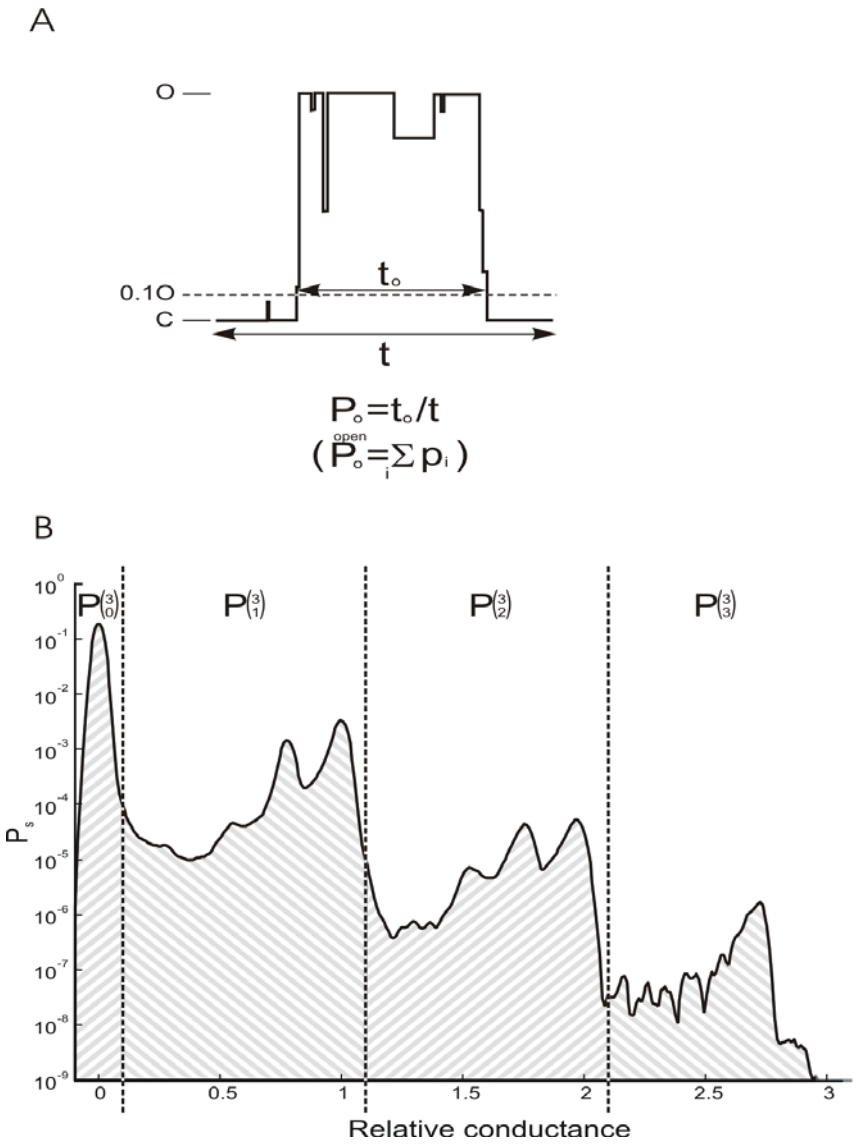


**Figure 2-4.** Determination of $P_o$ by the threshold method. (A) A hypothetic scheme represents a non-ideal channel containing several subconductive states. By carefully placing the threshold, the channel residing above the threshold is considered in the open state, otherwise, it is in the closed state. The $P_o$ can be defined as the fraction of time ($t_o$) the channel conducts above the certain threshold (0.1) to its total period (t). (B) An example of placing thresholds for a 3-channel patch from an all-point histogram. By knowing the open probability of the numbers of the channel out of the three channels, it permits us to calculate the single channel open probability ($P_o$).

*Assessment of open probability by integral current*

An ideal two-state channel resides in either the fully closed or the fully open state. The integral current at any tension is the product of the conductance of the fully open state ($g_O$) and its occupancy, i.e. $P_o$. If a channel has multiple conductive substates, the integral current will have contributions from all of them. We can define how the measured integral current depends on the probabilities and conductance of individual states. Suppose at a given tension γ, each of the $i^{th}$ conducting states of a channel is characterized by its probability of being in any conductive states, $p_i$, with conductance, $g_i$. Conductance $g_i$ can also be denoted through the fractional conductance $f_i = g_i/g_o$ , where $g_o$ is the conductance of the fully open state. The probability of being in any of the conductive states (fully open + sub-conductive state) can be presented as the sum:

$$P_o(\gamma) = \sum_{i_{OPEN}} p_i(\gamma) = 1 - P_c(\gamma),$$

$P_c(\gamma)$ here is the probability of being in any non-conducting state. Our assumption is that MscL channel has only one closed state (C).

The relative integral conductance of a channel at a tension γ will be the sum of the fractional conductance $f_i$ multiplied by the probability being in each conductive state $p_i$, which can be expressed by $\sum_{i_{OPEN}} f_i . p_i(\gamma)$

To describe the deviation of a channel containing substates from an ideal two-state channel, we use the following expression:

$$\langle f(\gamma) \rangle = \frac{\sum_{i_{OPEN}} f_i \cdot p_i(\gamma)}{\sum_{i_{OPEN}} p_i(\gamma)}$$

$\langle f(\gamma)\rangle$ is called time-averaged fractional conductance of the channel. 1- $\langle f(\gamma)\rangle$ therefore represents the reduction of the time-averaged conductance of a multistate channel from that of an ideal channel that displays only a fully open state.

The integral conductance at a given tension for a multistate one-channel patch can be written as:

$$G(\gamma) = \langle f(\gamma)\rangle \cdot g_o \cdot P_o(\gamma)$$

Assuming that the integral conductance at saturating tensions in which a multistate channel remains always conductive, i.e. $P_o(\gamma_{max}) = 1$, can be approximated as:

$$G_{\max} = \langle f(\gamma_{\max})\rangle \cdot g_o$$

If $\langle f(\gamma)\rangle$ of a multistate channel is close to $\langle f(\gamma_{max})\rangle$, i.e., in the wide range of tensions, the channel displays the same degree of deviation to the ideal two-state channel, then, $P_o(\gamma)$ can be expressed as

$$P_o(\gamma) = G(\gamma) / G_{\max}$$

For an ideal two-state channel without subconducting states, it can be shown that integral conductance through the multi-channel patch is proportional to the open probability of the single channel. In an N-channel patch, the integral conductance for the opening of k channel at any tension can be expressed as:

$$G_{IC} = \sum_{k=1}^{N} k \cdot G_o \cdot P(\tbinom{N}{K}) = G_o \cdot \sum_{k=1}^{N} k \cdot P(\tbinom{N}{K}) = G_o \cdot N \cdot P_o$$

So that $P_o = \dfrac{G_{IC}}{G_o \cdot N} = \dfrac{G_{IC}}{G_{o_{\max}}}$

where $G_o$ is the full conductance of the individual channel in a multiple channel patch.

The graph presented in Fig 2-3B shows those relative occupancies of conducting state as functions of tension. As a result of opposite tendencies for the short- and long-

lived substates, the combined relative occupancy of all sub-conducting states (open triangles, ∆) and the relative occupancy of the fully open state (solid squares, ■) remains practically constant. The numbers show that all sub-conducting states occupy approximately 26% of the time the channel conducts above the threshold of 0.1 and 74% of the time in the fully open state. These subconducting states reduce the mean integral current by about 6% relative to an 'ideal' open channel without substates, essentially independent of tension (Fig. 2-3B, open square, □). Thus, the integral current for MscL is always 94% of ionic current expected for an ideal two-state channel of the same open-state conductance. Having $\langle f(\gamma) \rangle$ constant and equal to 0.94, one can write $P_o = (G_{IC} \cdot 94\%) / (G_{max} \cdot 94\%) = G_{IC} / G_{max}$. Therefore, although MscL displays multiple subconducting states, we can treat it in a simplified two-state approximation, C→ $O_{effective}$, and estimate $P_o$ for individual channels from integral current measured on multi-channel patches.

**Dose-response curves**

After validating that integral current is an adequate measure of $P_o$, I analyzed 29 dose-response curves from patches with a few or multiple MscL channels obtained either without or with induction, respectively. The combined data are presented as $P_o/P_c$ in logarithm scale versus tension in Fig. 2-5A. Scaling of tensions was done for each dose-response curve using individually MscS as an internal gauge. Prior to fitting and statistical treatment, we compared the open probabilities estimated from the same traces with two different methods. As illustrated by the inset to Fig. 2-4, the $P_o/P_c$ values obtained from a 5-channel patch are the same when measured from the integral current (open circles) or using the threshold method (closed circles); the difference in parameters

ΔE and ΔA estimated from the fits was less than 1%. Note that the amplitude threshold technique can be easily applied when the number of MscL channels in the patch is less than 5; smearing of levels in recordings containing more channels, however, makes the threshold assignment difficult. Assessment of $P_o$ from integral current, in contrast, is insensitive to the number of channels in the patch. For uniformity, the entire dataset presented in Fig. 2-5 was obtained using the integral current only.

Each curve presented in Fig. 2-5A was fitted by the two-state model yielding a pair of parameters, ΔE and ΔA. The thick solid line represents the effective dose-response curve recreated with the mean values across the dataset, ΔE = 32.4 *kT* and ΔA = 12.8 $nm^2$. The individual curves (three examples are shown by thin lines), however displayed different slopes; as a result, the scatter of parameters was quite large, being ± 10.3 *kT* for ΔE and ± 4.2 $nm^2$ for ΔA (standard deviations). The minimum observed values of ΔE and ΔA were 13.7 *kT* and 5.8 $nm^2$, whereas the maximum values were 52.2 *kT* and 20.8 $nm^2$, respectively. The point of intersection with the x-axis, representing the tension midpoint ($\gamma_{1/2}$) for each curve was more consistent, with the mean position at 10.40 ± 0.8 dyne/cm. When ΔE and ΔA from each experiment were plotted against each other (Fig. 2-5B), the two parameters were linearly correlated (Pirson's correlation coefficient R = 0.98) with a slope of 10.4 dyne/cm. This reflects the fact that different activation curves have different slopes, but intersect with the x-axis close to the same point of 10.4 dyne/cm. As dictated by eqn. 1 (see Methods), the tension $\gamma_{1/2}$ that causes equipartitioning of the channel between the closed and open states is equal to the ΔE/ΔA ratio.

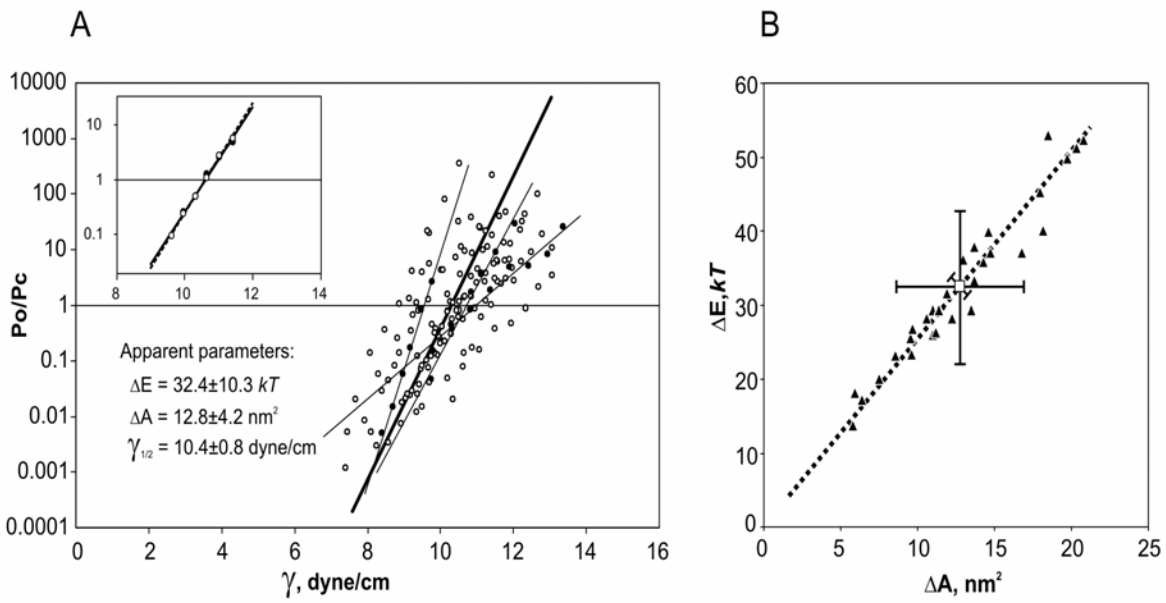


**Figure 2-5.** Dose-response curves and apparent gating parameters of MscL. (A) Twenty-nine independent curves (ten from induced and nineteen from un-induced patches) plotted as $P_o/P_c$ ratio (in a logarithmic scale) versus membrane tension and fitted to the two-state model. Apparent parameters ΔE, ΔA, and $\gamma_{½}$ were extracted from each fit, averaged and presented as the mean ± SD. The thick solid line represents the curve with the average parameters. Thin solid lines are examples of individual curves with varying slopes. Inset: $P_o/P_c$ versus tension plots obtained from the same trace with five active channels. Open circles represent $P_o$ obtained from the integral current; closed circles show $P_o$ determined using the amplitude threshold (0.1) detection technique. (B) Energies of MscL gating transition (ΔE) plotted against apparent protein area changes (ΔA) calculated from individual traces. Vertical, horizontal, and diagonal error bars represent standard deviations of ΔE, ΔA and $\gamma_{½}$ = ΔE/ΔA, respectively, around their mean values. Dotted line is the linear fit passing through the origin. Pirson's correlation coefficient of ΔE and ΔA values is 0.98.

**Intrinsic gating parameters and statistical modeling of population response**

To explain the correlated variation of $\Delta E$ and $\Delta A$, we hypothesized that a large scatter in the slope of the activation curves, and a much smaller scatter of $\gamma_{1/2}$ may be specifically due to heterogeneity of channel population in each patch. Indeed, if the midpoint positions of activation curves for individual channels in the patch are scattered around the mean, the midpoint of the curve measured on the entire population should not deviate much from that mean. However, because some channels activate earlier, and some later on tension, the 'smearing' of the resultant curve is expected to decrease the slope (see simulation below). Since we never observed any significant deviation of MscL unitary conductance from 3.1-3.2 nS, we presumed that the channel conformation in the open state is rather uniform and the protein expansion between the states, $\Delta A$, is most likely to be the same across the channel population. The local tension, however, may vary due to a local mechanical non-homogeneity of the membrane, and the term $\gamma\Delta A$ is expected to vary. Because only the product contributes to the free energy, the variation of $\gamma$ would be equivalent to variation of $\Delta A$. The intrinsic energy of the gating transition ($\Delta E$) of the channel may also be sensitive to the lipid or protein microenvironment in the membrane, in which a particular channel resides. The scatter of $\Delta E$ and/or $\Delta A$ among channels in the population is predicted to reduce the apparent slope of the combined activation curve, and this reduction would be more pronounced when standard deviations of $\Delta E$ and/or $\Delta A$ increase.

In order to choose realistic initial parameters, $\Delta E_o$ and $\Delta A_o$, reflecting the intrinsic behavior of channels (unperturbed by the surroundings), open conformation 11 from previously developed molecular models of MscL (Sukharev et al., 2001) was chosen

because it gives the closest prediction of the channel conductance (A. Anishkin, unpublished calculations). The open conformation 11 displays helical tilts of $72^{o}$ (M1) and cross-sectional pore area of 10 $nm^2$. This conformation is compared with the closed MscL in Fig. 2-6, where both models are shown with their solvent-accessible surfaces and the in-plane cross-sections. The mean cross-sectional areas of the open and closed conformations were computed as 40.8 and 17.5 $nm^2$, respectively. The difference of 23.3 $nm^2$ was taken as the initial parameter $\Delta A_o$. The energy of the transition, satisfying this area change and the midpoint tension of 10.4 dyne/cm in eqn 1 is 58.9 $kT$, which was taken as the initial $\Delta E_o$.

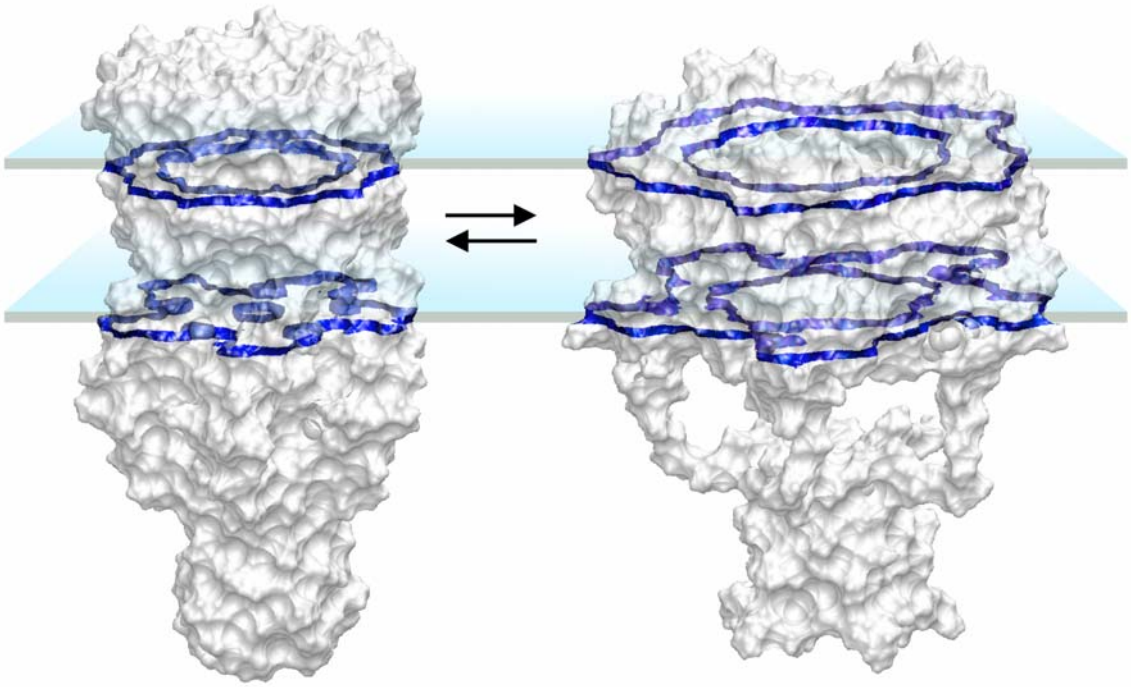

**Figure 2-6.** The models of the *E. coli* MscL in the open and closed conformations shown with solvent-accessible surfaces. The positions of the tansmembrane helices forming the barrel correspond to conformations 2 (closed) and 11 (open) from Sukharev et al. (2001), whereas the bundle-like arrangement of the C-terminal segments in the open state was supported by disulfide bridge experiments (see chapter 1). The cross-section planes are positioned approximately at the boundaries of the hydrophobic core of the membrane (±12 Å along the z axis). The average cross-sectional areas of the modeled closed and open states are 17.5 and 40.8 $nm^2$, respectively, predicting the transition-related area change of 23.3 $nm^2$.

Sets of normally distributed random numbers $\Delta E_i$ and $\Delta A_i$ with different standard deviations were generated using the "randn" function of Matlab. We started from one hundred random numbers and assumed these numbers follow the normal distribution. The standard deviations were varied, between 0 to 9 *kT* for $\Delta E_o$ (58.9 *kT*), and between 0 and 3.5 $nm^2$ for $\Delta A_o$ (23.3 $nm^2$). Fig. 2-7A represents a relatively uniform population of 100 channels (varying by 0.5% standard deviation from $\Delta E_o$ = 58.9 *k*T, i.e. SD ~0.3*k*T) and the simulated dose-response curve. The population response does not deviate substantially from that of a single channel. Panel B represents a population with the energy of transition scattered by 5% (SD ~3*k*T) relative to the $\Delta E_o$. The effective dose-response curve in this case is substantially inflected and the slope in the middle is about twice as lower than that in the left-most and right-most parts. A dispersion of $\Delta E$ by 3 *kT* around these mean parameters would reproduce the experimental dataset with an average 'apparent' $\Delta E$ of 32 *kT* and $\Delta A$ of 12 $nm^2$.The increase in the scatter to 10% further reduces the slope in the middle (not shown). One should note that the left-most and the right-most parts of the curve are close and parallel to the curve of the very first and very last channels activated by tension and the slopes of these parts correspond to that of a single channel and therefore reflect the intrinsic area change. A similar tendency was observed when a scatter between 0.5% and 5% was introduced to the $\Delta A_o$ parameter (~23.3 $nm^2$, SD ~0.1 and 1 $nm^2$) with the fixed $\Delta E_o$ (58.9 *k*T) in a uniform population of 100 channels. A dispersion of $\Delta A$ by 1 $nm^2$ around these mean parameters would also reproduce the experimental dataset with an average 'apparent' $\Delta E$ of 32 *kT* and $\Delta A$ of 12 $nm^2$ (not shown).

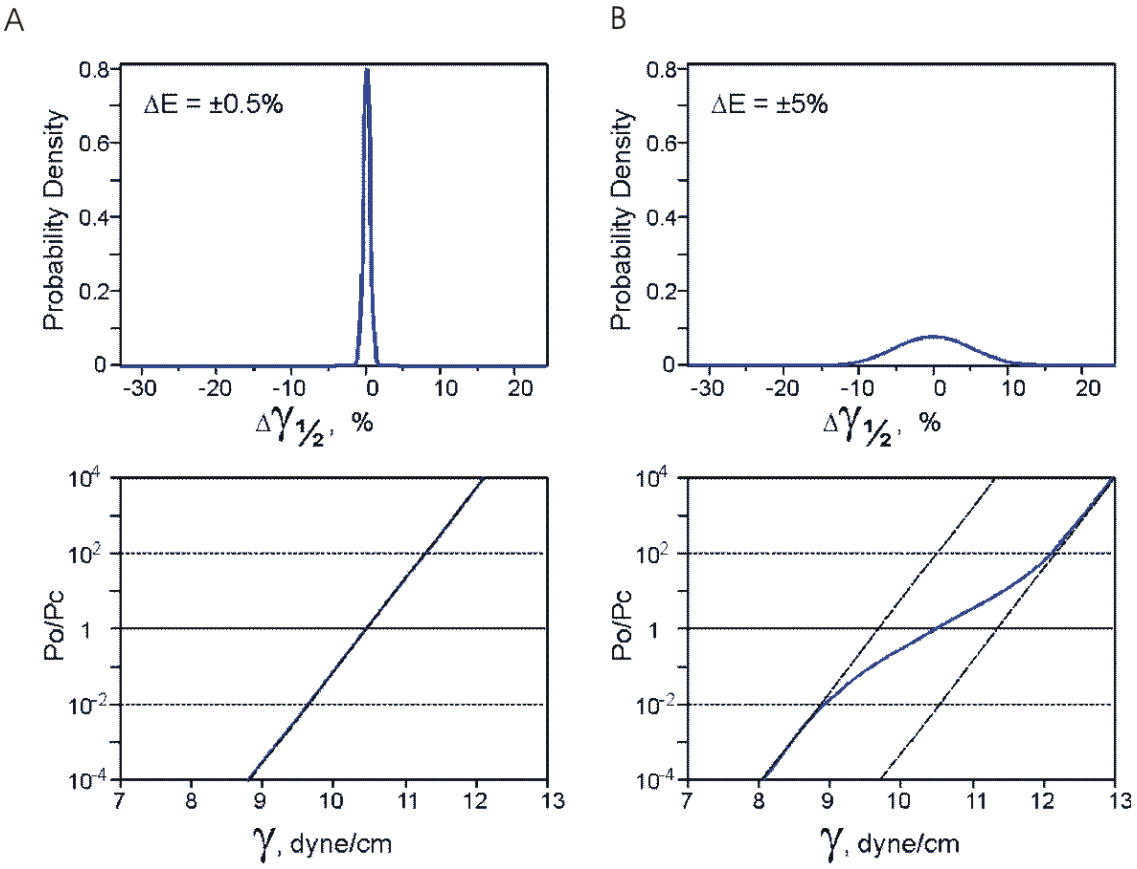


**Figure 2-7.** Statistical simulation of tension response of 100-channel populations. (A) Upper part is the distribution of ΔE of the 100 channels and their correspondent tension midpoint difference ($\Delta\gamma_{1/2}$, compare with 10.4 dyne/cm), obtained by scattering ΔE around initial 58.9 *k*T with standard deviation varying from 0.5% of ΔE and fixed ΔA = 23.3 $nm^2$ . Lower part is its simulated population dose-response curve. Note in (B), as the increase of the standard deviation of ΔE (5% of 58.9 *k*T), the simulated population dose-response curve is linear in the beginning and the end part but inflected in the middle part.

**Estimation of gating parameters from multi-channel traces**

The above analysis shows that 'true' thermodynamic parameters of gating could be readily estimated from single-channel traces. As mentioned above, those recordings were practically impossible to obtain due to the substantial 'leakage' of the promoter. From the simulated dose-response curves (Fig. 2-7B) one can see that the slope of the population response significantly deviates only in the middle, whereas the leftmost and rightmost parts of the curves have a slope close to that of an ideally uniform population, reflecting only the subpopulations of channels that activate very early or very late on tension. For this reason, we analyzed the slopes of left-most parts of multi-channel activation curves, i.e. the regions where only one or two channels were active. Examples of such curves are represented in Fig. 2-8. Like the simulated ones, these dose-response curves exhibit visible inflections. Fitting of the middle part of the left curve (dashed line) gives the estimation of $\Delta A$ of about 12 $nm^2$, whereas fitting the two initial points representing a sub-population of 'early' channels only (solid line) produces the slope of 22 $nm^2$. One needs to remember that, although the initial slope gives a better estimation of $\Delta A$, the intersection of the solid line with the x-axis represents the midpoint for the 'early' channels only. The correct midpoint position for the channel population in the patch can be obtained by fitting the entire curve. The inset in Fig. 2-8 illustrates two ways of treating such dose-response curves. In the scenario when only $\Delta E$ varies ($\sigma(\Delta E)>0$, $\Delta A$ = const), activation curves for individual channels are translated up and down relative to the mean position, therefore, a line passing through the whole-population midpoint with the slope estimated from two initial points would be a representation of the dose-response curve for the mean channel. If only $\Delta A$ varies, activation curves for individual channels

will be turning about the common intercept with the vertical axis ($\sigma(\Delta A)>0$, $\Delta E$ = const), crossing the horizontal axis at different points. In this case, a line connecting the population midpoint with the common intercept would represent mean parameters of the channel. In reality, both $\Delta E$ and $\Delta A$ may vary, and the resultant curve may lie anywhere in the shaded area between the two lines. The initial slope of eight independently measured curves with visible inflections yielded $\Delta A = 20.4 \pm 4.8$ nm$^2$, highly consistent with molecular models. With the midpoint for the entire population $\gamma_{½} = 10.4 \pm 0.8$ dyne/cm, the upper limits for $\Delta E$ and $\Delta A$ were estimated as 52.5 *kT* and 20.43 nm$^2$ (as if $\Delta E$ is variable), whereas the lower limits corresponding to variation in $\Delta A$ were estimated as 50.9 *kT* and 19.8 nm$^2$, respectively. After averaging, $\Delta E = 51.7\ (\pm 13)$ *k*T and $\Delta A = 20.1\ (\pm 4.8)$ nm$^2$ can be taken as a realistic experimental estimation of gross parameters of MscL gating.

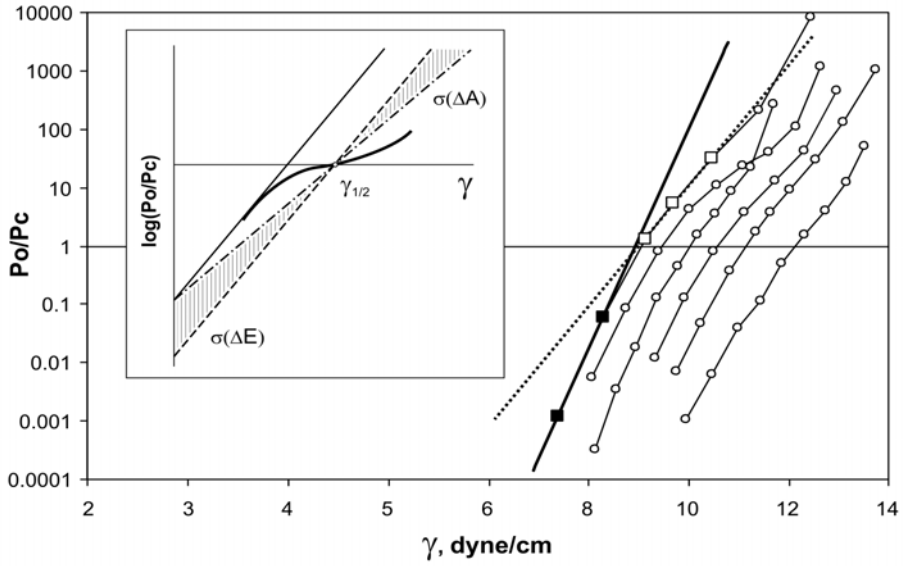


**Figure 2-8.** Examples of experimental activation curves of WT MscL exhibiting different degree of slope variation. The curves display a noticeable S-like shape with a steeper slope at the ends, and more shallow dependence near $\gamma_{1/2}$. The inflection was more pronounced in patches with smaller number of channels (3 to 7). Linear fit of initial points (solid line) defines the 'limiting slope', which gives higher estimates for $\Delta E$ and $\Delta A$ than the fit of the middle region (dotes line). The inset illustrates the procedure of reconstruction of the mean single-channel activation curve for channel populations of $\Delta A$. The inflected line represents the population dose-response curve. The fit of the initial region is shown by solid line. A parallel translation of this line to the population midpoint ($\gamma_{1/2}$) yields the mean for a population with varying $\Delta E$ only (dashed line). Rotating the initial fitting line around the its vertical axis intercept, such that it crosses the horizontal axis at $\gamma_{1/2}$, yields the mean curve for a population with varying $\Delta A$ (dot-dashed line). The hatched area represents possible intermediate line positions for populations in which $\Delta E$ and $\Delta A$ may vary simultaneously.

## Discussion

Previous analysis of MscL gating has been done on purified channels reconstituted in asolectin liposomes (Sukharev et al., 1999b). Patch-clamp recording was combined with video imaging to evaluate the curvatures of patches in a range of pressure gradients. Single-channel traces recorded in liposome patches were initially idealized with an amplitude threshold criterion. The open and closed time distributions were essentially monoexponential and the rate constants were fit with a two-state model reasonably satisfying the scheme with one closed and one open state. $P_o$ curves plotted against membrane tension gave the mid-point of MscL activation ($\gamma_{½}$) of 11.8 dyne/cm, and $\Delta A$ estimated from the steepness of the curves by the two-state model was 6.5 $nm^2$. This area change was suspiciously small for a molecule predicted to form a large conducting pore 3 nm in diameter.

Liposome patches are large enough for imaging, but mechanically unstable during continuous recordings having a tendency to slide up the pipette under pressure (Sukharev et al., 1999b). Here we presented an analysis of MscL activity recorded from smaller patches in spheroplasts. Instead of video imaging (which is inaccurate due to small patch size), we used MscS as an internal tension gauge (Fig. 2-1). A steep activation of MscS at around 5.5 dyne/cm in both liposomes (Sukharev, 2002) and spheroplasts (Cui and Adler, 1996) made this channel a good 'standard' for two reasons. First, MscS appears to exhibit a more consistent behavior in spheroplasts and liposomes, whereas MscL exhibits a time-dependent decrease in activity in liposomes (Hase et al., 1995). For this reason the midpoint of 11.8 dyne/cm determined in liposomes may be a slight overestimation compared to that in the native membrane. Second, MscS activation automatically gauges

the entire range of mechanical stimuli, including those situations where MscL was activated to low $P_o$. The established procedure of recording and treatment allows us to present disparate $P_o$-pressure curves in unified tension scale without patch imaging, as well as to compare different MscL mutants in other studies. The midpoint of MscL activation determined from 29 independent traces as 10.4±0.8 dyne/cm (Fig. 2-5), is a key parameter, which now permits thermodynamic analysis of MscL function in the native membrane. MscS, present in the majority of patches, also allowed us to assess the radius of curvature for each patch and its variability (Fig. 2-1, inset), which usually remains out of sight in most channel studies.

Out of the nine subconducting states detected by Gaussian fits of amplitude histograms (Fig. 2-2), three short-lived substates $S_{0.22}$, $S_{0.70}$ and $S_{0.93}$ reasonably correspond to the intermediate conductive states with relative amplitudes of 0.28, 0.71 and 0.90, previously identified in liposome-reconstituted MscL (Sukharev et al., 1999b). The occupancies of short-lived substates $S_{0.22}$ and $S_{0.93}$ are near $10^{-3}$ and $10^{-1}$ relative to the occupancy of the fully open state (O), and decrease with tension (Fig. 2-3 B). This is consistent with the notion that $S_{0.22}$ and $S_{0.93}$ are intermediate states characterized by smaller area changes between them, constituting about 74 and 85% of $\Delta A$ for the fully open state. The picture is highly consistent with the results of the previous kinetic analysis, which describe the transition from the closed to the first substate as the slowest, and the most tension-sensitive (Sukharev et al., 1999b). The occupancy of the long-lived substate $L_{0.78}$ increases with tension (Fig. 2-3 B). The dependencies of the $L_{0.78}$ occupancy on tension show that the $O \rightarrow L_{0.78}$ transition is associated with approximately 14% additional protein expansion. The occupancy of the second long-lived state $L_{0.64}$ is

visited directly from $L_{0.78}$. The fact that the long-lived substates are visited exclusively from the fully open state, places $L_{0.78}$ and $L_{0.64}$ beyond the open state in the kinetic scheme aligned with the coordinate representing the cross-sectional area of the protein (Fig. 2-9).

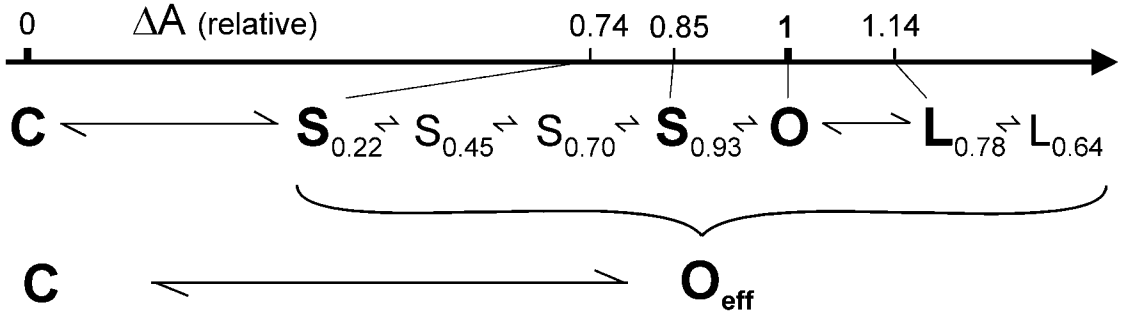


**Figure 2-9.** The kinetic scheme of MscL aligned with the reaction coordinate representing the protein in-plane area change. The main tension-dependent transition from C to $S_{0.22}$ is associated with a largest area increase. The long-lived subconducting states ($L_{0.78}$ and $L_{0.64}$) are characterized with larger in-plane areas than the open state (O). All conductive states can be grouped as $O_{eff}$, which conducts 94% of current relative to an ideal two state over the range of tensions. Uncorrected estimates of area and energy differences of the major states relative to the fully closed state (0 $nm^2$, 0 $kT$) are 9.3 $nm^2$ (31 $kT$) for $S_{0.22}$, 10.7 $nm^2$ (29.3 $kT$) for $S_{0.93}$, and 14.4 $nm^2$ (38.4 $kT$) for $L_{0.78}$ and 12.67 $nm^2$ (32.5 $kT$) for the fully open state. According to the data estimated in Fig. 2-8, the corrected area and energy changes between the fully closed (C) and fully open (O) states are about 20.1 $nm^2$ and 51.7 $kT$. Correspondingly, the distances from the fully closed state to substates can be re-scaled as 14.8 $nm^2$ (49 $kT$ ) for $S_{0.22}$, 17.0 $nm^2$ (47 $kT$) for $S_{0.93}$, and 22.9 $nm^2$ (61 $kT$) for $L_{0.78}$.

The experimentally observed $\langle f(\gamma) \rangle$ stays at the level of 0.94in the range of $P_o$ between 0.02 and 0.85 (Fig. 2-3B). This follows from the fact that 74% of the time channels spend in the fully open state, and two major substates - $S_{0.93}$ and $L_{0.78}$ have opposite tension dependencies (Fig. 2-3B). The $S_{0.22}$ substate has low conductance, but its contribution is negligibly small due to very low occupancy. The combined relative occupancy of all substate together counts for 26% of the channel opening time and remains unchanged over the range of tensions. Thus, simple two-state formalism can be applied safely to calculate the single channel open probability and characterize gross parameters for WT MscL. This rule, however, may not hold for gain-of-function MscL mutants (see Chapter 3) or other mechanosensitive channels in which the occupancies of prominent substates substantially change with tension (Yao et al., 2001).

In the two-state approximation, the average expansion and energy of the C→O transition estimated from twenty-nine independent curves were 12.8±4.2 $nm^2$ and 32±10.3 *k*T. These effective parameters measured on populations, as was mentioned above, may not reflect the intrinsic parameters for individual channels. The energies and areas were found to be linearly correlated, but at the same time strongly scattered. The inference that this distribution of parameters is a consequence of non-uniformity of the channel populations was well supported by statistical simulations. A much narrower scatter of the midpoint position, $\gamma_{½}$, reflects a symmetrical character of distributions of the actual ΔE and ΔA in channel populations, centered about the median, which reproduces well from trial to trial. These conclusions explain the relationships between the observed and predicted ΔA and ΔE values. ΔA predicted from the atomic-scale models is in the range of 23 $nm^2$, which, implies ΔE=59 *kT* (to satisfy $\Delta E/\Delta A = \gamma_{½} = 10.4$

dyne/cm). A dispersion of either ΔE by 3 *kT* or ΔA by 1 $nm^2$ around these mean parameters would reproduce the experimental dataset with an average 'apparent' ΔE of 32 *kT* and ΔA of 12 $nm^2$. The data also suggest that 'smearing' of the activation curves leads not only to reduction of the gross gating parameters that reflect the C→O transition, but may also result in a proportional reduction of the parameters for the sub-transitions. For instance, the protein expansion during the $O \rightarrow L_{0.78}$ transition estimated as 1.7 $nm^2$ under conditions that produce ΔA=12 $nm^2$ for the entire C→O transition, in reality should be 2.8 $nm^2$ (see Fig. 2-9, and legend). On the other hand, the analysis of only left-most regions of inflected experimental activation curves allows to overcome 'smearing' of activation curves (Fig. 2-8). It yields average ΔE ~51.7 *k*T and ΔA~20.1 $nm^2$, which appear to be reasonable experimental estimations of the 'true' gating parameters. The areas and energies for the substates can be rescaled as 14.8 $nm^2$ (49 *k*T) for $S_{0.22}$, 17.0 $nm^2$ (47 kT) for $S_{0.93}$ and 22.9 $nm^2$ (61 kT) for $L_{0.78}$. These values should help relating the substates with modeled intermediate conformations and prompt further studies of physical interactions contributing to the total energy of gating transition in MscL.

Why are channel populations non-uniform? The deviations of gating parameters within channel populations can be ascribed to heterogeneity of the native membrane, creating a slightly different physical environment for each channel. This heterogeneity may emerge from the formation of clusters among MscL proteins or variations of local protein/lipid environment in the native membrane, in which channels are subjected to different tensions depending on the actual position in the cluster. Does this functional heterogeneity have any biological meaning for a cell? Probably, because in this case the early openings of few MscLs would aid in coping with an abrupt osmotic downshock or

automatically generate a more graded permeability response to varied osmotic challenges.

In conclusion, the analysis of MscL gating in spheroplasts is consistent with the kinetic scheme in which the major tension-sensitive step is the transition from the closed to the short low-conducting substate. This substate represents a highly pre-expanded conformation characterized by a relative area only 25 % smaller than of that of the fully open state with essentially the same intrinsic energy. In contrast to the short-lived substates, the long-lived substates do not appear to be intermediates, but rather alternative open states. Since the wild type MscL always conducts 94% ionic current relative to an ideal two-state channel with all tensions, this validates the use of integral current as a means for estimating $P_o$, and the two-state approximation for gross thermodynamic treatment. Since a small heterogeneity of the population is capable of severely reducing the apparent $\Delta E$ and $\Delta A$ parameters, the slope can be evaluated using only the initial, left-most regions of activation curves. The total protein expansion obtained in this fashion reasonably corresponds to that predicted from structural models of MscL.

# Chapter 3

# Gain-of-function mutations reveal expanded intermediate states and a sequential action of two gates in MscL


## Abstract

The tension-driven gating transition in the large mechanosensitive channel MscL proceeds through a number of detectable intermediate states. Gain-of-function (GOF) mutants with polar or charged substitutions in the main hydrophobic gate display altered patterns of subconducting states providing valuable information about gating intermediates. Here I present thermodynamic analysis of several GOF mutants to clarify the nature and position of low-conducting conformations in the transition pathway. Unlike wild-type (WT) MscL, which predominantly occupies the closed and fully open states with very short substates, the mild V23T GOF mutant frequently visits a multitude of short-lived intermediates. Severe mutants V23D and G22N open in sequence: closed (C) → low-conducting substate (S) → open (O), with the first sub-transition occurring at lower tensions. Analyses of the state occupancies as a function of membrane tension show that the C→S sub-transition in WT MscL is associated with only a minor conductance increment, but the largest in-plane expansion and free energy change. The GOF substitutions strongly affect the first sub-transition by reducing $\Delta A$ and $\Delta E$ between C and S states commensurably with the severity of mutation. GOF mutants also exhibited a considerably larger $\Delta E$ associated with the second (S→O) sub-transition, but $\Delta A$ similar to WT. The area changes indicate that closed conformations of GOF mutants are physically pre-expanded. The tension dependencies of rate constants for channel closure

($k_{off}$) predict different rate-limiting barriers on the energy landscapes for WT and GOF MscL. The data support the two-gate mechanism in which the first sub-transition can be viewed as opening of the central (M1) gate, resulting in an expanded water-filled 'leaky' conformation (S). Strong facilitation of this step by polar GOF substitutions suggests that separation of M1 helices and hydration of the pore in WT MscL is the major energetic barrier for opening. The bulk of conductance gain occurs in the second sub-transition (S→O) through the separation of the N-terminal (S1) gate. Extensions of S1-M1 linkers increase the occupancy of low-conducting intermediates; in GOF mutants they also prevent full opening. This indicates that the linkers are coupling elements between the M1 and S1 gates and their length is critical.

## Introduction

Single –channel currents are the main source of direct information about the gating process. The gating pattern of wild-type MscL is complex and shows a number of subconducting states as described in the chapter 2, some of which were interpreted as conformational intermediates between the closed and fully open states, while the others were shown to be alternative open states. The initial survey of EcoMscL gating in liposome patches (Sukharev et al., 1999b) has identified three prominent short-lived substates and estimated the tension dependencies of rate constants for each sub-transition. The kinetics revealed that the major tension-dependent step in the process of opening is the transition from the closed state to the lower subconducting state, suggesting that this transition must be characterized by a relatively large in-plain area change (Sukharev et al., 1999b) and, despite low conductance, it must resemble more the open than the closed conformation. The analysis of substate occupancies of wild type EcoMscL in native membranes, as discussed in Chapter 2, revealed a larger number of subconducting states and confirmed the presence of low-conducting expanded intermediates. Thus, the necessity of a structural element that partially occludes the pore in the expanded state evoked the hypothesis of a second gate (Sukharev et al., 2001). The additional gate was modeled as a bundle of short N-terminal (S1, residue 1~ 12) domains, which were unresolved in the original TbMscL structure (Chang et al., 1998). As reported in Chapter 1, EcoMscL with its conserved phenylanaline 10 replaced by cysteine is non-functional according to patch-clamp examination, but after treatment with a reducing reagent, the channel shows full openings. This result suggests that S1 domains are likely to separate during the gating process.

The isolation and functional analysis of toxic gain-of-function (GOF) mutants (Ou et al., 1998) revealed that many of them are characterized by low-tension activation and fast kinetics (Ou et al., 1998; Yoshimura et al., 1999). The most severe GOF mutants exhibited a prominent low-conducting substate, which was appreciably occupied even at zero tension, whereas the subsequent transition to the fully open state required higher tensions (Yoshimura et al., 1999). The stable low substate was initially interpreted as partial opening of the main hydrophobic gate formed by M1 helices (Yoshimura et al., 1999). The question of whether the prominent low substate in GOF mutants is a result of partial opening of a single gate, or is in an intermediate in the alternative two-gate mechanism suggested for WT MscL (Sukharev et al., 2001), becomes mechanistically important. If the latter is the case, then GOF mutations simply stabilize the low-conducting intermediate and separate the two parts of transition in time and on the tension scale.

In the present work, I record single-channel traces from three GOF mutants of different severity (V23T, V23D, and G22N) and compare them with WT. The analysis of substate occupancies using HISTAN ( a software written by Dr. Andriy Anishkin) shows that with the proper statistical treatment the two major sub-transitions are indeed separable even in the mild mutant (V23T). I demonstrate that hydrophilic substitutions in the pore constriction, when compared to wild-type MscL, affect primarily the first sub-transition associated with the opening of the M1 gate, making M1 gate easily unlocked. The mutants are characterized by the reduction of $\Delta A$ and $\Delta E$ in the first transition (C→S), which implies critical role of hydration in the opening of the M1 gate. Hydrophilic substitutions have smaller effect on the second transition (S→O) ascribed to

the separation of the hypothetical S1 gate, displaying an increase in ΔE, but with ΔA similar to that of wild type. The results indicate that the two-gate mechanism offers a better explanation of MscL gating. I also studied the role of S1-M1 linker connecting the two gates and find its length critical for the second sub-transition and proper coordination of the entire gating process. I acknowledge technical assistance from Mrs. Monica Betanzos in generation of V23T MscL and mutants with extended likers.

## Results

### GOF mutations change gating patterns

The three mutations, V23T, V23D and G22N are hydrophilic substitutions in the pore constriction of MscL and all confer gain-of-function phenotypes of different magnitude. In in-vivo plate assays, full expression of V23T driven by the $P_{lacUV}$ promoter in the presence of 1 mM IPTG shows little effect on bacterial growth. In contrast, the growth of cells expressing the G22N and V23D mutants with IPTG induction was severely depressed (not shown), which is consistent with the data reported previously (Ou et al., 1998). In liquid culture, the growth rate of G22N is the slowest one, which ranks it the most severe GOF mutant. Patch-clamp trials have clearly indicated that these substitutions make the channel more sensitive to pressure. G22N and V23D MscLs were activated before MscS, whereas V23T MscL was gated at approximately the same pressure as MscS. The MscL opening threshold (relative to MscS) for G22N, V23D and V23T was 0.18 ± 0.24 (n=10), 0.31 ± 0.26 (n=13) and 1.02 ± 0.12 (n=18) respectively, whereas the threshold for wild type MscL was 1.55 ± 0.16 (n=15).

Fig. 3-1 shows fragments of typical single-channel traces recorded in WT MscL, mild V23T, and two severe gain-of-function mutants V23D and G22N at five different pressures. Their open probabilities range from about $10^{-2}$ to about 0.9. The right part of the figure shows expanded episodes with better-resolved characteristic transitions. Wild-type MscL displays an almost binary character of behavior with high occupancies of fully closed and fully open states. Short sojourns to lower subconducting levels occur predominantly from the fully open level. The expanded fragment shows that in addition to the downward deflections from the fully open state the channel also displays short stops on the way up or down, previously documented in liposome-reconstituted MscL (Sukharev et al., 1999b).

The mild V23T mutant displays a faster kinetics of main transitions relative to WT. The downward deflections from the fully open level are deeper and more frequent. The channel visits intermediate conducting states more often, with a slightly higher probability of low levels at lower tensions. The expanded fragment of trace shows especially frequent excursions from the baseline to the low sublevels.

The more severe V23D mutant displays short openings to the low sublevel very early on tension. This low substate resides in more in the middle of the stimulation range and flickers to the upper substate or open state. As the open state becomes considerably populated at higher tensions, the channel practically never visits the fully closed state, returning always to one of the low-conducting levels. The most severe G22N mutant behaved in a manner similar to V23D. However, at lower tensions the channel even more stably populates the low-conducting level with low noise. At intermediate tensions, the channel remained mostly to the lower substates, flickered to the high-conductance states,

and returned to the lower substates. At higher tensions, G22N tends to dwell more in the higher conductive states and practically never visits the closed state, always returning to the substates. For all three GOF mutants, the maximal conductance is ~ 3.1 nS, similar to that of WT.

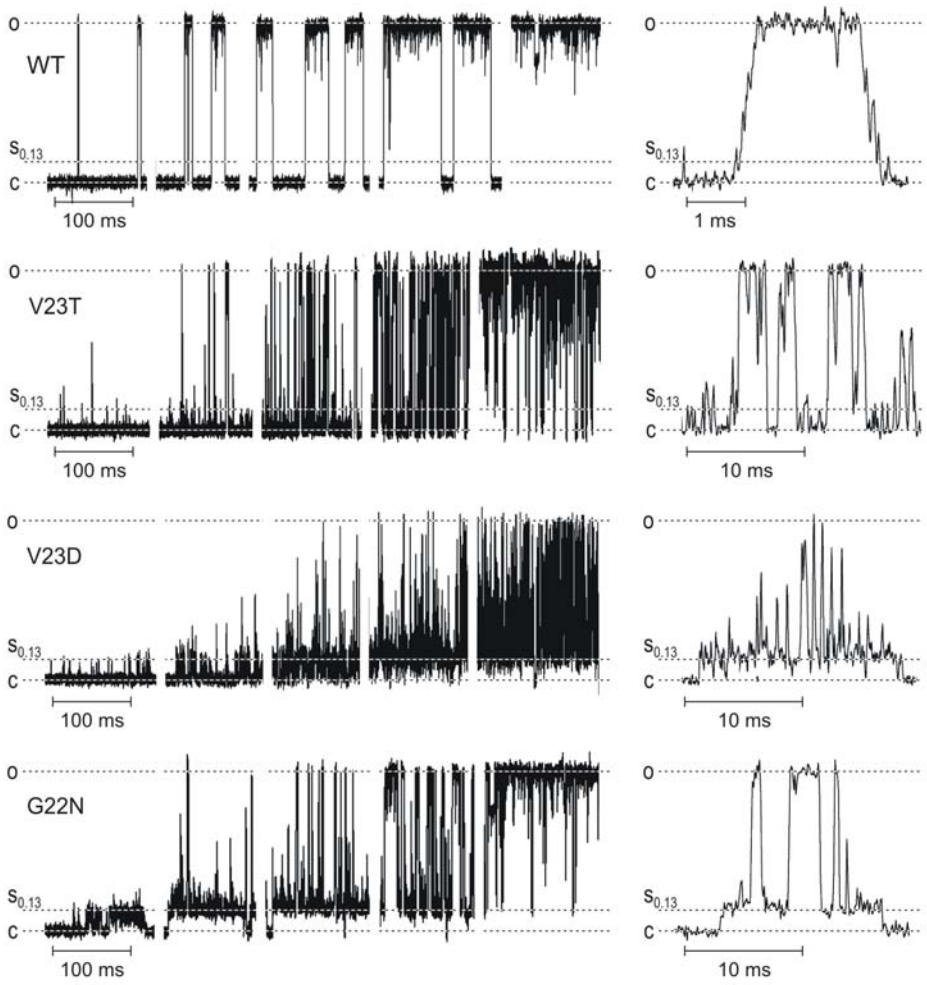


**Figure 3-1.** Typical gating patterns of WT MscL, mild GOF mutant V23T and more severe V23D and G22N mutants. Recordings were done in inside-out patches at –20 mV (pipette positive). Low-pass filtering was at 30 kHz and sampling rate was 100 kHz.The fragments of traces in a 'magnified' time scale are shown on the right. The occupancy of low-conducting substates increases with the severity of the mutation.

**Positions of prominent substates**

To assess the occupancies of each of the conducting states, all-point amplitude histograms for WT and each mutant were constructed by uniformly fitting them with eleven Gaussian peaks of different amplitude and width (Fig. 3-2). The histograms represent fragments of traces recorded at tensions activating each channel to $P_o$ between 0.1 and 0.2. The number of peaks was initially chosen as the minimum requirement for accurate fitting of wild-type histograms discussed in the Chapter 2 (Fig. 2-2). As shown in panels, essentially the same set of Gaussian peak positions reflecting similar substate amplitudes (some of which are not easily identifiable on traces by eye) provides good quality of fitting for all versions of MscL. The occupancies of intermediate peaks are substantially higher for GOF mutants than that of WT. The lower subconducting states, $S_{0.13}$ and $S_{0.22}$, experience the most drastic increase in occupancies as the severity of GOF mutation increases. To evaluate the open probability of individual substate with tensions in detail, 2-D representations of probability density for different conducting states along the tension gradient were built from several combined activation curves for WT, V23T, V23D and G22N (Fig. 3-3). The ridges on the far left and on the far right represent the closed and the fully open states, respectively. As seen from the Fig. 3-3, the tension required for the first full opening decreases with the severity of GOF mutation and is ~8 dyne/cm for WT , ~6 dyne/cm for V23T, ~4.5 dyne/cm for V23D and only about 1.8 dyne/cm for G22N. Their occupancy of the full opening increases as tension goes up. In wild-type MscL, the prominent ridge next to the full opening represents the long-lived satellite state $L_{0.78}$, which is characterized with a slightly larger area than the open state (see Chapter 2). As the tension increases, a few intermediate states become visible, but

with probabilities $10^2$-$10^3$ times lower than that of the fully open state. V23T occupies more intermediate levels, but does not display prominent long-lived states. More severe V23D also shows high occupancy of intermediates. The two low substates, $S_{0.13}$ and $S_{0.22}$, appear early and at higher tensions become substantially more occupied than the closed state. G22N, the most severe mutant, shows a significant occupancy of the low substate already at zero tension in all three traces examined, it also reaches intermediates relatively early on tension compared to other mutants and the sharp ridge of long-lived substate at 0.78 is clearly visible.

**Figure 3-2.** All-point amplitude histograms for WT and GOF mutants, each fit with eleven Gaussian distributions. The data for WT and the amplitude histogram fit are taken from the chapter 2, where the positions of obvious and implied subconducting states were first determined. Gaussians with essentially the same positions permitted accurate fitting of histograms for all mutants, their sums (grey dashed line) overlap with experimental histograms (black continuous line). The occupancies of the closed (0.00), fully open (1.00) and two lower substates with relative amplitudes of 0.13 and 0.22 were further used for thermodynamic analysis. The peaks for these states are presented in red.

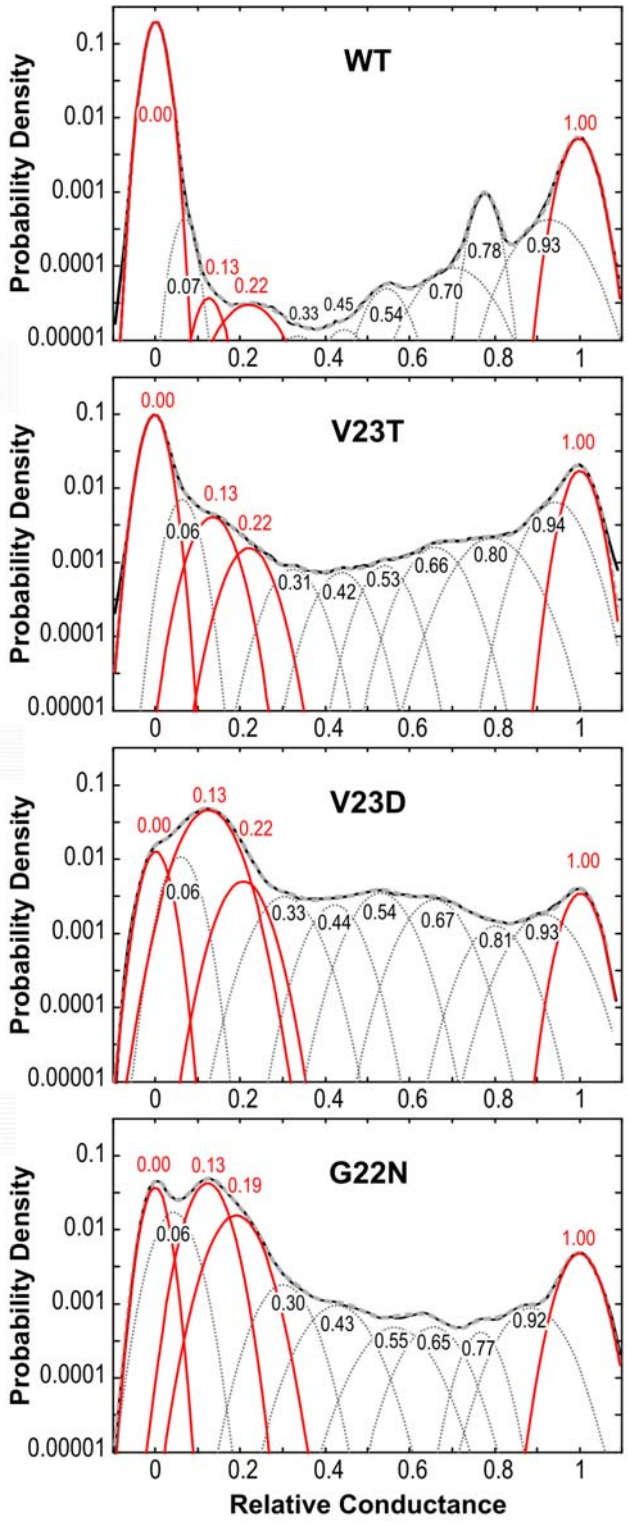
WT
0.00
0.07
0.13
0.22
0.33
0.45
0.54
0.70
0.78
0.93
1.00
V23T
0.00
0.06
0.13
0.22
0.31
0.42
0.53
0.66
0.80
0.94
1.00
V23D
0.00
0.06
0.13
0.22
0.33
0.44
0.54
0.67
0.81
0.93
1.00
G22N
0.00
0.06
0.13
0.19
0.30
0.43
0.55
0.65
0.77
0.92
1.00
Probability Density
0.1
0.01
0.001
0.0001
0.00001
0
0.2
0.4
0.6
0.8
1
Relative Conductance

**Figure 3-3.** Two-dimensional amplitude histograms for WT MscL and GOF mutants. The x-axis, as in a regular amplitude histogram, represents the relative conductance, y-axis represents tension and the z axis is the density of probability of occupying the specific conducting state. The ridges on the left and on the right represent the baseline and the fully open state. Note that in G22N, the most severe mutant, the low substate (ridge next to the baseline) is occupied at zero tension. The number of independent traces taken for analysis: WT, n=10; V23T, n=4; V23D, n=6; and G22N, n=3.

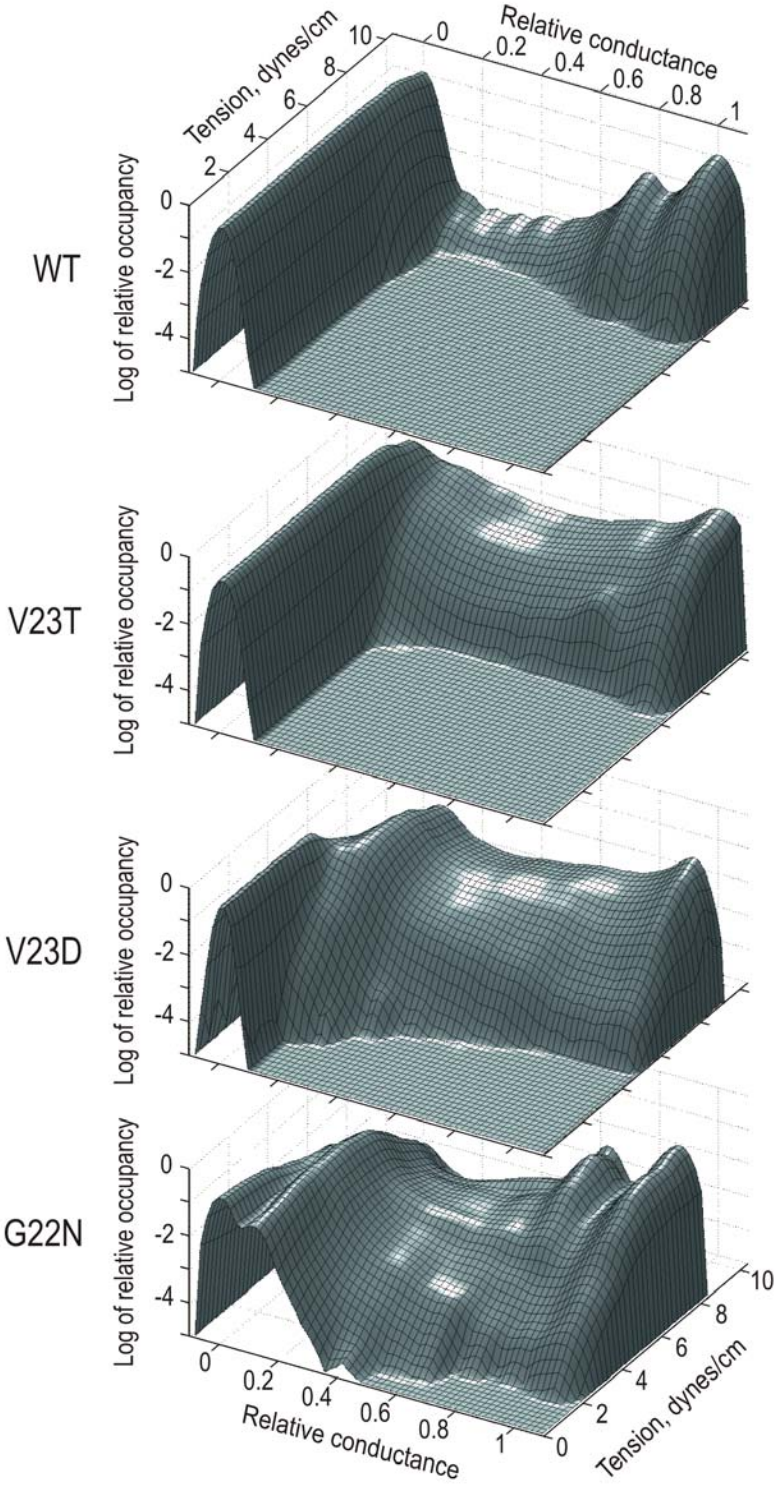
WT
V23T
V23D
G22N
Log of relative occupancy
0
-2
-4
Tension, dynes/cm
0
2
4
6
8
10
Relative conductance
0
0.2
0.4
0.6
0.8
1

**Thermodynamic analysis**

Fig. 3-4 shows ratios of occupancies of three individual conducting states, closed (C), low substate ($S_{0.13}$) and fully open (O) for WT and V23D MscL. Data points were obtained by fitting individual histograms, as shown in Fig. 3-2, recorded at different tensions. For WT MscL, the data are taken from the chapter 2 describing the positions and occupancies of substates and evaluation of gating parameters based on the analysis of non-uniform population responses. The curves presented here are reconstructed with the parameters extracted from initial slopes of dose-response curves measured with integral current. The occupancy of the low-conducting substate $S_{0.13}$ and its position between the closed and open states on the ΔA scale were determined from the analysis of cumulative amplitude histograms based on ten independent traces (see Fig. 2-3, Fig. 2-9, Chapter 2). The right panel shows fitted curves and extracted parameters for the V23D mutant. The curve for the C→ $S_{0.13}$ sub-transition is shifted upwards compared to that of wild-type, signifying high occupancy of $S_{0.13}$. The entire curve for the second sub-transition $S_{0.13}$ →O moved downward, reflecting low occupancy of the fully open state compared to $S_{0.13}$. For both the WT and the V23D mutant, the slopes for the second sub-transition $S_{0.13}$ →O are similar, corresponding to an approximately 5-6 $nm^2$ expansion. Note for the C→O transition, the increase of mean integral current with tensions (open squares, □) exhibits a considerably lower slope, producing an apparent total expansion of only 4.1 $nm^2$. The value is much smaller than the total expansion predicted from the ratio of open and closed state occupancies (15.0 $nm^2$) or the sum of expansions for the two sub-transitions (15.1 $nm^2$), which appear to be additive. In contrast, the total expansion from C→O transition for wild type gauged by either the integral current or the ratio of

occupancies is the same. This is a clear consequence of differences between WT and V23D; the former has a single rate-limiting step for the entire C→O transition, whereas the two sub-transitions for the mutant are separated on the tension scale. Thus, the integral current can be used as measure of $P_o$ for channels with an apparent single-transition (two-state) behavior, as WT MscL, but would be inappropriate for channels with separated prominent sub-transitions. The figure illustrates that the procedure of log ($P_j/P_i$) fitting produces reliable slopes for individual sub-transitions ($i \rightarrow j$) in WT and mutant MscLs. While the figure shows just two examples, the cumulative data for the closed, open and two low-conducting intermediates, $S_{0.13}$ and $S_{0.22}$, for all mutants are given in Table 3-1. The data illustrates that the two substates are positioned relatively close to each other on the energy and area scales and their relative positions between the two end states (C and O) vary depending on the mutation. The area and especially energy differences between the closed state and low-conducting intermediates remarkably decrease with the severity of the mutation.

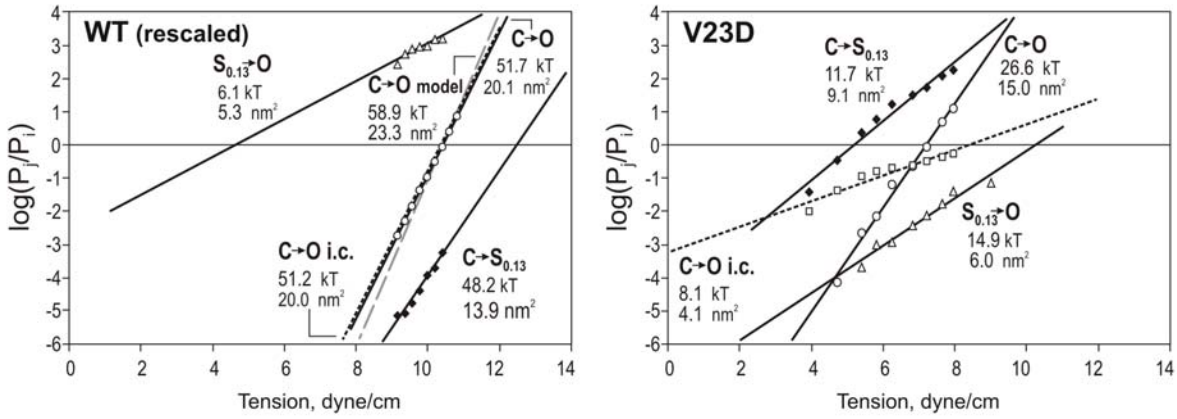


**Figure 3-4.** Paired ratios of probabilities for the closed (C), low substate ($S_{0.13}$) and the fully open state (O) for WT and V23D MscL, shown as functions of tension. Boltzmann fitting (straight solid lines) gives thermodynamic parameters of energy change and in-plane protein expansion between the two particular states. Dashed lines represent dose-response curves determined with integral current. For the V23D mutant, the integral current curve has much lower slope than the dose-response determined from the ratio of O and C occupancies.

**Table 3-1**. Energy and area differences between the closed (C), substates $S_{0.13}$ and $S_{.022}$, and fully open state (O) determined from the slopes of their occupancy dependencies on tension for WT MscL and three mutants.

* The standard deviations are not shown because the ΔE and ΔA parameters for WT were determined from one unified dataset based on ten independent traces.

| | **WT* (n=10)** | | **V23T (n=9)** | | **V23D (n=6)** | | **G22N (n=3)** | |
|---|---|---|---|---|---|---|---|---|
| **Sub-state** | **ΔE, kT** | **ΔA, nm²** | **ΔE, kT** | **ΔA, nm²** | **ΔE, kT** | **ΔA, nm²** | **ΔE, kT** | **ΔA, nm²** |
| **C** | 0 | 0 | 0 | 0 | 0 | 0 | 0 | 0 |
| **$S_{0.13}$** | 48 | 14 | 27±8 | 11±3 | 12±5 | 10±3 | 1±2 | 3±0 |
| **$S_{0.22}$** | 49 | 15 | 31±10 | 13±4 | 17±5 | 11±3 | 4±1 | 4±1 |
| **O** | 52±13 | 20±5 | 41±14 | 18±6 | 26±4 | 15±2 | 13±3 | 12±2 |

**Kinetics of closing transitions**

In addition to finding the positions of the energy wells for the subconducting states, I attempted to locate the main barriers that limit the rate of entering/exiting the fully open state for WT and V23D MscL. Using the QuB suite, I idealized the traces in the simplest two-state approximation taking into account the full C→O transition for the WT and only the $S_{0.13}$→O transition for V23D (Fig. 3-5 A). It is obvious that this crude approximation ignores low-amplitude spikes from the closed state (WT) or from lower level $S_{0.13}$ (in V23D), as well as brief downward deflections from the fully open state. The energetic closeness of short-lived high-conducting states adjacent to the fully open state (see Chapter 2) and fast transitions between them nevertheless suggest that grouping these states together with the open state may be a reasonable simplification allowing us to locate the main transition barrier. Thus, I focused my analysis primarily on the rate of backward transitions ($k_{off}$) from the fully open state to either low substate or fully closed state, as a function of tension. For the closed and open states separated by a single barrier, the two rate constants can be written in the Eyring's form:

$$k_{on} = k_0 \exp[-(\Delta h_b - \gamma \Delta A_{cb})/kT] \qquad \text{and} \qquad k_{off} = k_0 \exp[-(\Delta h_b - \Delta E + \gamma \Delta A_{ob})/kT]$$

where $\Delta E$ is the energy difference between closed and open wells, $\Delta h_b$ is the height of the barrier looking from the closed well, $\Delta h_b$-$\Delta E$ is the height of the barrier as seen from the open well, and $\Delta A_{cb}$ and $\Delta A_{ob}$ are the area differences between the bottoms of closed or open well to the tip of the barrier. By taking logarithms and then derivatives on γ, the logarithmic slopes of the rate constants give area differences between the equilibrium positions of the states and that of the rate-limiting barrier.

$$\frac{d \ln k_{on}}{d\gamma} = \Delta A_{cb} / kT \qquad \text{and} \qquad \frac{d \ln k_{off}}{d\gamma} = -\Delta A_{ob} / kT$$

Fig. 3-5B depicts $k_{on}$ and $k_{off}$ as functions of tension for WT and V23D MscL. The slope of $k_{off}$ is higher for WT MscL and reflects the area change of -7.2 ±1.5 $nm^2$ (n=3) between the open state and the rate-limiting transition state, which places the barrier between the closed and the low substates, but close to $S_{0.13}$ (Fig. 3-7). The rate constants for V23D mutant are about 2 orders of magnitude higher than that for WT, indicating a transition barrier that must be at least 5 kT smaller. The lower slope suggests that the top of the barrier is only 2.2 $nm^2$ away from the fully open state, situating between $S_{0.22}$ and O states (Fig. 3-7).

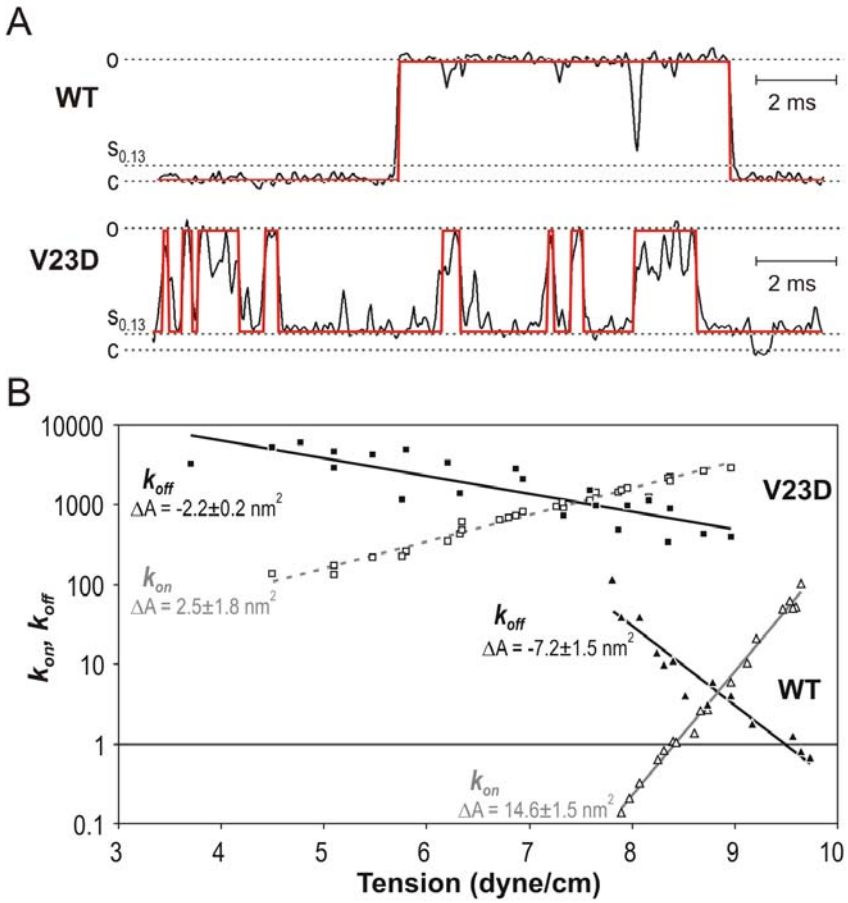


**Figure 3-5.** The kinetics of closing events in WT and V23D MscL channels. (A) Examples of simplified two-state idealization of traces using SKM protocol with level tolerances (standard deviations) for the closed and open states set at 2 and 5% of the unitary conductance, respectively. For WT MscL the complete C→O transition was fit, whereas only S→O sub-transition was accounted for V23D. (B) Semi-logarithmic plots of $k_{off}$ and conditional $k_{on}$ as functions of tension. The slopes of $k_{off}$ in each case suggest the distance between the open state and the rate-limiting barrier on the ΔA reaction coordinate.

**S1-M1 linker extensions and the second sub-transition**

According to the previously proposed model of MscL gating, expansion of transmembrane barrel strains the linkers connecting M1 helices with N-terminal (S1) segments. The hypothetical S1 bundles (S1 gate) held together by hydrophobic interactions between conserved phenylalanines (F7 and F10) were predicted to expand and then eventually disrupt (see chapter 1) under tension exerted by the linkers ($^{13}R^{14}G^{15}N$). The linker length was then suggested to be important for normal gating. To test this hypothesis, linker mutants with the insertion of an extra glycine next to the 'hinge' residue G14 (GG14 mutation) and two extra amino acids, GAG14, were generated. The opening threshold of GG14 was 1.39 ± 0.18 (n=46), slightly smaller than that of wild- type (1.55 ± 0.16, n= 15), whereas GAG14, opens at a similar membrane tension (1.59 ± 0.21, n=30) relative to wild type. Figure 3-6 shows how the gating patterns change with one- and two-amino acid insertions into the linker. GG14 mutation increases its occupancy of short-lived subconducting states, especially those of low conductance. When introduced on the V23D genetic background, V23D-GG14 mutant was gated at a lower tension (threshold, 0.69 ± 0.44, n=14). This mutant resides mostly in the low subconducting state ($S_{0.13}$), but practically never visits the fully open state. The two-amino acid linker extension, GAG14, produced an unexpected phenotype. Instead of a further increase in probability of intermediate states, upon activation, GAG14 mutant channel usually shows several seconds of continuous activity, and then closes irreversibly even with the same suction applied (Fig. 3-6A, inset of GAG trace). It was impossible to reactivate the channel by applying higher suctions. In addition, GAG14 mutant channel displayed an unusual behavior when it occasionally gated for minutes in which a burst of

short and incomplete openings frequently occurred before channel activities ran down. After GAG14 was introduced on the V23D background, this mutant was also gated at a lower tension (threshold, 0.56 ± 0.48, n=12), but it was impossible to attain full openings at any attainable tension. It appears that the length of the S1-M1 linker is critical for the proper gating of wild-type MscL with intact M1 gate, especially when the channel is driven into the open state by high tensions. For the easily opened V23D, in which M1 gate is perturbed, longer S1-M1 linkers have less effect on its conformationally stable intermediates; however diminish the maximal conductance of the mutated channels.

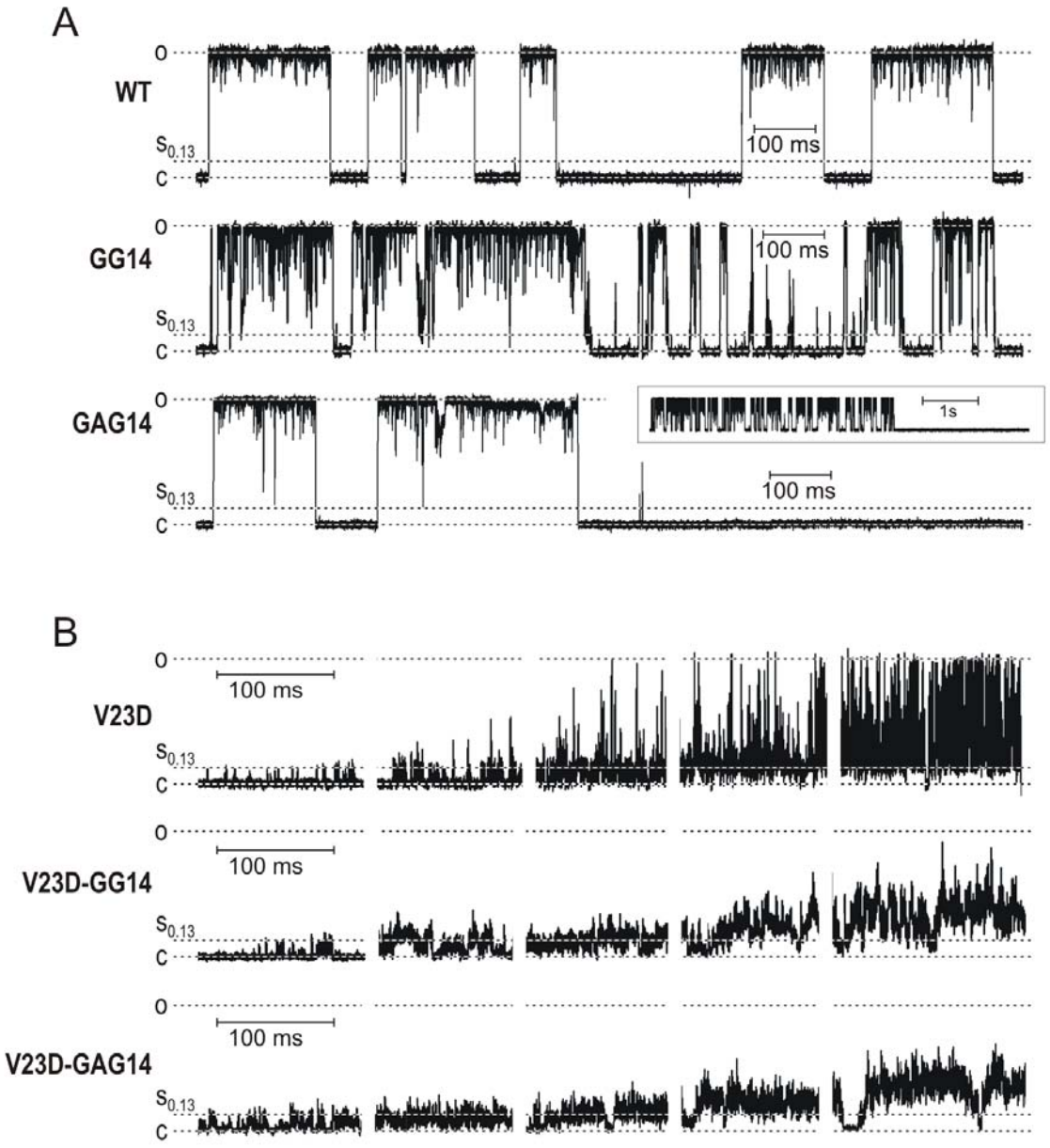


**Figure 3-6.** Gating patterns of channels with extensions of S1-M1 linker introduced on WT and V23D backgrounds. The inset next to the GAG14 trace illustrates the typical irreversible inactivation of the mutant. The extension mutants generated on V23D background never attain fully open state.

## Discussion

GOF mutations of MscL were first isolated in random mutagenesis trials exhibiting a slow- or no-growth phenotype (Ou et al., 1998). Most of the mutations grouped in the cytoplasmic half of the first transmembrane domain M1 shown to form the hydrophobic constriction of the pore (M1 gate). The toxicity of mutations and the leftward shifts in dose-response curve (early activation) correlated with the hydrophilicity of the substitute residue (Yoshimura et al., 1999). Some of the severe mutants (G22N, G22K) were shown to stably occupy low subconducting states which split the entire transition into two sub-transitions (Yoshimura et al., 1999). The analysis of GOF mutant gating presented above shows that via analysis of all-point histogram similar sub-transitions become separable in less severe mutant, V23T, and in WT. Quantification of state occupancies and thermodynamic analysis show that GOF mutations affect the overall energetics of gating with the strongest impact specifically on the first sub-transition.

The relative energy and area changes (Table 1) combined with the positions of major rate-limiting barriers obtained from kinetic data (Fig. 3-5) allow reconstruction of free energy profiles for the transitions. Fig. 3-7A shows the profiles for all four mutants calculated for zero-tension conditions and aligned by the open state areas. This type of alignment appears to be better than an alignment by the closed-state areas for two reasons. First, the conductance of fully open states for all four versions of MscL was indistinguishable, indicative of similar pore geometry and high likelihood that the outer dimension of the barrel is the same. Second, charged or polar side chains packed in the narrow pore constriction are expected to influence primarily the closed conformation, but would be far separated in the open state, with less overall influence on its conformation.

The energetic cost of the open conformation of wild-type and mutant MscLs moving from the vacuum to water environment were calculated by Dr. Andriy Anishkin. Then the curves on the vertical (free energy) scale, according to estimated energy differences between open-state conformations for different mutants, were separated. Each curve was shifted as a whole, keeping the constant relative distances among the states. The down-shifts for the V23T and G22N mutants by -14.5 and -39.5 kT reflect more favorable hydration of polar and more exposed substitute side chains calculated from estimated water-exposed areas. The shift of -24.9 kT for the charged V23D mutant includes both the hydration energy (-38.9 kT) and the positive contribution of electrostatic repulsion between equivalent side chains in the pentamer (+14.0 kT). Because the exact open structures of wild-type and GOF mutant MscL are not known, the procedure of energy assignment and curve separation illustrates the tendencies only.

The energy landscape for WT shows that the major barrier for opening is between C and $S_{0.13}$. The two states not perturbed by tension are separated by the major 48 kT gap, whereas only 2-3 kT separate $S_{0.13}$ from the fully open state. Such a large energy difference predicts that in the absence of tension $P_o$ must be about $10^{-21}$, qualifying MscL as a leak-proof channel at rest. Fig. 3-7B shows the same profiles re-calculated for 10.4 dyne/cm, which is the equipartitioning tension ($\gamma_{1/2}$) for WT MscL as described in Chapter 2. In the assumption that membrane tension produces a linear distortion of the entire profile, application of $\gamma_{1/2}$ not only equalizes the energies of the

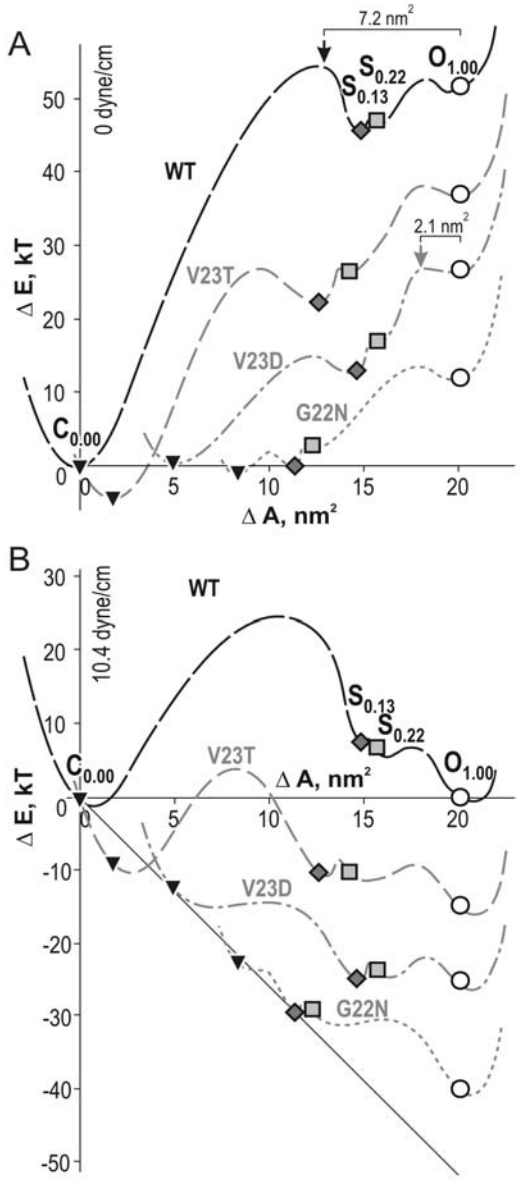


**Figure 3-7.** Energy landscapes for WT MscL and the four mutants reconstructed with parameters presented in Table 1. The distances between the curves on the energy axis were estimated mainly from hydration energies of the primary sidechains and that of substitutes. The positions of energy barriers for WT and V23D mutants were taken from the kinetic analysis (Fig. 3-5). The profiles calculated for zero tension (A) and for tension of 10.4 dyne/cm (B).

closed and fully open states, but also places $S_{0.13}$ and $S_{0.22}$ about 10 kT above the open state. The C $\rightarrow S_{0.13}$ transition brings the major expansion (~70% of the total expansion) and this makes it the most tension-sensitive step in the gating of WT MscL. From the kinetic analysis of WT MscL (Fig. 3-5), I determined that the main rate-limiting barrier is separated from the open state by 7.2 $nm^2$ (~64% of the total expansion), just left of the substate $S_{0.13}$., as illustrated in Fig. 3-7B. Under tensions near $\gamma_{1/2}$ the small barrier between $S_{0.22}$ and O states is largely reduced, thus the low substates in WT MscL are extremely short-lived as the latter steps $S_{0.13} \rightarrow S_{0.22} \rightarrow ... \rightarrow O$ come immediately after the first sub-transition.

The helical models of the MscL barrel illustrating the closed, expanded and open conformations are shown in Fig. 3-8. The opening of the main gate formed by V23 (red) and the preceding residues, $L^{19}A^{20}V^{21}G^{22}$, results in the hydration of pore interior. The expanding barrel at the same time puts stress on S1-M1 linkers that leads to separation of S1 domains (yellow) and complete opening. The cylinders below approximate protein shapes and dimensions as the channel proceeds through sequential opening. The area increments of 17 and 6 $nm^2$ for the first and second sub-transitions predicted by models are reasonably well supported by the results of thermodynamic analysis indicating $\Delta A$'s of about 15 and 5 $nm^2$ for the C $\rightarrow S_{0.13}$ and $S_{0.13} \rightarrow O$ sub-transitions in WT MscL (Table 1).

The fist major expansion of the transmembrane barrel (~70% of the total expansion) is associated with a minor gain of conductance (13% of the total conductance). Such a behavior can hardly be explained by a partial opening of a single

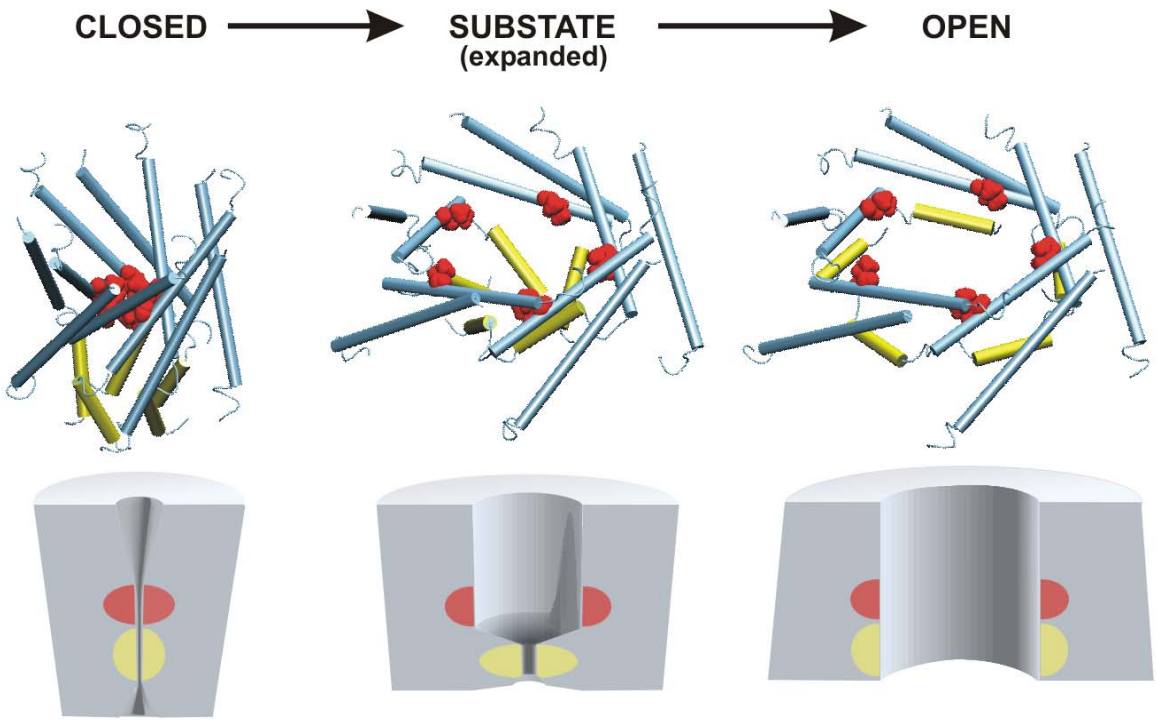


**Figure 3-8.** Structural models of the transmembrane barrel of MscL along the transition pathway. The transmembrane helices M1 and M2 forming pentamic assemblies are shown in blue, N-terminal S1 helices in yellow and the side chains of V23 are presented as red spheres. The periplasmic loops and cytoplasmic domains are not shown. The cylinders below show approximate dimensions of the barrel. According to the atomic-scale models, the in-plane area of the closed conformation may be around 19 $nm^2$, increasing to 36 $nm^2$ in the substate and then to 42 $nm^2$ in the fully open state. The locations of the main (M1) and the cytoplasmic (S1) gates are shown in red and yellow, respectively.

gate. With the simplifying assumption that the pore cross-section increases proportionally with the in-plane protein area, one may expect the conductance increase commensurate with expansion. A 70 % protein area increase should then produce a substate conducting at least 2 nS (3.1 nS * 0.70 = 2.1 nS), five times higher than observed (3.1 nS * 0.13 = 0.40 nS). The strong disparity between the area and conductance changes shows that the low substates are unlikely to be produced by partial opening of the single M1 gate as was proposed previously (Yoshimura et al., 1999), and implies the second gate.

Although the $S_{0.13}$ and $S_{0.22}$ substates are classified as low (relative to the fully open state), their conductance is appreciable (0.4-0.7 nS) and when combined with large in-plane area, it clearly signifies that the pore interior in those substates is well hydrated. The substates are apparently sequential intermediates in the opening process and the $S_{0.13} \rightarrow S_{0.22}$ transition itself may be associated with a small barrel expansion; yet the exact nature of the two-fold conductance increase remains unclear. One may speculate that at least in $S_{0.13}$ the S1 gate likely remains closed and the leakage takes place through gaps between S1-M1 linkers. Our preliminary data show that cross-links between S1 domains via cysteins at positions 3 (I3C) or histidine at positions 10 (F10H) prevented full openings, yet permitted low substates, thus supporting this idea.

In the closed conformation, the hydrophobic core of the transmembrane barrel of WT MscL appears to be completely de-hydrated according to molecular dynamics (Gullingsrud and Schulten, 2003). The reduction of the free energy difference between the closed and low substates by GOF mutations clearly correlates with the hydrophilicity of the substitute. The V23D mutation places five negative charges in the pore constriction instead of closely positioned aliphatic side chains (Fig. 3-8). Besides electrostatic

repulsion pushing M1 helices apart, a strong hydration of the pore interior is also expected as a consequence of such substitution. The mild V23T mutant that was generated by the inference of interior pore would have similar effect as V23D, but of lower magnitude, which appears to be the case. The most severe G22N mutation introduces a bulky and hydrophilic side chain in the tight contact between closely packed M1 helices, sterically pushing the helices apart. This mutation causes the largest effect resulting in about equal occupancies of C and $S_{0.13}$ even at zero tension. However, full openings are still prohibited, since a 12-15 kT separate $S_{0.13}$ from O (Table 1, Fig. 3-7A). This characteristic increase in energy gap between the low substates and the open state likely in all GOF mutants makes the substate stable at low and intermediate tensions. More tension is required to facilitate further transition to the fully open state.

Compared to WT, the in-plane expansion ($\Delta A$) associated with the first sub-transition decreases with the severity of GOF mutation, whereas $\Delta A$ associated with the second sub-transition is only slightly changed. The alignment by the open state, as seen from Fig. 3-7, suggests that the initial closed-state areas of GOF proteins are considerably larger than that of WT MscL. This means that the GOF channel complexes reside in pre-expanded conformations due to either partial hydration (V23T), electrostatic conflict of the pore constriction (V23D), or hydration on top of strong steric conflict in the interhelical contacts (G22N). The molecular details about how GOF mutants stabilize in the pre-expanded closed conformation remain to be clarified. The kinetic analysis suggests that the nature of the barriers that limit the access to the fully open state in WT and GOF MscLs is different. For WT MscL, the position of the rate-limiting state on the area coordinate is just left of the substate $S_{0.13}$ (Fig. 3-7), meaning that the transition state

just precedes the arrival to the low substate and is probably non-conductive. Overcoming this main barrier and probably instant (in the electrophysiological time scale) hydration of the entire pore makes the full open transition in WT MscL highly cooperative, in which the central hydrophobic regions and S1 domains in WT channel unlock coherently. The easy hydration of the pore in GOF mutants lowers specifically this barrier, stabilizes the intermediate state and shifts the rate-limiting step to the second sub-transition, which involves separation of S1 domains making it inherently less cooperative. The questions of whether the association energy of S1 helices creates the second barrier (positioned close to the fully open state in V23D), or other factors such as the angular positions of M1 helices also determine the parameters of the second sub-transition, are the ones for further investigation. Nonetheless, the analysis of GOF mutants suggests that the two-gate mechanism offers a reasonable view about the MscL gating, in which M1 gate is first broken followed by the separation of the S1 bundles.

The putative role of S1 bundles is supported by the extension of S1-M1 linker, which connects between S1 and M1 helices. The gating pattern is clearly influenced by the length of the S1-M1 linker. The increased occupancy of short-lived low-conducting substates in the GG14 mutant (Fig. 3-6A) is consistent with the reduction of stress that the linkers exert on the S1 domains and increased conformational freedom allowing S1s to recombine together forming the transient intermediate. However, the longer linker extension with the two-amino acid insertion (GAG14) does not produce the same amount or more of substates, but makes the open conformation unstable (Fig. 3-6A). It appears that while the separation of the S1 bundle is the last event in the opening process, recombination of these flexible domains may well be the first event on the way back to

the closed state. If for some reason the S1 bundle formation cannot prime and guide the reformation of the closed state properly, then there would be a higher rate of misfolding in MscL, then generating a non-functional channel. The irreversible inactivation of the GAG14 mutant (Fig. 3-6A) suggests this scenario.

The same extensions introduced on the V23D background dramatically increased the probabilities of dwelling in the intermediate states at higher tensions and at the same time completely abolished visits to the fully open state (Fig. 3-6B). This is consistent with a lower stress in extended linkers and a higher propensity to recombination. The result also illustrates that in a mutant with unstable open state (open dwell time in V23D is indeed very short, Figs. 3-1), extension of linkers further lowers the probability of the fully open state. One- or two-amino acid extensions produce qualitatively similar effects on the GOF background. The comparison of gating patterns between WT and V23D as well as between GG14 and V23D-GG14 (Fig. 3-6A, B) clearly shows that V23D mutation dramatically destabilizes the open state (increases the off-rate), and in the later instance simply prevents the stable occupancy in the open state. It appears that V23D mutation increases the re-association rate of putative S1 domains, or prevents their docking to the barrel wall properly as was proposed in structural models of the open state (Sukharev et al., 2001). The successful docking of S1 domains may depend on the conformation of the S1-M1 linkers, but also on the angular position of M1 helix, which was predicted to change during the gating process (Yoshimura et al., 1999).

In conclusion, the data presented above strongly support the two-gate mechanism of MscL. The opening of the main (M1) gate is associated with the major barrel expansion, whereas separation of the second (S1) gate leads to the major gain in

conductance. The energetics and kinetics of the rate-limiting first sub-transition in wild-type MscL is largely defined by the process of hydration of the transmembrane pore interior. It is highly suggestive of a similar role of pore hydration in defining gating characteristics for other channels with hydrophobic gates.

# GENERAL CONCLUSIONS

MscL is a ubiquitous emergency release valve regulating turgor in bacteria. At the same time, it had emerged as a convenient model system for biophysical studies of mechanosensitive channel gating. Residing in the inner membrane of *E. coli*, MscL opens a large aqueous pore in response to a mechanical stress of a magnitude that is close to the lytic limit of the lipid bilayer (~10 dynes/cm). Cloning of MscL (Sukharev et al. 1994), extensive mutagenesis (Ou et al., 1998) and subsequent crystallographic determination of the structure of its homolog from *Mycobacterium tuberculosis* (Chang et al., 1998) have opened unique opportunities for structure-based studies of tension-driven conformational changes in membrane proteins.

The entire project presented above was based on a model of MscL opening through the tilting and outward movement of transmembrane helices (iris model). The special feature of the hypothetical gating mechanism is the presence of two gates that open sequentially. The hydrophobic constriction between the tightly packed M1 helices was identified as the main (M1) gate (Chang et al., 1998). The structural arrangement of the main gate was in a good agreement with the location of multiple gain-of-function mutations destabilizing the tight helical packing. The second gate was inferred to explain the presence of intermediate states characterized by low conductance (13-22% of the full), and at the same time large in-plane area, comparable (70~75%) to that of the fully open state, according to the kinetic and thermodynamic analyses. The second gate was modeled as a bundle of short N-terminal (S1) helices absent in the original TbMscL structure. The opening of the first (M1) gate by tension transmitted through the lipid bilayer to the transmembrane helices was proposed to be associated with the critical event

of pore hydration. During the further barrel expansion, the tension is transmitted to the second gate through short S1-M1 linkers leading to separation of S1 domains, which results in a complete channel opening.

The first chapter presents experiments in which I have tested the iris-like model of the barrel expansion. The helical positions in the closed-state model of EcoMscL, built by homology to the crystal structure of TbMscL, were well supported by I24C-G26C and I32C-N81C cross-links. The expanded conformation of the barrel was trapped by a unique A20C-L36C cross-link that also stabilized the open state of the channel. This cross-link constrains the M1 helices in a highly tilted position (~ $70^{o}$ relative the normal to the membrane plane), making the overall open conformation highly expanded and extremely flat. The transition form the predicted closed conformation to the cross-link-constrained open state produces the pore of about 10 $nm^2$ in cross-section, which satisfies the observed conductance. The estimated outer boundary area change accompanying this transition is about 23 $nm^2$.

The data presented in Chapter 1 also provide partial support for the model of the second (N-terminal) gate. The amphipathic S1 helices are held together, in part, by apolar interactions between highly conserved phenylalanines (F7 and F10) hidden in the core of the helical bundle. Cysteines in F7C and F10C mutants form disulfide bonds spontaneously, cross-linking pairs of subunits and locking the channel in the closed conformation, consistent with the model.

The data also provided strong support for the stable character of the cytoplasmic bundle assembly (S3). In early models, the S3 bundle was depicted as separating upon opening. However, inter-subunit cross-links between cysteines in positions 121 and 122,

as well as 128 and 129 did not affect the normal gating of MscL. Conversely, destabilization of the bundle by removing most of the hydrophobic residues (L121T/L122T/L128T/L129T) did not affect gating either, though mutant occasionally resides longer in lower substates, supporting the fact that the S3 bundle is energetically uncoupled from the barrel expansion and most likely remains inseparable in all states.

While Chapter 1 clarifies the stereochemical aspect of the transition in MscL, the analysis of single- and multi-channel records presented in Chapter 2 shows that MscL gating pattern is complex and exhibits many conducting states. With the aid of the HISTAN software, it was possible to assess occupancies for individual states. It takes eleven gaussian peaks to accurately fit amplitude histograms from WT MscL. The peaks reflect the closed and fully open states, as well as nine substates. Some of these substates are not easily recognized on traces by eye, but revealed by the fitting procedure. Fitting of multiple histograms from traces recorded at different tensions in the range of open probabilities from $10^{-2}$ to 0.8 has shown that in WT MscL, all substates occupy approximately 26% of the open time and reduce the mean integral current by about 6% (relative to the current expected for an ideal channel without substates), practically independent of tension or open probability. Having the major rate-limiting step associated with the early sub-transition leading from the closed state to the low substate ($C \rightarrow S_{0.13}$), it was possible to simplify the entire kinetic scheme to two states by unifying all conducting states in a single effective conducting state $O_{eff}$ . The fact that WT MscL with its multi-state behavior permits a two-state approximation has validated the use of integral current as an adequate measure of open probability and enabled thorough analysis of multi-channel traces.

The dose-response curves allowed realistic estimation of the energetic and spatial scales for the entire transition. The analysis of the open probability as a function of membrane tension has been done in the linear Boltzmann approximation, in which the slope of $ln(P_o/P_c)$ on tension is equal to $\Delta A$/kT, thus directly reporting the area difference between any C and O states. The earlier estimations ΔE and ΔA associated with the entire C→O transition from multi-channel dose-response curves measured in liposomes (Sukharev et al., 1999b) gave unexpectedly low values for protein area changes (ΔA~6 $nm^2$), hardly accommodating the large conducting pore estimated to be 9-10 $nm^2$ in cross-section. This indicated that, for some reason, the slope of activation did not exactly reflect the expansion. I revisited this problem by recording dose-response curves in spheroplasts. Without direct measurements of membrane curvature, pressure-to-tension conversions were done by scoring the pressure activating the small channel MscS, usually found in the same patch. Dose-response curves from native multi-channel patches gave a larger ΔA (~12 $nm^2$), and revealed a small variation of the mid-point position from trial to trial, however, slope variation was unexpectedly large. To explain such a behavior we inferred that the populations of channels in each patch are slightly non-uniform, having channels activated earlier or later on tension. Statistical simulations of responses of normally distributed channel populations produced a large correlated scatter of apparent ΔE and ΔA parameters, with a fairly constant ratio ΔE/ΔA (corresponding to the mid-point tension $\gamma_{1/2}$), exactly as observed in experiments. The simulations indicated that a small scatter of either ΔE or ΔA (s.d. = 4-5% of the mean) is enough to reduce the midpoint slope of the population curve twice, leading to a 50% underestimation of both ΔA and ΔE. The simulations also predicted that the curves measured on scattered

populations must be inflected. Only the initial slope of left-most parts of such curves is close to the intrinsic slope for an individual channel, whereas the slope near the midpoint can be substantially lower and should not be trusted. Fitting the initial slopes of several inflected experimental dose-response curves produced $\Delta A = 20.1$ nm$^2$ and $\Delta E = 51.7$ kT for the entire gating transition. With this approach, the estimated area change is highly consistent with $\Delta A = 23$ nm$^2$ predicted by molecular models of the two end states. The problem of population non-uniformity is general and should be always considered in dose-response analysis of various types of channels (see Ruiz et al., 1999, for instance).

The values of $\Delta A$ and $\Delta E$ above are the gross parameters for the complex C→O transition. The observed subconducting states provided additional information on the gating intermediates. Measurements of substate occupancies from histograms at different tensions and treatment with the linear Boltzmann model allowed me to determine the $\Delta A$ and $\Delta E$ parameters for each individual sub-transition. The tension dependencies for several prominent substates in WT MscL allowed assigning their positions on the area scale ($\Delta A$) and clearly discerning whether they are intermediates, as all short-lived substates with $\Delta A$ smaller than that for the open state, or alternative open states, as $L_{0.78}$ and $L_{0.64}$, whose conformations are wider than that of the fully open state.

In Chapter 3, I continued the analysis of WT MscL gating and compared it to the gating of several gain-of-function mutants. The substate analysis confirmed the presence of expanded low-conducting intermediates and strongly supported the two-gate mechanism of MscL. The first major expansion of the transmembrane barrel (~70% of the total area change) is associated with a minor (13%) gain of conductance (0.4 nS). Such a behavior can hardly be explained by partial opening of a single gate. With the

simplifying assumption that the pore cross-section increases proportionally with the in-plane protein area, one may expect the conductance increase commensurate with expansion. A 70% protein area increase should then produce a 2.1 nS substate, five times higher than observed. The strong disparity between the area and conductance changes shows that the low substates are unlikely to be produced by partial opening of the single M1 gate as was proposed previously and implies the second gate.

I have accomplished thermodynamic analysis of several GOF mutants to clarify the nature and position of low-conducting conformations in the transition pathway. Gain-of-function (GOF) mutants of MscL carrying hydrophilic or charged substitutions in the hydrophobic constriction (M1 gate) open at lower tensions. Most severe and toxic GOF mutants open through a stable low-conducting substate. This stable substate has the same conductance as short-lived $S_{0.13}$ in WT and appears to be structurally analogous. A substate occupancy analysis revealed that gain-of-function mutations have strong effect specifically on the first sub-transition. The $\Delta E$ and $\Delta A$ parameters for the two sub-transitions show that the V23D GOF mutation reduces the area and especially energy parameters for the first $C \rightarrow S_{0.13}$ step compared to that of WT MscL. Other GOF substitutions affect the first sub-transition by reducing $\Delta A$ and $\Delta E$ between C and $S_{0.13}$ states commensurably with the severity of mutation. GOF mutants exhibited a larger $\Delta E$ associated with the second ($S_{0.13} \rightarrow O$) sub-transition, but $\Delta A$ similar to WT. The area changes indicated that resting conformations of GOF mutants are likely to be physically pre-expanded. The tension dependencies of rate constants for channel closure ($k_{off}$) predicted different rate-limiting barriers on the energy landscapes for WT and GOF MscL. The main barrier for WT is positioned at $\Delta A = 0.64$, between the C and $S_{0.13}$

states, whereas the barrier limiting the access to the O state in V23D is between the $S_{0.13}$ and O states, very close to O. The data support the two-gate mechanism in which the first sub-transition can be viewed as opening of the central (M1) gate, resulting in an expanded water-filled 'leaky' conformation (S). Strong facilitation of this step by polar or charged GOF substitutions suggests that separation of M1 helices is associated with hydration of the pore posing the major energetic barrier for opening of WT MscL.

In contrast to mutations in the pore constriction, extensions of S1-M1 linker alter the second sub-transition specifically. According to the previously proposed model, expansion of transmembrane barrel strains the linkers connecting M1 helices with N-terminal (S1) domains. Insertion of an extra glycine next to the 'hinge' residue G14 (GG14 mutation) on the WT background increases the occupancy of short-lived subconducting states, especially those of low conductance. When introduced on the V23D background, this mutation also increases the presence of intermediate states, but reduces the maximal conductance of the channel by abolishing transitions to the fully open state. This suggests that longer linkers experience less effective tension (become slack) and the driving force pulling the S1 bundle apart is lower. The two-amino acid linker extension (GAG14) produced an unexpected phenotype when introduced on the WT background. Instead of a further increase in probability of substates, the GAG14 mutation actually did not increase their presence during periods of channel activity (compared to WT), but was inactivated. It appears that the length and conformation of the S1-M1 linker is critical for the conformational stability of MscL with intact M1 gate, especially in the open state under high membrane tension. This behavior leads us to hypothesize that S1 domains may serve as primers for the proper closing transition. The

length of linkers seems to be less critical for the conformational stability of the easily opened V23D mutant with more stable intermediates. Thus, the iris-like mechanism involving two gates acting in a sequential manner had been tested. What remains unclear? The following points should be considered as the specific objectives for the future work: (1) In the 'iris' model, the large change in internal volume requires significant tilting of both M1 and M2 helices. The flattening and expansion of the M1/M2 barrel, has to extend periplasmic loops and M2-S3 linkers substantially. Both non-helical elements are likely to participate in forming of the conductive passage for water and ions. It has been known that single residue deletion (ΔQ56) in the periplasmic loops makes the channel stiffer requiring double tension to open it, whereas substitutions at the same position makes the channel softer (Blount et al., 1996b), suggesting that the structure of these region is critical for normal gating. Following the proteolytic cleavage in the loops, the channel was still functional but the open probability increases dramatically when the suction applied, indicating that the loop acts as a spring to restrain the opening of the channel and promotes its closure when it is open (Ajouz et. al., 2000). Thus, the conformational rearrangements of the periplasmic regions and their energetic impact in the channel in gating remain to be firmly established. S3 domains that form a cytoplasmic bundle stay together in all conformations. The M2-S3 liker is hypothesized to constitute a pre-filter at the cytoplasmic entrance to the pore that prevents the escape of large molecules. Its length and composition may affect normal channel gating and *in vivo* bacterial survival. A more thorough examination is needed to elucidate the function role of M2-S3 linker as a putative pre-filter.

(2) The biochemical and electrophysiological examinations of S1 domains support the two-gate mechanism. When the major M1 gate is perturbed by hydrophilic substitutions, the low-conducting substate, $S_{0.13}$, is stabilized in severe GOF mutants: V23D and G22N. What is the conformational structure of this substate? We envisage that the gaps between S1-M1 linkers ($^{13}R^{14}G^{15}N$) could conduct some ionic flux, creating in the substate $S_{0.13}$. While the low-conducting substate is extremely short in the wild type, in GOF mutant it lasts for much longer periods probably because S1 gate remains closed although M1 gate is open and at the same time, holes between M1-S1 linker are conductive. To test this hypothesis, single channel recordings should be performed in mutants in which S1 domains are restrained in a bundle-like arrangement on both the wild-type or GOF background. We expect to capture long periods of low-conducting states without or few full openings in GOF background, where the M1 gate is destabilized. The nature of the $S_{0.13} \rightarrow S_{0.22}$ sub-transition may be clarified by detailed analysis of GOF mutants. Through these investigations, we will obtain a better understanding about how sequential two gates work upon channel opening.

(3) The helix-tilt model predicts that upon the channel opening the S1 domains swing away and attach to the M1/M2 barrel. In the wild-type MscL, the proper docking may permit the additional stabilization of the fully open state. Kinetic analysis shows that the severe GOF mutants have hundred times faster on/off rate than that of wild type, showing a short full opening in the low and intermediate tensions. It suggests that the S1 domains are unable to dock properly in the GOF mutations. The roles of highly conserved S1 domains, their conformations in the closed state and the arrangement of the 'docking' site in the open state need to be addressed.

# REFERENCES


Adams, C. M., Anderson, M. G., Motto, D. G., Price, M. P., Johnson, W.A., Welsh, M. J. (1998) Ripped pocket and pickpocket, novel Drosophila DEG/ENaC subunits expressed in early development and in mechanosensory neurons. *J Cell Biol.* 140: 143-52.

Ajouz, B., Berrier, C., Besnard, M., Martinac, B., and Ghazi, A. **(**2000) Contributions of the different extramembranous domains of the mechanosensitive ion channel MscL to its response to membrane tension. *J Biol Chem.* 275:1015-22.

Ainsley, J.A., Pettus, J. M., Bosenko, D., Gerstein, C.E., Zinkevich, N., Anderson, M.G., Adams, C.M., Welsh, M.J., and Johnson, W.A. (2003) Enhanced locomotion caused by loss of the drosophila DEG/ENaC protein Pickpocket1. *Curr Biol.* 13: 1557-63.

Alvarez de la Rosa D, Zhang, P., Shao, D., White, F., Canessa, C. M.. (2002) Functional implications of the localization and activity of acid-sensitive channels in rat peripheral nervous system. *Proc Natl Acad Sci U S A*. 99: 2326-31.

Barr, M. M. and Sternberg, P. W. (1999) A polycystic kidney-disease gene homologue required for male mating behaviour in C. elegans. *Nature* 401, 386-389.

Bass, R. B., Strop, P., Barclay, M., and Rees, D. C. (2002) Crystal structure of Escherichia coli MscS, a voltage-modulated and mechanosensitive channel. *Science.* 298:1582-7.

Batiza, A. F., Rayment, I., and Kung, C. (1999) Channel gate! Tension, leak and disclosure. *Structure Fold Des.* 7:R99-103.

Blount, P., Sukharev, S.I., Moe, P.C., Schroeder, M.J., Guy, H.R., and Kung, C. (1996a) Membrane topology and multimeric structure of a mechanosensitive channel protein of *Escherichia coli*. *EMBO J.* 15: 4798-805.

Blount, P., Sukharev S. I., Schroeder M. J., Nagle S. K., and Kung C. (1996b) Single residue substitutions that change the gating properties of a mechanosensitive channel in *Escherichia coli*. *Proc. Natl. Acad. Sci. U. S. A* 93, 11652-11657.

Blount, P., Schroeder, M.J., and Kung, C. (1997) Mutations in a bacterial mechanosensitive channel change the cellular response to osmotic stress. *J Biol Chem*. 272: 32150-7.

Canessa, C.M., Horisberger, J. D., and Rossier, B. C. (1993) Epithelial sodium channel related proteins involved in neurodegeneration. *Nature.* 361, 467-70.

Canessa, C. M., Schild, L., Buell, G., Thorens, B., Gautschi, I., Horisberger, J.D., and Rossier, B.C. (1994) Amiloride-sensitive epithelial Na+ channel is made of three homologous subunits. *Nature.* 367:463-7.

Chang, G., Spencer, R.H., Lee, A.T., Barclay, M.T., and Rees, D.C. (1998) Structure of the MscL homolog from *Mycobacterium tuberculosis*: a gated mechanosensitive ion channel. *Science.* 282: 2220-6.

Colbert, H.A., Smith, T.L., and Bargmann, C.I. (1997) OSM-9, a novel protein with structural similarity to channels, is required for olfaction, mechanosensation, and olfactory adaptation in Caenorhabditis elegans. *J Neurosci.* 17: 8259-69.

Cosens, DJ, and Manning, A. (1969) Abnormal electroretinogram from a Drosophila mutant. *Nature.* 224: 285-7.

Cruickshank, C.C., Minchin, R.F., Le Dain, A.C., and Martinac, B. **(**1997) Estimation of the pore size of the large-conductance mechanosensitive ion channel of *Escherichia coli*. *Biophys J.* 73: 1925-31.

Cui, C., Smith, D.O., and Adler, J. (1996) Characterization of mechanosensitive channels in *Escherichia coli* cytoplasmic membrane by whole-cell patch clamp recording. *J Membr Biol.* 144:31-42.

Darboux, I., Lingueglia, E., Pauron, D., Barbry, P., Lazdunski, M. (1998) A new member of the amiloride-sensitive sodium channel family in Drosophila melanogaster peripheral nervous system. *Biochem Biophys Res Commun.* 246: 210-6.

Delany, N.S., Hurle, M., Facer, P., Alnadaf, T., Plumpton, C., Kinghorn, I., See, C.G., Costigan, M., Anand, P., Woolf, C.J., Crowther, D., Sanseau, P., and Tate, S.N. (2001) Identification and characterization of a novel human vanilloid receptor-like protein, VRL-2. *Physiol Genomics.* 4: 165-74.

Driscoll, M., and Chalfie, M. (1991) The mec-4 gene is a member of a family of *Caenorhabditis elegans* genes that can mutate to induce neuronal degeneration. *Nature.* 349:588-93.

Drummond, H. A., Price, M. P., Welsh, M. J., and Abboud, F. M..(1998) A molecular component of the arterial baroreceptor mechanotransducer. *Neuron* 21:1435-41.

Drummond, H.,A., Abboud, F..M., and Welsh, M. J. **(**2000) Localization of beta and gamma subunits of ENaC in sensory nerve endings in the rat foot pad. *Brain Res.* 884:1-12.

Ernstrom, G. G. and Chalfie, M. (2002) Genetics of sensory mechanotransduction. *Annu. Rev. Genet.* 36, 411-453.

Fricke, B., Lints, R., Stewart, G., Drummond, H., Dodt, G., Driscoll, M., and von During M. (2000) Epithelial Na+ channels and stomatin are expressed in rat trigeminal mechanosensory neurons. *Cell Tissue Res.* 299:327-34.

Garcia-Anoveros, J., Samad, T.A., Zuvela-Jelaska, L., Woolf, C. J., and Corey, D. P. (2001) Transport and localization of the DEG/ENaC ion channel BNaC1alpha to peripheral mechanosensory terminals of dorsal root ganglia neurons. *J Neurosci*. 21: 2678-86.

Goodman, M. B. and Schwarz, E. M. (2003) Transducing touch in *caenorhabditis elegans. Annu Rev Physiol* 65, 429-52.

Guharay, F., and Sachs, F. (1984) Stretch-activated single channel currents in tissue culture embryonic chick skeletal muscle. *J. Physiol* 352, 685-701.

Gullingsrud, J., and Schulten, K. (2003) Gating of MscL studied by steered molecular dynamics. *Biophys J.* 85:2087-99.

Gustin, M. C., Zhou, X. L., Martinac, B., and Kung, C. (1988) A mechanosensitive ion channel in the yeast plasma membrane. *Science.* 242, 762-765.

Hamill, O. P., Marty, A., Neher, E., Sakmann, B., and Sigworth, F. J. (1981) Improved patch-clamp techniques for high-resolution current recording from cells and cell-free membrane patches. *Pflugers Arch.* 391:85-100.

Hamill, O. P., and Martinac, B. (2001) Molecular basis of mechanotransduction in living cells. *Physiol. Rev*. 81, 685-740.

Hase, C. C., Le Dain, A. C., and Martinac, B. (1995) Purification and functional reconstitution of the recombinant large mechanosensitive ion channel (MscL) of *Escherichia coli. J Biol Chem.* 270:18329-34.

Howard, J., Roberts, W.M., and Hudspeth, A.J. (1988) Mechanoelectrical transduction by hair cells. *Annu Rev Biophys Biophys Chem.* 17:99-124.

Huang, M. and Chalfie, M. (1994) Gene interactions affecting mechanosensory transduction in *Caenorhabditis elegans*. *Nature.* 367, 467-470.

Hudspeth, A. J. (1997) How hearing happens. *Neuron.* 19:947-50.

Ingber, D. E. (2003) Tensegrity I. Cell structure and hierarchical systems biology. *J Cell Sci.* 116:1157-73.

Kellenberger, S., and Schild, L. (2002) Epithelial sodium channel/degenerin family of ion channels: a variety of functions for a shared structure. *Physiol Rev.* 82:735-67.

Kim, J., Chung, Y.D., Park, D.Y., Choi, S., Shin, D.W., Soh, H., Lee, H.W., Son, W., Yim, J., Park, C.S., Kernan, M.J., Kim, C.A. (2003) TRPV family ion channel required for hearing in *Drosophila*. *Nature.* 424: 81-4.

Kloda, A. and Martinac, B. (2001) Mechanosensitive channels in archaea. *Cell Biochem. Biophys.* 34, 349-381.

Koprowski, P., and Kubalski, A. (1999) Glutathione (GSH) reduces the open probability of mechanosensitive channels in *Escherichia coli* protoplasts. *Pflugers Arch.*438: 361-4.

Krishtal, O. (2003) The ASICs: signaling molecules? Modulators? *Trends Neurosci.* 26, 477-483.

Levina, N., Totemeyer, S., Stokes. N.R., Louis, P., Jones, M.A., and Booth, I.R. (1999) Protection of Escherichia coli cells against extreme turgor by activation of MscS and MscL mechanosensitive channels: identification of genes required for MscS activity. *EMBO J.* 18: 1730-7.

Liedtke, W., Choe, Y., Marti-Renom, M.A., Bell, A.M., Denis, C.S., Sali, A., Hudspeth, A.J., Friedman, J.M., and Heller, S.(2000) Vanilloid receptor-related osmotically activated channel (VR-OAC), a candidate vertebrate osmoreceptor. *Cell* 103: 525-35.

Littleton, J. T, and Ganetzky, B. (2000) Ion channels and synaptic organization: analysis of the Drosophila genome. *Neuron.* 26:35-43.

Maingret, F., Fosset, M., Lesage, F., Lazdunski, M., and Honore, E. (1999) TRAAK is a mammalian neuronal mechano-gated K+ channel. *J Biol Chem.* 274: 1381-7.

Malashkevich, V.N., Kammerer, R.A., Efimov,V.P., Schulthess,T. and Engel, J. (1996) The crystal structure of a five-stranded coiled coil in COMP: a prototype ion channel? *Science.* 274:761–765.

Martinac, B, Buechner, M, Delcour, A. H., Adler, J., and Kung, C. (1987) Pressure-sensitive ion channel in *Escherichia coli. Proc Natl Acad Sci U S A.* 84: 2297-301.

Maurer, J. A., Elmore, D. E , Lester, H. A., Dougherty, D. A. (2001) Comparing and contrasting Escherichia coli and Mycobacterium tuberculosis mechanosensitive channels (MscL). New gain of function mutations in the loop region. *J Biol Chem.* 275:22238-44.

Maurer, J.A., and Dougherty, D.A. (2003) Generation and evaluation of a large mutational library from the Escherichia coli mechanosensitive channel of large conductance, MscL: implications for channel gating and evolutionary design. *J Biol Chem.* 278:21076-82.

Minke, B, Wu, C., and Pak, W..L. (1975) Induction of photoreceptor voltage noise in the dark in *Drosophila* mutant. *Nature.* 258: 84-7.

Moe, P.C., Levin, G., and Blount, P. (2000) Correlating a Protein Structure with Function of a Bacterial Mechanosensitive Channel. *J Biol Chem.* 275: 31121-31127.

Nauli, S.M., Alenghat, F.J., Luo, Y., Williams, E., Vassilev, P., Li, X., Elia, A.E., Lu, W., Brown, E. M., Quinn, S.J., Ingber, D.E., and Zhou, J. (2003) Polycystins 1 and 2 mediate mechanosensation in the primary cilium of kidney cells. *Nat Genet.* 33: 129-37.

Oakley, A. J., Martinac, B., Wilce, M. C. (1999) Structure and function of the bacterial mechanosensitive channel of large conductance. *Protein Sci.* 8:1915-21.

Ou, X., Blount, P., Hoffman, R.J., and Kung, C. (1998) One face of a transmembrane helix is crucial in mechanosensitive channel gating. *Proc Natl Acad Sci U S A.* 95: 11471-5.

Pakula, A.A., and Simon, M.I. (1992) Determination of transmembrane protein structure by disulfide cross-linking: the Escherichia coli Tar receptor. *Proc Natl Acad Sci U S A.*89:4144-8

Patel, A.J., and Honore, E. (2001) Properties and modulation of mammalian 2P domain K+ channels. *Trends Neurosci*. 24: 339-46.

Patel, A.J., Lazdunski, M., and Honore, E. (2001) Lipid and mechano-gated 2P domain K(+) channels. *Curr Opin Cell Biol.* 13: 422-8.

Perozo, E., Cortes, D..M., Sompornpisut, P., Kloda, A., and Martinac, B. (2002 ) Open channel structure of MscL and the gating mechanism of mechanosensitive channels. *Nature.* 418: 942-8.

Pivetti, C.D., Yen, M. R., Miller, S., Busch, W., Tseng, Y. H., Booth, I. R., Saier, M. H. Jr. (2003) Two families of mechanosensitive channel proteins. *Microbiol Mol Biol Rev.* 67:66-85.

Pleumsamran, A. and Kim, D. (1995) Membrane stretch augments the cardiac muscarinic K+ channel activity. *J. Membr. Biol.* 148, 287-297.

Price, M. P., Lewin, G. R., McIlwrath, S. L., Cheng, C., Xie, J., Heppenstall, P. A., Stucky, C. L., Mannsfeldt, A.G., Brennan, T.J., Drummond, H.A., Qiao, J., Benson, C.J., Tarr, D.E., Hrstka, R.F., Yang, B., Williamson, R.A., and Welsh, M.J. (2000) The mammalian sodium channel BNC1 is required for normal touch sensation. *Nature.* 407: 1007-11.

Price, M.P., McIlwrath, S.L., Xie, J., Cheng, C., Qiao, J., Tarr, D.E., Sluka, K.A., Brennan, T.J., Lewin, G.R., and Welsh, M.J. (2001) The DRASIC cation channel contributes to the detection of cutaneous touch and acid stimuli in mice. *Neuron.* 32: 1071-83.

Qin, F., Auerbach, A. and Sachs, F. (2000) A direct optimization approach to hidden Markov modeling for single channel kinetics. *Biophys. J.* 79:1915-1927
in mechanosensitive channel gating. *Proc Natl Acad Sci U S A.* 95: 11471-5.

Ruiz, M., Brown, R.L., He, Y., Haley, T.L., and Karpen, J.W. (1999) The single-channel dose-response relation is consistently steep for rod cyclic nucleotide-gated channels: implications for the interpretation of macroscopic dose-response relations. *Biochemistry.* 38:10642-8.

Sachs, F. (1992) Stretch-sensitive ion channels: an update. *Soc Gen Physiol Ser.* 47:241-60.

Sackin, H. (1995) Mechanosensitive channels. *Annu. Rev. Physiol* 57, 333-353.

Sidi, S., Friedrich, R.W., and Nicolson, T. (2003) NompC TRP channel required for vertebrate sensory hair cell mechanotransduction. *Science.* 301: 96-9.

Smith, C.U.M. (2000) Biology of sensory system. John Wiley & Sons Ltd.

Spencer RH, Chang G, Rees DC. (1999) 'Feeling the pressure': structural insights into a gated mechanosensitive channel. *Curr Opin Struct Biol.* 9:448-54.

Strotmann, R., Harteneck, C., Nunnenmacher, K., Schultz, G., and Plant, T. D. (2000) OTRPC4, a nonselective cation channel that confers sensitivity to extracellular osmolarity. *Nat Cell Biol.* 2: 695-702.

Sukharev, S.I., Martinac, B., Arshavsky, V.Y., and Kung, C. (1993) Two types of mechanosensitive channels in the *Escherichia coli* cell envelope: solubilization and functional reconstitution. *Biophys J.* 65: 177-83.

Sukharev, S.I., Blount, P., Martinac, B., Blattner, F.R., and Kung, C. (1994) A large-conductance mechanosensitive channel in *E. coli* encoded by mscL alone. *Nature.* 368: 265-8.

Sukharev, S. I., Blount, P., Martinac, B., Kung, C. (1997) Mechanosensitive channels of *Escherichia coli*: the MscL gene, protein, and activities. *Annu. Rev. Physiol* 59, 633-657

Sukharev, S.I., Schroeder, M.J., and McCaslin, D.R. (1999a) Stoichiometry of the large conductance bacterial mechanosensitive channel of E. coli. A biochemical study. *J Membr Biol.* 171: 183-93.

Sukharev, S.I., Sigurdson, W.J., Kung, C., and Sachs, F. (1999b) Energetic and spatial parameters for gating of the bacterial large conductance mechanosensitive channel, MscL. *J Gen Physiol.* 113: 525-40.

Sukharev, S., Durell, S. R., and Guy, H. R. (2001) Structural models of the mscl gating mechanism. *Biophys. J.* 81, 917-936.

Sukharev, S. (2002) Purification of the small mechanosensitive channel of *Escherichia coli* (MscS): the subunit structure, conduction, and gating characteristics in liposomes. *Biophys. J.* **83**, 290-298.

Sukharev, S. and Anishkin, A. (2004) Mechanosensitive channels: what can we learn from 'simple' model systems? *Trend in Neurosci.* 27:345-351

Suzuki, M., Mizuno, A., Kodaira, K., Imai, M.(2003) Impaired pressure sensation in mice lacking TRPV4. *J Biol Chem*. 278: 22664-8.

Tang, Q. Y., Qi, Z., Naruse, K. and Sokabe, M. (2003) Characterization of functionally expressed stretch-activated BKca channel cloned from chick ventricular myocytes. *J Mem Biol.* 196: 185-200

Tobin, D., Madsen, D., Kahn-Kirby, A., Peckol, E., Moulder, G., Barstead, R., Maricq, A., and Bargmann, C. (2002) Combinatorial expression of TRPV channel proteins defines their sensory functions and subcellular localization in *C. elegans* neurons. *Neuron.* 35: 307-18.

Van Wagoner, D. R. (1993) Mechanosensitive gating of atrial ATP-sensitive potassium channels. *Circ. Res.* 72, 973-983.

Vriens, J., Watanabe, H., Janssens, A., Droogmans, G., Voets, T., and Nilius, B. (2004) Cell swelling, heat, and chemical agonists use distinct pathways for the activation of the cation channel TRPV4. *Proc Natl Acad Sci U S A.* 101: 396-401.

Walker, R.G., Willingham, A.T., Zuker, C.S. (2000) A Drosophila mechanosensory transduction channel. *Science*. 287: 2229-34.

Welsh, M. J., Price, M. P., and Xie, J. (2002) Biochemical basis of touch perception: mechanosensory function of degenerin/epithelial Na+ channels. *J. Biol. Chem.* 277, 2369-2372.

Wissenbach, U., Bodding, M., Freichel, M., and Flockerzi, V. (2000) Trp12, a novel Trp related protein from kidney. *FEBS Lett.* 485: 127-34.

Yao, X., Kwan, H-Y, and Huang Y. (2001) Stretch-sensitive switching among di°erent channel sublevels of an endothelial cation channel. *Biochimica et Biophysica Acta* 1511, 381-390

Yoshimura, K., Batiza, A., Schroeder, M., Blount, P., and Kung, C. **(**1999) Hydrophilicity of a single residue within MscL correlates with increased channel mechanosensitivity. *Biophys J.* 77: 1960-72.

Yoshimura, K., Batiza, A., and Kung, C. (2001) Chemically charging the pore constriction opens the mechanosensitive channel MscL. *Biophys J.* 80: 2198-206.

Zhou, X. L., Batiza, A. F., Loukin, S. H., Palmer, C. P., Kung, C., and Saimi Y. (2003) The transient receptor potential channel on the yeast vacuole is mechanosensitive. *Proc Natl Acad Sci U S A* 100, 7105-10.

Zoratti, M. and Petronilli, V. (1988) Ion-conducting channels in a Gram-positive bacterium. *FEBS Lett* 240, 105-109.